

STRUCTURAL AND SEDIMENTOLOGICAL STUDIES  
OF BADAMI SEDIMENTS AND ITS IMPLICATION ON  
URANIUM MINERALIZATION ALONG DESHNUR-  
GUJANAL TRACT, BELGAUM DISTRICT, KARNATAKA

*by*

PRANAV RAJ TYAGI

ENGG1G201801007

**Bhabha Atomic Research Centre, Mumbai**

*A thesis submitted to the  
Board of Studies in Engineering Sciences*

*In partial fulfillment of requirements  
for the Degree of*

MASTER OF TECHNOLOGY

*of*

**HOMI BHABHA NATIONAL INSTITUTE**

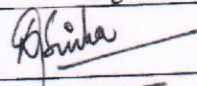
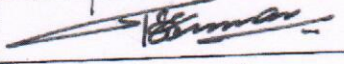
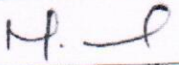
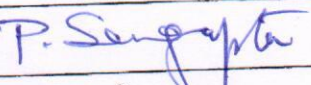
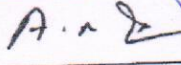
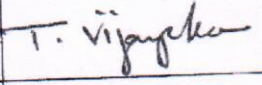
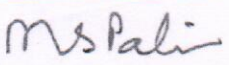
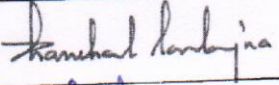



**February, 2021**

# Homi Bhabha National Institute

## Recommendations of the Thesis Examining Committee

As members of the Thesis examining Committee, we recommend that the thesis prepared by Pranav Raj Tyagi entitled "Structural and Sedimentological studies of Badami sediments and its implication on uranium mineralization along Deshnur-Gujanal tract, Belgaum district, Karnataka" be accepted as fulfilling the thesis requirement for the Degree of Master of Technology.

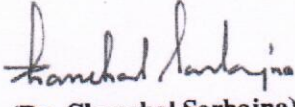
	Name	Signature
Member-1	Dr. D. K. Sinha	
Member-2	Dr. T. S. Sunil Kumar	
Member-3	Dr. Navin Goyal	
Member-4	Dr. Pranesh Sengupta	
Member-5	Dr. A. Rama Raju	
Technical advisor	T. Vijaya Kumar	
Examiner	Prof. M.S. Pandian	
Guide & Convener	Dr. Chanchal Sarbajna	
Chairman	Prof. Vivekanand Kain	

Final approval and acceptance of this thesis is contingent upon the candidate's submission of the final copies of the thesis to HBNI.

I hereby certify that I have read this thesis prepared under my direction and recommend that it may be accepted as fulfilling the thesis requirement.

Date: 11-02-2021

Place: Hyderabad

  
(Dr. Chanchal Sarbajna)  
Guide

## **DECLARATION**

I, hereby declare that the investigation presented in the thesis has been carried out by me. The work is original and has not been submitted earlier as a whole or in part for a degree / diploma at this or any other Institution / University.



(Pranav Raj Tyagi)

## **ACKNOWLEDGEMENT**

I express my sincere gratitude to my guide, Dr. Chanchal Sarbajna, Adjunct Professor, HBNI, for his valuable guidance, enriched suggestions, supervision and generous help during the course of work to complete this project.

I would also like to thank my technical advisor Shri T. Vijaya Kumar, SO/F for his support and guidance during the course of study. I am deeply indebted to Dr. D.K. Sinha, Director, AMD, for providing all the facilities and the opportunity to pursue this M. Tech programme. I am thankful to Shri Sandeep Hamilton, Additional Director (Operations-I), Shri B. Saravanan, Additional Director (Operations-II) and Dr. T.S. Sunil Kumar, Additional Director (R&D) for their encouragement and administrative support. I express my deep sense of gratitude to Shri D. K. Choudhury, SO-H, Regional Director, AMD, Southern Region, for providing the infrastructural facilities and co-operation extended throughout this project work. I thank the Deputy Regional Director and Incharge, Kaladgi Basin Investigation, AMD, Southern Region as well for their cooperation and support.

I am also thankful to the competent authority of HBNI for providing the opportunity to pursue the M. Tech. degree. I am thankful to Incharge, BARC Training School, AMD Campus for his support.

I would like to acknowledge my gratitude to Shri. Prathamesh Samant, SO-D, AMD-SR, Shri. Vinod Maurya, SO-D, AMD-SR for their support during the field work and technical discussions. I would like to extend my gratitude to Smt. Kusum Prakash, SO-F, Incharge, Petrology Lab, and other staff of Petrology Lab, AMD, SR for their generous support. Further, I would like to acknowledge the officers and Incharge of Physics, Chemistry and XRF laboratories of AMD for the analytical support which have been essential for the progress of the work.

Pranav Raj Tyagi

# CONTENTS

(Page No.)

<b>SYNOPSIS</b>	<b>iii</b>
<b>LIST OF FIGURES</b>	<b>vii</b>
<b>LIST OF TABLES</b>	<b>xi</b>
<b>CHAPTER 1 – INTRODUCTION</b>	<b>1</b>
1.1    PREVIOUS WORK	3
1.2    URANIUM MINERALIZATION IN KALADGI BASIN	4
1.3    PRINCIPAL OBJECTIVES	6
1.4    RESEARCH PLAN/METHODOLOGY	7
1.5    DELIVERABLES	7
<b>CHAPTER 2 – GEOLOGY</b>	<b>8</b>
2.1    LOCATION, COMMUNICATION AND ACCESSIBILITY	8
2.2    PHYSIOGRAPHY AND CLIMATE	8
2.3    REGIONAL GEOLOGY	9
2.4    MAPPING	13
2.5    LOCAL GEOLOGY	15
2.6    BADAMI SEDIMENTS	15
2.7    SEDIMENTARY STRUCTURES	18
2.8    DEFORMATIONAL STRUCTURES	19
<b>CHAPTER 3 – SEDIMENTOLOGY</b>	<b>21</b>
3.1    SEDIMENTARY LOGS	22
3.2    LITHOFACIES ANALYSIS	24
3.3    PALEOCURRENT ANALYSIS	38
3.4    DEPOSITIONAL SETTING	39
3.5    URANIUM MINERALIZATION	42

3.6	MINERALIZED HOST ROCK CHARACTERISTICS	49
<b>CHAPTER 4 – PETROGRAPHY</b>		<b>50</b>
4.1	METHODOLOGY	50
4.2	BADAMI SEDIMENTS	52
4.2.1	PEBBLY FELDSPATHIC ARENITE	53
4.2.2	FELDSPATHIC ARENITE	57
4.2.3	QUARTZ ARENITE	59
4.3	RADIOACTIVITY	62
4.4	DIAGENETIC HISTORY	63
4.5	INTERPRETATION	64
<b>CHAPTER 5 – HEAVY MINERALS STUDIES</b>		<b>66</b>
5.1	METHODOLOGY	66
5.2	MORPHOMETRIC ANALYSIS OF ZIRCON	71
5.2.1	ROUNDNESS	71
5.2.2	ELONGATION	74
5.2.3	SURFACE CHARACTERISTICS	76
<b>CHAPTER 6 – GEOCHEMISTRY</b>		<b>81</b>
6.1	CAVE TEMPLE ARENITE SANDSTONES	81
6.2	PALEOWEATHERING	86
6.3	TECTONIC SETTING	89
6.4	GEOCHEMISTRY OF PEBBLY FELDSPATHIC ARENITE/LOWER CONGLOMERATE	90
<b>CHAPTER 7 – DISCUSSION</b>		<b>100</b>
<b>CHAPTER 8 – CONCLUSION</b>		<b>105</b>
<b>REFERENCES</b>		<b>108</b>

## SYNOPSIS

The study area, along Deshnur-Gujanal tract, Belgaum district, Karnataka is located in the western part of Proterozoic Kaladgi basin. The area exposes Cave Temple Arenite Member of Badami Group of sediments unconformably overlies basement rocks comprising of Chitradurga metasediments. Sub-surface exploration by AMD established significant correlatable uranium mineralisation in lower part of Badami sediments at Deshnur and Gujanal areas. Present study on the structural and sedimentological aspects of Badami Group of rocks will help in establishing control of uranium mineralisation.

Geological mapping in 1:25,000 scale over an area of about 20 sq km, mainly exposes sequence of conglomerate to pebbly feldspathic arenite and quartz arenite overlying the basement garnetiferous quartz chlorite schist with an angular unconformity. The general attitude of Badami sediment is ENE-WSW strike direction, dipping gently with 5-10° due NW direction. The area is traversed by two major sub-vertical fractures trending along NE-SW and NW-SE directions (n=179).

Sedimentological studies by preparing lithologs and facies analysis were taken up in exposed surface outcrops and borehole cores in Deshnur (43P 472370m E/1759475m N) and Gujanal (43Q 465649m E/1770659m N) areas respectively, Belgaum district, Karnataka. Paleocurrent analyses (n=65) on cross-beds from mainly quartz arenite units exposed near Deshnur area indicate the movement of paleocurrent flow from SE to NW direction.

As a part of present work based on the process based sedimentological studies, the presence of three major sedimentary cycles (300m total thickness) are inferred, starting from alluvial fan type environment characterized by presence of clast to matrix supported conglomerate and culminating in braided fluvial system characterized by cross stratified sandstone. A small interval of marginal-marine transition represented by presence of

intercalated black shales within quartz arenite is interpreted in the upper part of second sedimentary cycle. The mineralisation is confined to second major cycle (80-100m thick) represented by 30 minor channel fill cycles starting with matrix supported conglomerate, grading into pebbly feldspathic arenite and ending with thinly laminated silty-shale intercalations. Thickness of individual channel fill cycles ranges from 30cm to 4m with shale units ranges from 2 to 15cm thickness. The mineralisation is recorded in minor cycles from 11<sup>th</sup> to 13<sup>th</sup> at 6 different levels confined to 40m thick horizon in borehole SLD-100, whereas it is recorded from 26<sup>th</sup> to 30<sup>th</sup> cycles in SLD-102. The host rock is greyish white to greenish white, matrix supported pebbly feldspathic arenite intercalated with thin shale bands and associated with sulphides. The dominant clasts (1 to 6 mm size) are quartz and feldspars with vein quartz, set in quartzo-feldspathic matrix. It is soft and friable at places due to minor fracture and alteration in which feldspars are highly altered to clay.

Petromineralogical study identified the mineralized samples as matrix supported conglomerate / pebbly feldspathic arenite. It is texturally and mineralogically immature characterized by poorly sorted, sub-rounded to angular clasts of quartz (70-80%), microcline, perthite, orthoclase and plagioclase feldspar (15-30%) and rock fragments of chert, quartzite and mylonite as framework clast set in quartzo-feldspathic and clayey matrix. K-feldspar are in abundance relative to plagioclase. Feldspar and biotite are altered to sericite, illite and chlorite also contributing as matrix at places. The cement is iron oxide and silica. Silica overgrowth and pressure solution are indicating diagenetic modification. Sericite as flowage texture surrounding clast and replacing them are evidence of post diagenetic changes. Due to size constrains, it is difficult to distinguish between different clay phases and their transformation in response to changing physio-chemical conditions.

Discrete uranium phases identified are pitchblende, uraninite and coffinite grains, under ore microscopic studies, occurring predominantly as disseminated form along the grain



boundaries, inter-granular spaces of poorly sorted matrix portion and as micro fracture filling in quartz in association with sulphides. Pitchblende with varying shades of grey occupying the secondary pores formed due to dissolution of quartz along the etched grain boundaries is also observed. Radioactive accessories are identified as zoned zircon and monazite. Clusters of titanites and apatite grains occur as accessories. Pyrite, chalcopyrite, covellite and bornite are the associated sulphide minerals. The association of uranium phases with sulphide minerals indicates a reducing environment which helped in precipitation of uranium. Paragenetically pyrite is being replaced by chalcopyrite which in turn is replaced by pitchblende and coffinite along grain boundaries and cleavage plane suggest uranium precipitation in later phases to sulphides. Uranium bearing samples show significant amount of clayey matter occurring as matrix in comparison to non-radioactive samples which are compact, mature and bounded by ferruginous matter indicating relatively oxidized nature

Geochemical analyses (n=24) show very high and wide range of  $\text{SiO}_2$  with moderate to high  $\text{Al}_2\text{O}_3$ ,  $\text{K}_2\text{O}$  and moderate  $\text{Na}_2\text{O}$ ,  $\text{MgO}$ ,  $\text{Fe}_2\text{O}_3$  indicating presence of predominant quartz with moderate amount of K-feldspar / plagioclase feldspar, mica and clay minerals as accessories. The studied rock samples mostly fall in arkose to sub-arkose field with few falling in lithic arenite to quartz arenite fields.

The provenance study from major oxides indicate that the detritus involved in the formation of sandstone were derived from quartzose sedimentary provenance, which represent ultimate granitic provenance, it is further substantiated by high Index of Compositional Variation (ICV), moderate Chemical Index of Alteration (CIA) values and morphometric studies of Zircon. Completely unrounded grains of zircon with less surface fracturing and cracks, indicates quick burial of detrital sediments from nearby source, thus indicating less transport history. The sediments were deposited in humid climate in passive margin tectonic setting.

Geochemically mineralised (n=11) and non-mineralised (n=10) samples show overlapping chemical composition with depletion of SiO<sub>2</sub>, CaO and enrichment of Al<sub>2</sub>O<sub>3</sub>, Fe<sub>2</sub>O<sub>3</sub>, K<sub>2</sub>O, Ni, Rb, Sr, Zr and Ba with respect to Average Proterozoic Cratonic Sandstone. Besides, mineralised samples show enrichment of Cu, Pb, U and depletion of TiO<sub>2</sub> with respect of non-mineralised samples. Both samples show presence of zircon, apatite, monazite, sphene, rutile, ilmenite as accessories and illite as clay mineral. Weak to moderate correlation of uranium with copper (309 to 7195 ppm, r=0.35), and good correlation with lead (19 to 239 ppm, r=0.69) and zinc (22 to 207 ppm, r=0.71) is noticed in mineralised samples.

The basinal oxidised fluids might have leached the uranium from refractory minerals such as zircon, monazite, sphene from sediments and/or basement. Activity of hydrothermal solution from basement is evidenced by the anomalous content of Cu, Pb, Zn, Ni, Ba in sediments. The close association of uranium minerals formed by replacement of copper sulphides, indicate precipitation of sulphides during earlier phase of hydrothermal activity, thus suggesting the uranium mineralization to be hydrothermal and epigenetic in nature.

## LIST OF FIGURES

Figure No.	Description	Page No.
1.1	Geological map of Kaladgi Basin, after Jayaprakash 2007	6
2.1	Geological map along Deshnur-Gujanal tract. Survey of India Toposheet Number 47 L/12 & 48 I/9)	14
2.2	Geological cross section along Deshnur-Gujanal tract.	17
2.3	Planar cross bedding from Quartz arenite, Cave temple arenite member, Deshnur	17
2.4	Radioactive, fine grained Quartz arenite, Cave temple arenite member, Deshnur.	17
2.5	Upper conglomerate, displaying different fracture sets at Deshnur	18
2.6	Gritty feldspathic arenite, Cave temple arenite member, Nelganti	18
2.7	Lithosection representing three sedimentary cycles	19
2.8	Rose diagram displaying fracture set data. Trends of prominent fracture affecting: a) Basin Margin, b) Basin Interior	20
3.1	(a) Cross-section along Deshnur-Gujanal tract, (b) Litholog prepared from borehole SLD-99, (c) Litholog prepared from vertical exposed section in Deshnur	23
3.2	a): Lithofacies A - Clast supported conglomerate; b): Lithofacies B - Matrix supported conglomerate; (c, d): Lithofacies C - Cross-stratified pebbly sandstone; e): Lithofacies D - Thinly laminated silty-shale intercalations; f): Lithofacies E - Trough cross-stratified sub-feldspathic arenite; (g, h): Lithofacies F - Tabular cross stratified quartz arenite; (i, j, k, l, m): Lithofacies G - Trough cross stratified quartz arenite; (n, o, p): Lithofacies H - Wavy parallel laminated shale; (q, r, s): Lithofacies I - Clast supported conglomerate; (t, u): Lithofacies J - Trough cross stratified feldspathic arenite.	37

3.3	Well preserved trough and planar cross beds	39
3.4	Paleocurrent direction in basin margin	39
3.5	Feldspathic arenite; (a) cross-stratification, b) ferruginisation along fracture plane (c) gritty feldspar and quartz grains.	40
3.6	Intercalations of conglomerate and silty-shale horizons.	41
3.7	Quartz arenite.	41
3.8	Sulphides along S <sub>0</sub> plane within black shale	41
3.9	Detailed litholog of pebbly feldspathic arenite/lower conglomerate unit from borehole SLD-99	43
3.10	Silty shale intercalations in pebbly feldspathic arenite/lower conglomerate.	44
3.11	i), ii), iii) Mineralized horizons in SLD-100	45, 46, 47
3.12	Mineralized horizons in SLD-102	48
4.1	(a) Non-radioactive conglomerate, polycrystalline quartz (PQ), clay and K feldspar (kfs), TL 1N, (b) RL, XN, (c) perthite clast (PC), (d) feldspar altering to clay, Pitchblende (P) and Pyrite (Py) TL, XN, (e) detrital biotite and diagenetic clay occurring as matrix around framework grains of Quartz (Q) and feldspar (Kfs)	55
4.2	Radioactive conglomerate, (a), (b) & (c) Uraninite and copper sulfide in quartz microfractures and replacing quartz and clay minerals present as matrix, (d) Uraninite (U) and suspected coffinite (Cf) associated with chalcocite TL, 1N, (e)) Uraninite occupying secondary dissolution pore-spaces (indicated by small arrows) and also engulfing etched quartz fragment (inset), RL, 1N., (f) Different generation of copper sulfides, wherein chalcopyrite is replaced by bornite which is replaced by covellite.	56

4.3	Feldspathic arenite showing compact nature with less matrix content (a) TL, 1N (b) TL, XN; Uranium minerals associated with chalcopyrite along grain boundaries replacing clay matrix (c) TL, 1N, (d) TL, XN. Magnified view of uraninite (U) associated with chalcopyrite TL, 1N, (e) RL, 1N; (f) RL. Biotite can be seen converting to clay minerals in matrix (g) TL XN, (h) TL, 1N. Occurrence of sulphides along grain boundaries (i) TL, XN (j) RL, XN,	58, 59
4.4	(a) Non-radioactive quartz arenite showing interlocking texture TL, XN (b) Silica overgrowth TL, XN	60
4.5	(a) Pitchblende (P) vein in hairline fractures in quartz arenite giving very dense tracks, TL, XN, (b) Fractured Pyrite (Py) surrounded and infiltrated by pitchblende, RL, 1N, (c) Pitchblende present in the intergranular spaces, Offset track image RL, XN, (d) TL, 1N	61
4.6	(a,b) Irregular grain boundaries (filled with clay minerals) creating pore spaces due Quartz dissolution due to acidic brines.	65
5.1	Zircon 20X, TL, 1N (a), (c); Zircon 20X, TL, XN (b), (d); Monazite 10X, TL, 1N (e), (g), Monazite 10X, TL, XN (f), (h); Iron coating 10X, TL, 1N (i), (k); Iron coating 10X, RL, XN (j), (l); Sphene 20X, TL, 1N (m), (n), (o), (p).	70
5.2	Completely unrounded Zircon grains with sharp edges 20X, TL, 1N (a), (b), Zircon 20X, TL, XN (c)	71
5.3	Elongate Zircon grains 20X, TL, 1N, (a), (b), (c), (d), (e). (f)	75
5.4	Zircon grains exhibiting fracturing perpendicular to c axis in a & b, TL, 1N; Zircon grains with cracks developing in c, d, e and f, TL, 1N.	77
5.5	Zoned zircons with fluid inclusions 50X, TL, XN	78
5.6	A representative spider plot showing the interrelations between roundness, collision marks, type of fraction, cracks at the crystal surface. After (Gartner et al 2013	79

6.1	Geochemical classification of sandstones. (a) $\log (\text{Fe}_2\text{O}_3/\text{K}_2\text{O})$ versus $\log (\text{SiO}_2/\text{Al}_2\text{O}_3)$	84
6.2	Bivariate diagram $\text{K}_2\text{O}$ wt.% versus $\text{Na}_2\text{O}$ wt.% bivariate diagram (after Crook 1974).	85
6.3	Provenance discrimination plot (after McLennan et al., 1980; Schieber, 1992)	85
6.4	Provenance discrimination plot $\text{TiO}_2$ wt% vs $\text{Al}_2\text{O}_3$ wt% (after McLennan et al., 1980). The “granite line” and “3 granite + 1 basalt line” are after Schieber, (1992).	86
6.5	$\text{SiO}_2$ (wt%) vs $\text{Al}_2\text{O}_3+\text{K}_2\text{O}+\text{Na}_2\text{O}$ (wt%) binary variation plot (After Muhs, 2002)	88
6.6	$\text{SiO}_2$ vs $\text{K}_2\text{O}/\text{Na}_2\text{O}$ plot after Roser and Korsch, (1986) shows passive continental margin setting of the studied conglomerate	89
6.7	Average Proterozoic Cratonic Sandstone (APCS) normalized spider diagram for uraniferous and non uraniferous conglomerate	92
6.8	A-CN-K diagram showing the weathering trend of the high and low uraniferous matrix-supported conglomerate of the Badami Formation (After Nesbitt and Young, 1982). $\text{A}=\text{Al}_2\text{O}_3$ , $\text{CN}=\text{CaO}+\text{Na}_2\text{O}$ , $\text{K}=\text{K}_2\text{O}$ (molecular proportions).	97
6.9	Binary plot between $\text{MgO}/\text{Al}_2\text{O}_3$ versus $\text{K}_2\text{O}/\text{Al}_2\text{O}_3$ (after Sopuck, 1988)	98

## LIST OF TABLES

<b>Table No.</b>	<b>Description</b>	<b>Page No.</b>
2.1	Lithostratigraphy of Kaladgi Basin. After Jayaprakash et al. (1987), Jayaprakash (2007).	11
3.1	Facies encountered within Cave Temple Arenite Member of Badami Group	34
5.1	The ten classes of roundness, after Pupin 1980	72
5.2	Ratios and classification after Mitterer (2001) for both common possibilities of calculation of elongation	76
6.1	Correlation coefficient data of major and minor oxides of Cave Temple Arenite sandstones`	82
6.2	Major, minor and trace elements of selected non-radioactive samples	90
6.3	Major, minor and trace elements of selected radioactive samples	91
6.4	Average of major, minor and trace elements of pebbly feldspathic arenite/lower conglomerate against Proterozoic Cratonic Sandstone after Condie, 1993	92
6.5	Correlation matrix of major and trace elements composition of uraniferous pebbly feldspathic arenite/lower conglomerate	94
6.6	Correlation matrix of major and trace elements composition of non-uraniferous pebbly feldspathic arenite/lower conglomerate	95

## CHAPTER 1

### INTRODUCTION

Uranium is a dense naturally occurring radioactive trace element. It is the heaviest naturally occurring element ( $z=92$ ) and is an incompatible element because of its high charge and large ionic radius (e.g.,  $U^{4+} = 1.03\text{\AA}$ ,  $U^{+6} = 0.87\text{\AA}$ ) and remains concentrated in upper continental crust relative to other earth geochemical reservoirs. Concentration of uranium is normally low, averaging only 2.7 ppm in the upper continental crust, 0.015 ppm in mantle (Clark 1966). Uranium is a Large Ion Lithophile Element (L.I.L.E.) which occurs in the tetravalent ( $U^{+4}$ ), pentavalent ( $U^{+5}$ ) and in the hexavalent ( $U^{+6}$ ) states, the  $U^{+6}$  form being stable under highly oxidizing conditions. The most abundant radioactive isotope of this element,  $^{238}\text{U}$ , has a long half-life of  $4.5 \times 10^9$  years which is similar to the age of the earth. In highly differentiated rocks (granite, pegmatite and especially in peralkaline rocks), uranium is associated with Th, Zr, Ti, Nb, Ta and Rare Earth Elements (REE) (Cuney, 2010; Cuney and Kyser, 2009). In sedimentary rocks like sandstone, uranium occurs in association with redox-sensitive elements like Mo, V, Se, As and Cu (Fayek et al., 2011). Owing to this geochemical character, uranium deposits occur in a wide range of temperatures and pressures throughout the geological cycle, occurring in different geological settings belonging to wide range of geological age.

Exploration in middle Proterozoic sedimentary basins received great impetus all over the world, ever since high-grade uranium mineralization was brought to light in the Proterozoic unconformity deposits as found in Athabasca basin of Canada and Pine Creek Geosyncline of Australia (Kyser & Cuney, 2009b, and Fayek, 2013). High concentrations of Uranium occurrences are reported from Proterozoic basins of the world. Proterozoic sedimentary basins provide valuable information on the evolution of lithosphere and ore-forming processes of



significant metal deposits like Uranium (Deb & Pal, 2015). Major global drivers such as changes in global geotectonic conditions and Great Oxidation Event (~2.4 bya.) (Cuney, 2005) supplemented by discovery of high-grade large-tonnage unconformity type deposits (33% of world's Uranium resource) in Canada and Pine creek geosyncline of Australia made Middle to Late Proterozoic basins the primary focus of uranium exploration.

Further, Proterozoic unconformity uranium deposits are of three sub types (IAEA, 2013) viz. Unconformity-contact deposits as found in Cigar Lake, Collins bay, Breccia or fractured controlled as found in Rabbit lake, Eagle point, McClean Lake, Millenium Athabasca basin, Canada Jabiluka and Ranger, Australia and Stratiform structure control deposits (IAEA, 2013) e.g., Chittril and Lambapur. The less deformed and unmetamorphosed Paleo-Mesoproterozoic basins occupying a significant part of peninsular India overlie the deformed and metamorphosed Archean/Proterozoic basement (Chakraborty et al. 2010). The broad similarities in, styles of crustal evolution, tectonic setup and metallogeny of Archean and Proterozoic terrains of Canada and Australia, underlies the significance of Proterozoic basins of India as potential zones for uranium mineralization. (Krishnamurthy, 1996). The Meso-Neoproterozoic Kaladgi basin encompassing characteristic geological setting, stratigraphy, structure, age and underlying fertile basement, is one of the major thrust areas of exploration for potential high-grade uranium mineralization.

In India, Middle Proterozoic basins have been under intensive exploration, particularly in the Southern and Central Peninsular India, for locating Unconformity type/related uranium deposits. The Proterozoic history of Indian shield includes Mesoproterozoic Mobile Belts (MPMB: Radhakrishna and Naqvi, 1986) and epicratonic, platform basins (Purana basins) that host Mesoproterozoic and Neoproterozoic cycles of sediments that flank five Archean cratonic nuclei (Radhakrishna, 1987, Ramakrishnan & Vaidyanthan, 2010; Mazumdar and Erickson,

2015). The Purana basins developed in an extensional tectonic regime, display structural contacts with the adjoining MPMB that evolved in compressive tectonic regimes.

### **1.1 Previous work**

The Kaladgi basin on the northern edge of the Dharwar craton differ from the other Purana basins in that, it does not have any geographic proximity with Mid Proterozoic Mobile Belts (MPMB). The three Proterozoic basins of the southern Peninsular India, namely, Cuddapah basin, Kaladgi basin and Bhima basin have been under active exploration by AMD, as a result of which, many uranium occurrences have come to light. Meso-Neoproterozoic intracratonic Kaladgi basin (Fig.1) is exposed over an irregular E-W trending area and located on the northern fringes of the Western Dharwar craton exposed mostly in northern parts of Karnataka, Maharashtra and Goa, South India (Jayaprakash et al., 1987).

Different aspects of Kaladgi basin such as the lithology, structure, geochemistry, structure etc. have been studied and reported by several authors. Bruce foote (1876) developing on the contributions from pioneers in early 19th century, was the first to systematically map the basin on the regional scale. He classified the sedimentary succession into Upper and Lower Kaladgi series. Nautiyal (1966) attributed the Lower and Upper Kaladgi series, to separate but overlapping Kaladgi and Badami basins respectively (Jayaprakash, 1987). A distinctive angular unconformity separating the undeformed younger and flat-lying sandstone-shale unit of Badami group from the underlying older and folded sedimentary sequence of Kaladgi group of rocks was identified by Vishwanathaiah (1977). Jayaprakash et al., 1987 critically reviewed and revised the entire sequence as Kaladgi supergroup thereby dividing it lithostratigraphically into lower Bagalkot and upper Badami group separated by an unconformity. Kale (1991) and Pillai (2007, 2018) through their detailed investigation and close examination in field study regarding geotectonic framework and its control on sedimentation have significantly contributed in the evolutionary history of the Kaladgi basin. Dey (2009, 2015) with shreds of

evidence from sandstone petrography and geochemistry established the composition and tectonics of provenance thereby contribution towards an understanding of the geological history of the basin.

## **1.2 Uranium mineralization in Kaladgi basin**

Uranium exploration in Proterozoic Kaladgi Basin of Southern India was initiated in the year 1961. Investigation strategies and approaches were modified as newer ideas emerged globally with time when the exploration for uranium in the basin was renewed on the basis of unconformity related model. Significant surface uranium mineralization up to 0.83%  $U_3O_8$  was located in the Badami arenite for the first time during F.S. 2004 (AMD, 2004-2005). Exploration activities gained new impetus after the discovery of uranium mineralization up to 0.13%  $eU_3O_8$  x 63.00m with high order uranium values up to 3.57%  $eU_3O_8$  hosted by Badami sediments in Deshnur, proximal to the unconformity between Badami sediments and basement Chitradurga metasediments.

Based on the same exploration strategy, subsurface exploration carried out in Gujanal area (AMD, 2013-2014) 18 km NNW of Deshnur village in Belgaum district, Karnataka. The sub-surface exploration by drilling has established rich grade and thick zones of uranium mineralization nearer to unconformity contact hosted in the lower part of the Badami sediments and basement metasediments of Chitradurga Group. Mineralized lower conglomerate and basal arenite extend over a strike length of over 1800 m at Suldhall-Gujanal block along NE-SW direction (AMD, 2017-2018).

Since, Kaladgi-Badami basin is one of the prime targets and under active uranium exploration, understanding the controls of mineralization and its genesis will be helpful in exploration in Suldhall-Gujanal area in particular and in the Kaladgi-Badami basin in general. Preliminary petrological studies indicated presence of uraniferous minerals, like pitchblende

and coffinite within the lower conglomerate. Detailed petromineralogical studies, to understand the paragenetic sequence of uranium and associated ore minerals in the host rock, corroborated by-geochemical characterization, may throw light into the genesis of uranium mineralization in the Suldhah-Gujanal area. The occurrence of such uranium rich minerals within Badami sediments is encouraging and warrants further studies in terms of the petromineralogy, geochemistry of the mineralized host rock. The study area occupying South-western part of the basin exposes Badami group of rocks unconformably overlying Chitradurga group of metasediments. The area extends from basin margin at Deshnur to Gujanal, thereby covering an area of 20 sq km. Paleocurrent analysis in south western part of Kaladgi basin exposing Cave Temple Arenite member in areas of Deshnur, Kardiguddi and Sulebhavi has been undertaken by Ghosh et al. 2016. However, detailed sedimentological studies encompassing the paleocurrent analysis, and lithofacies study of sediments with special reference to characterization of matrix portion uraniferous Badami sediments along Deshnur-Gujanal tract of had not been carried out so far. The present work covering sedimentological and structural studies will help in understanding the genesis of uranium mineralization of the Badami sediments.

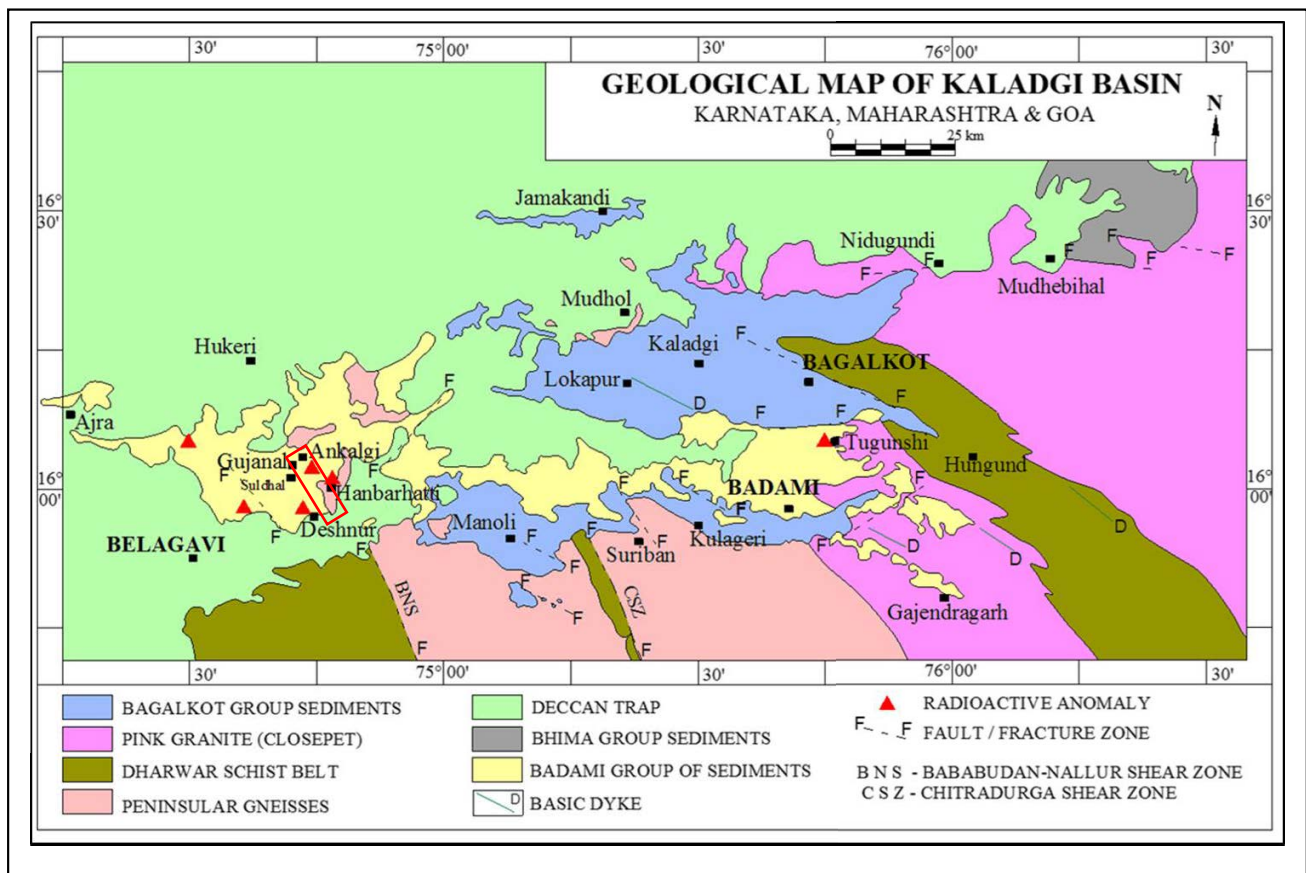


Figure 1.1 Geological map of Kaladgi Basin (after Jayaprakash 2007)

### 1.3 Principal objectives

Sediment hosted, unconformity related uranium mineralization processes are often to large scale movement of active fluids (Kyser and Hiatt, 2003). Porosity and permeability of the sediments dictate transportation of mineralizing fluids and subsequent precipitation under favorable locales. Thereby systematic study of sedimentological attributes of Badami sediments is critical in understanding the mineralization processes and deciphering its genetic aspects.

Correspondingly, the objectives of the study are as listed below.

- i. Structural and sedimentological studies of Badami sediments.

- ii. Characterization of uraniferous Badami sediments with special reference to matrix portion in feldspar clast rich conglomerate.
- iii. Provenance reconstruction studies.
- iv. Identify the controlling factors on Uranium mineralization.
- v. Develop a conceptual genetic model on uranium mineralization and associated base metals.

#### **1.4 Research Plan/Methodology**

To achieve the aforementioned objective, following methodology will be undertaken:

- i. Geological mapping on 1:25,000 scale from the basin margin to interior along Deshnur-Gujanal tract, Belgaum district in an area of 20 sq km, T.S. No. 48 I/9, 47 L/12.
- ii. Study of lithological and structural attributes by examination of borehole cores and with surface outcrops.
- iii. Petromineralogical studies of uraniferous Badami sediments.
- iv. Heavy mineral studies of pebbly feldspathic arenite/lower conglomerate.

#### **1.5 Deliverables**

- i. Geological mapping (1:25,000 scale) showing lithology and structural data from basin margin to interior along Deshnur-Gujanal tract.
- ii. Interpretation of depositional environment using facies analysis.
- iii. Characteristics of uraniferous Badami sediments.
- iv. Genesis of uranium mineralization and its controls.

## **CHAPTER 2**

### **GEOLOGY**

#### **2.1 Location, commutation and accessibility**

The study area undertaken for structural and sedimentological studies in Badami group of sediments, covering an area of 20 sq km extends from basin margin along Deshnur – Gujanal tract. The area taken up is covered in Survey of India Toposheet no. 47L/12 and 48I/9 between latitude 15°30' to 16°30' and longitude 74°40' to 74°45'. It lies near Deshnur Village in Belgaum district of Karnataka. A Major part of the field area is occupied by reserve forest with intermediate locations like Nelganti, Suldhhal and Budihal connected by all-season metal road. The study area is well connected by road and rail services. Nearest railway station at Belgaum is very well connected (~600 km) with Bangalore by all means. The airport in the suburbs of Sambra, 10 km east of Belgaum connects with major domestic airports of the country.

#### **2.2 Physiography and Climate**

Deshnur-Gujanal tract is situated east of Markandeya river, which joins east west flowing Ghataprabha river near Gokak. The area is mostly undulatory with sparsely distributed knolls and tors between intermittently flat plains. Hill tops are marked by long stretches of flat-lying rocks and are mostly barren with scanty scrubby vegetation. Plains are covered by thick soil profile and are used for cultivation.

Belgaum district experience general dryness, except during monsoon season. The region during the month of March to May experience a steady increase in temperature with April being the hottest month of the year. Beginning of June marks, the arrival of monsoon which starts retreating from October to November. This is followed by winter season culminating in February.

## 2.3 Regional geology

Kaladgi basin is an intracratonic Meso-Neoproterozoic basin, occupying North-western part of Western Dharwar Craton (WDC) exposed mostly in northern parts of Karnataka, Maharashtra and Goa, South India (Jayaprakash et al., 1987). The basin has an irregular elliptical outline which extends in east-west direction, spreading over 8300 sq km and a thickness of 4500m. A good part of the northerly and westerly extension of the basins is covered by Deccan Traps. Earlier workers have contributed in understanding several aspects of Kaladgi basin including lithology, and structure.

Kaladgi Supergroup is divided into older Bagalkot and younger Badami Group of sediments separated by a distinct angular unconformity (Table 2.1). On the basis of the presence of a disconformity and a basal conglomerate unit, the Bagalkot Group is further subdivided into the Lokapur Subgroup and the Simikeri Subgroup. The underlying basement rocks in the south and south-western part of the basin comprises of Peninsular Gneiss and Chitradurga greenstone belt, while the north-eastern, eastern and south-eastern parts are dominated by Closepet granite and Hungund Kushtagi schist belt. The evolution of the Kaladgi–Badami Basin was controlled by movements along east–west-trending normal faults under an extensional stress regime. The deformation, upliftment and subsequent erosion of the Bagalkot Group were followed by the formation of new basinal areas hosting the Badami Group sediments (Vishwanathaiah, 1977). The Bagalkot Group consists mainly of quartzites, shales and limestones with an appreciable amount of stromatolitic dolomites and chert breccias. It is deformed into the east–west-trending elongated doubly plunging synclines and anticlines. The upper part of the succession (Badami Group) comprising of horizontal to gently dipping beds of arenites, shales and limestones is undeformed and unconformably overlies the Bagalkot group of sediments. At places, the Badami group of sediments directly overlie basement granitoids and Dharwar greenstone belts. The northern and western extension of the basin is



covered by the Deccan Trap. Several outliers surrounded by basement rocks and granitoid inliers are exposed at many places across the basin.

Table 2.1 Lithostratigraphy of Kaladgi Basin. *After Jayaprakash et al. (1987), Jayaprakash (2007).*

Supergroup	Group	Subgroup	Formation	Member	Thickness (m)	Sedimentary structures	Sedimentary environment
Kaladgi	Badami		Katageri	Konkankoppa Limestone	85	Profuse cross-bedding (tabular, trough and tangential), ripple marks, graded bedding, parting lamination, sandstone dykes and convolute lamination in Cave-Temple Arenite	Dominantly fluvial with subordinate lacustrine (Jayaprakash 2007; Mukhopadhyay et al. 2013)
				Halkurki Shale	67		
				Belikhindi Arenite	39		
			Kerur	Halgeri Shale	3		
				Cave-Temple Arenite	89		
				Kendur Conglomerate	3		
	----- <i>Angular unconformity</i> -----						
	Bagalkot	Simikeri	Hoskatti	Argillite	695	Cross-bedding (trough and tabular) and ripple marks (symmetrical and asymmetrical) in Muchkundi Quartzite	High-energy beach deposits grading upwards to tidal flats (Kale & Phansalkar 1991) with minor fluvial deposits (terrestrial fan; Jayaprakash 2007). Dominantly fluvial in the lower part of the Muchkundi Quartzite (Mukhopadhyay et al. 2013).
				Arlikatti	Lakshanhatti Dolomite		
			Kerkalmatti Ferruginous Member		42		
			Neralkeri Chert		39		
			Govindkoppa Argillite		80		
			Kundargi	Muchkundi Quartzite	182		
				Bevinmatti Conglomerate	15		

		----- <i>Disconformity</i> -----					
		Lokapur	Yadhalli	Argillite	58	Small- and large-scale cross-bedding (trough and tabular, at places herringbone type), symmetrical and asymmetrical ripple marks, mud and shrinkage cracks, graded bedding, crude parting lineation, rain prints and load casts in Saundatti Quartzite. Erosional parting surfaces and mud cracks in Manoli Argillite (Jayaprakash et al. 1987; George 1999; Jayaprakash 2007)	Transgressive beach and intertidal suite with minor fluvial deposits (terrestrial scree and fan deposits grading down slope into braided river sediments) at the base, grading upwards to cycles of alternating carbonate and muddy tidal flat deposits (Kale & Phansalkar 1991; Kale et al. 1996; Bose et al. 2008).
			Muddapur	Bamanbudni Dolomite	402		
				Petlur Limestone	121		
				Jalikatti Argillite	43		
			Yendigere	Nagnapur Dolomite	93		
				Chikkashellikere Limestone	883		
				Hebbal Argillite	166		
			Yargatti	Chitrabhanukot Dolomite	218		
				Muttalgeri Argillite	502		
			Malaprabha	Mahakut Chert	133		
				Manoli Argillite	61		
			Ramdurg	Saundatti Quartzite	383		
				Salgundi Conglomerate	31		
----- <i>Non-conformity</i> -----							
Archaean granitoids, gneisses and greenstone belt metavolcanic and metasedimentary rocks							

## **2.4 Mapping**

Geological mapping was undertaken over an area of 20 sq km. at a scale of 1:25000 to understand the major variation in lithology along Deshnur-Gujanal tract. Besides sedimentological studies, structural data was documented to provide supplementary information towards generating a comprehensive geological map of the area. Data plotting was done using AutoCAD® software (2020 student version).

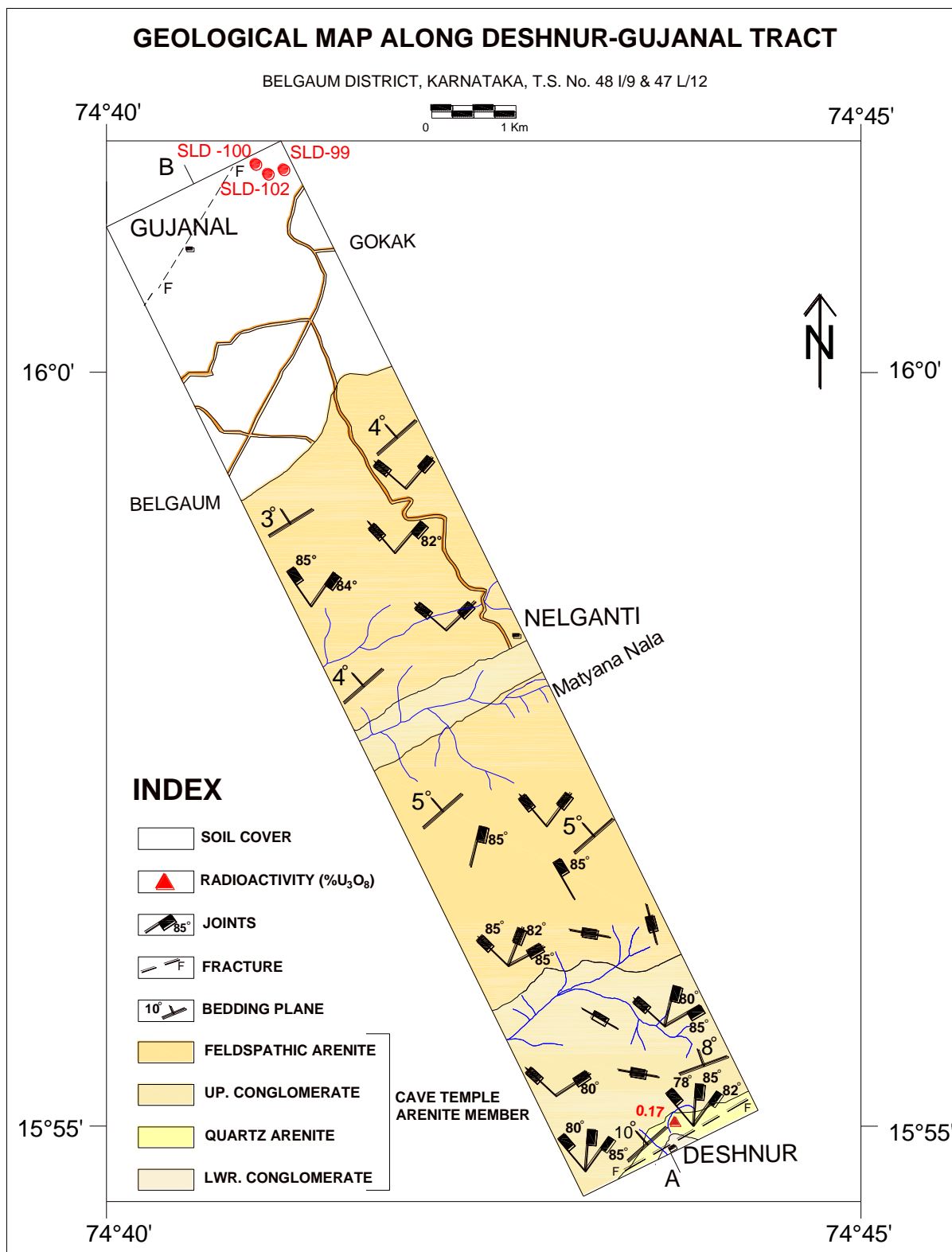


Figure 2.1 Geological map along Deshnur-Gujanal tract

### 3.4 Local geology

The study area (Fig. 2.1) exposes Cave Temple Arenite member of Badami Group of sediments along the Deshnur-Gujanal tract, unconformably overlies garnetiferous quartz-sericite-chlorite schist of Chitradurga Group. Badami sediments comprise low dipping (Fig. 2.2), alternate conglomerate and arenite sequences dissected by NW- SE, NE- SW and ESE-WNW trending faults/fracture zones. Stratigraphic succession corroborated with borehole data at the basin margin in Deshnur indicates three major sedimentary cycles starting with deposition of conglomerate and culminating with sandstone.

### 2.5 Badami sediments

- A. Basal conglomerate:** It is a polymictic, lensoid shape, clast supported conglomerate overlying the Chitradurga group of rocks with an average thickness of 5-10 m. It exhibits sharp contact with underlying basement and gradational contact with overlying sedimentary rocks. Poorly sorted framework grains of quartzite, vein-quartz, chert and Banded Iron Formation (BIF) set in arenaceous matrix defines the composition of the rock. Sub-angular to rounded clasts suggests some transportation before deposition. Ferruginous material is precipitated in interstitial spaces as cementing material indicates deposition under oxidizing conditions.
- B. Basal arenite:** It is fine to medium grained thinly laminated sandstone composed of mainly quartz and some lithic fragments with an average thickness of 10-20m. The grains are well-sorted and tightly packed with relatively less amount of feldspar.
- C. Lower conglomerate:** This lensoid conglomerate unit (80-100 m thick) is clast supported and polymictic in nature with grain size ranging from coarse sand to granule. Major framework grains constitute quartz, lithic fragments, chert, BIF and fresh as well as altered feldspars. Matrix component is dominated both by quartz and feldspars. The

intergranular spaces are filled with clayey material which is contributed by alteration of feldspars.

- D. Quartz arenite:** This tabular lithounit exhibits gradational contact with underlying lower conglomerate and overlying upper conglomerate. It consists of medium to fine grains of quartz and feldspar. Different sedimentary structures like ripple marks, planar and trough cross stratification (Fig. 2.3) ranging in size from 5 cm to 10 cm can be identified in outcrops exposed at basin margin in Deshnur area. It is observed that from lower to upper part feldspar content decreases, besides well good sorted quartz grains and their fine grain size indicates the influx of marine environment. Radioactivity was recorded in this unit (Fig. 2.4)
- E. Upper conglomerate:** This polymictic unit consisting of rounded to sub-rounded pebbles of vein quartz, quartzite, chert, jasper, Banded Hematite Jasper (BHJ) and Banded Hematite Quartz (BHQ) is clast supported in nature. Its average thickness is 60-170m (Fig. 2.5). This unit shows relatively less in feldspar content in comparison to Lower Conglomerate.
- F. Feldspathic arenite:** This top most unit overlying Upper conglomerate exhibit an average thickness of 5-45 m. Being exposed approximately 5 km interior from the basin margin this unit is relatively rich in feldspar content and display gritty appearance (Fig. 2.6).

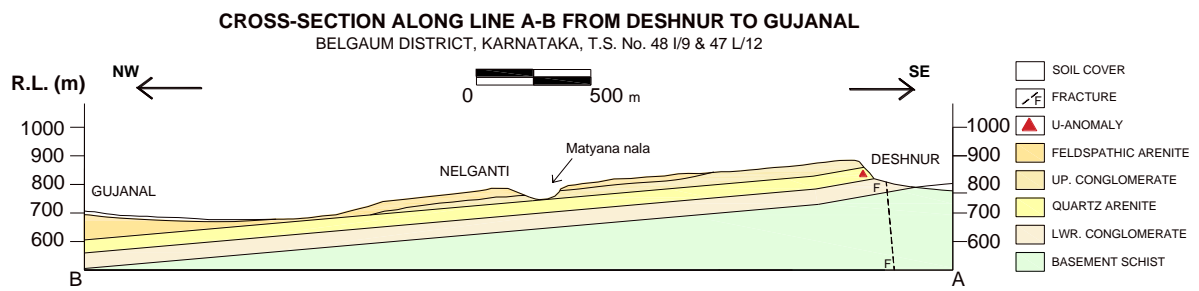


Figure 2.2 Geological cross section along Deshnur-Gujanal tract.

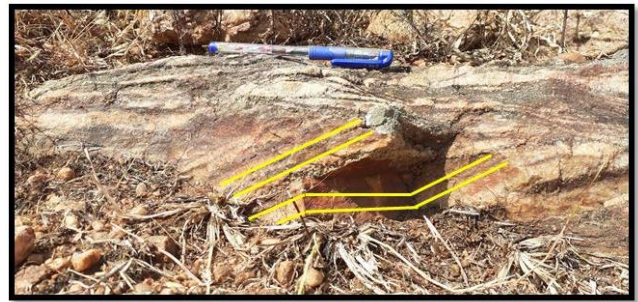
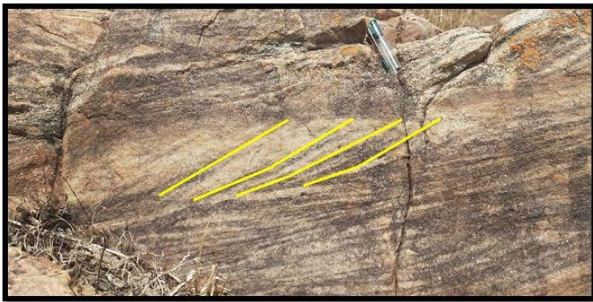


Figure 2.3 Planar cross bedding from Quartz arenite, Cave temple arenite member, Deshnur.



Figure 2.4 Radioactive, fine grained Quartz arenite, Cave temple arenite member, Deshnur.



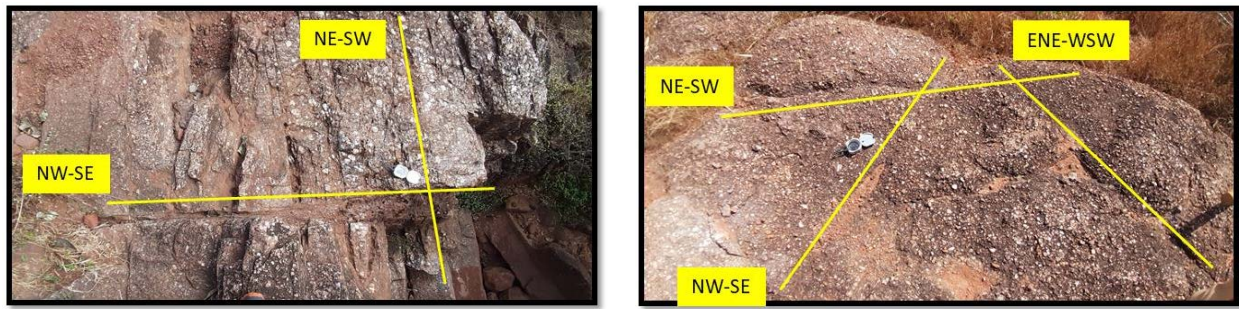


Figure 2.5 Upper conglomerate, displaying different fracture sets at Deshnur

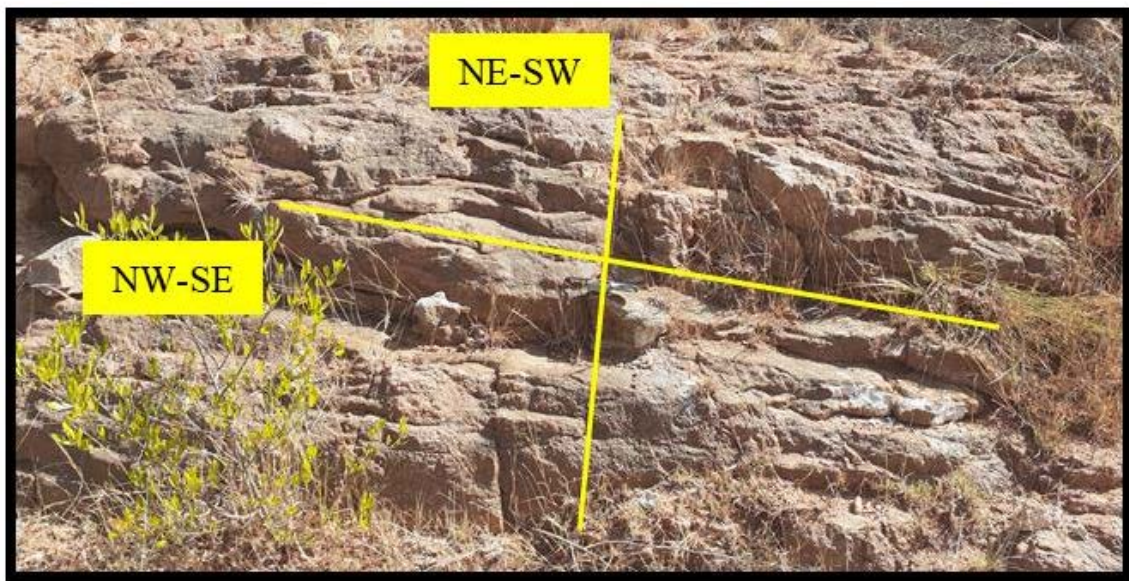


Figure 2.6 Gritty feldspathic arenite, Cave temple arenite member, Nelganti

## 2.6 Sedimentary structures

Badami sediments of Cave Temple Arenite exhibits three sedimentary cycles (Fig. 2.7). Conglomerate horizons are poorly sorted and lack imbrications. The arenite horizons display well developed stratification with quartz arenite accentuating good sorting and development of distinct planar and trough cross stratification structures. These sedimentary structures were further used to decipher the directional variability by the paleocurrent analysis.

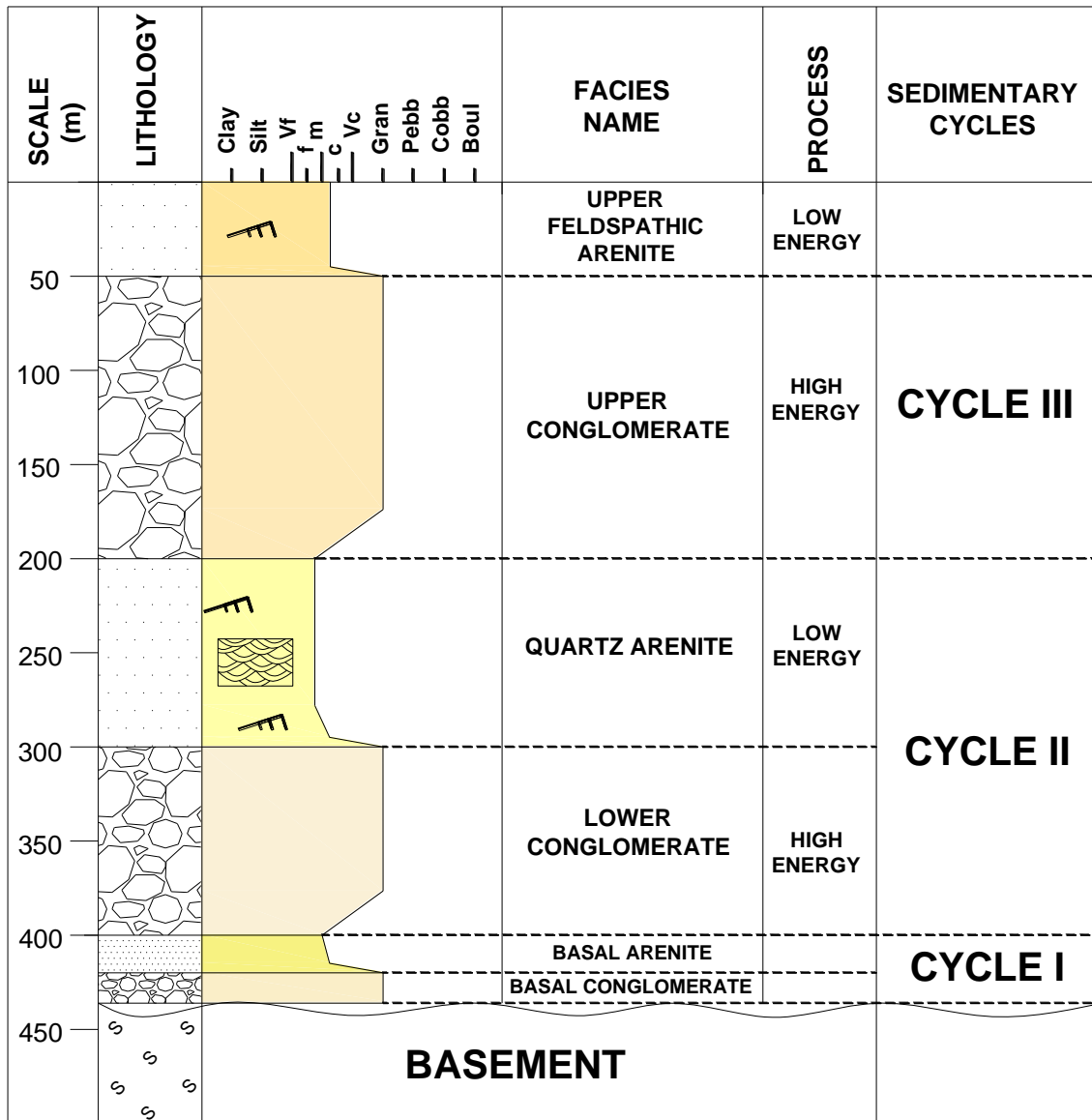


Figure 2.7 Lithosection representing three sedimentary cycles

## 2.7 Deformational structures

Badami sediments exposed in the study area strike  $060^{\circ}/10^{\circ} \rightarrow$  NW. The sediments along the basin margin at Deshnur, dip gently while further interior they maintain sub-horizontal disposition. As observed, high density of fracture sets in cover sediments are identified on basin margin trending in NE-SW, E-W and NNW-SE. However, two major fracture trends are seen to exhibit in basin interior, trending NE-SW and NNW-SSE. Rose

diagram representing the fracture set data is generated by plotting different fracture trends (Fig 2.8).

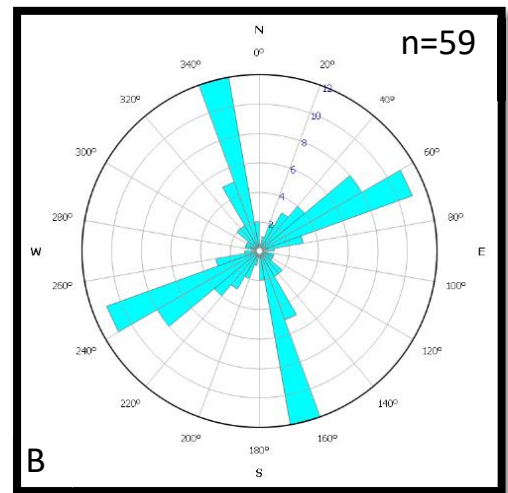
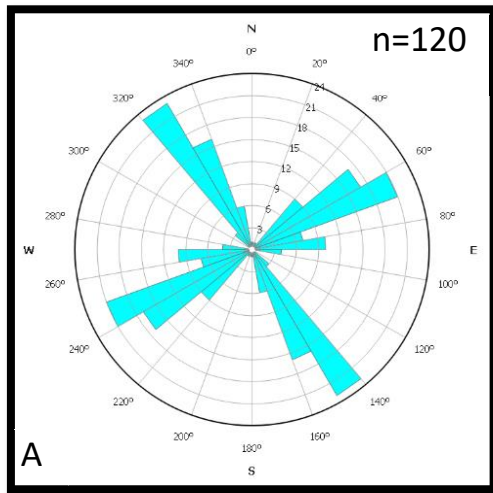


Figure 2.8 Rose diagram displaying fracture set data. Trends of prominent fracture affecting

A. Basin margin

B. Basin interior

## CHAPTER 3

### SEDIMENTOLOGICAL STUDIES

The Proterozoic Kaladgi is an intracratonic basins occurring over the Archaean Dharwar craton. It contains arenites, shales and carbonates with minor cherts and conglomerates deposited in continental, transitional and shallow-marine environments presumably during the late Paleoproterozoic/Mesoproterozoic to Neoproterozoic (Dey 2015). Badami Group of rocks is undeformed and unconformably overlies the older deformed succession of Bagalkot Group.

Detailed sedimentological studies include understanding of the process–product relationship, palaeogeographical interpretation and sequence stratigraphic analysis of the Kaladgi–Badami Basin, are less understood. The whole sedimentary package of the basin was deposited in at least three cycles bounded by unconformities. These cycles can tentatively be given depositional sequence status. Each cycle starts with local conglomerate and extensive arenite developed in a low stand system tract (when rate of sediment supply exceeded the rate of accommodation space) followed by repeated intercalations of shale and chemical precipitates (limestone, dolomite or chert) deposited under transgressive system tract (Dey 2015). The lower two cycles are represented by the Lokapur and Simikeri Subgroups (Bagalkot Group) whereas the Badami Group represents the uppermost one. The present study area in the western part of Kaladgi basin covers Cave Temple Arenite Member of Kerur Formation.

The sandstones and conglomerates of Cave Temple Arenite Member have been interpreted to be an expression of deposition under alluvial fan system grading into fluvial system (Ghosh *et al.* 2016). In total there are three major fluvial cycles identified which start

from conglomerate depositing in alluvial fan type deposit and culminating in sandstones deposited under braided fluvial system.

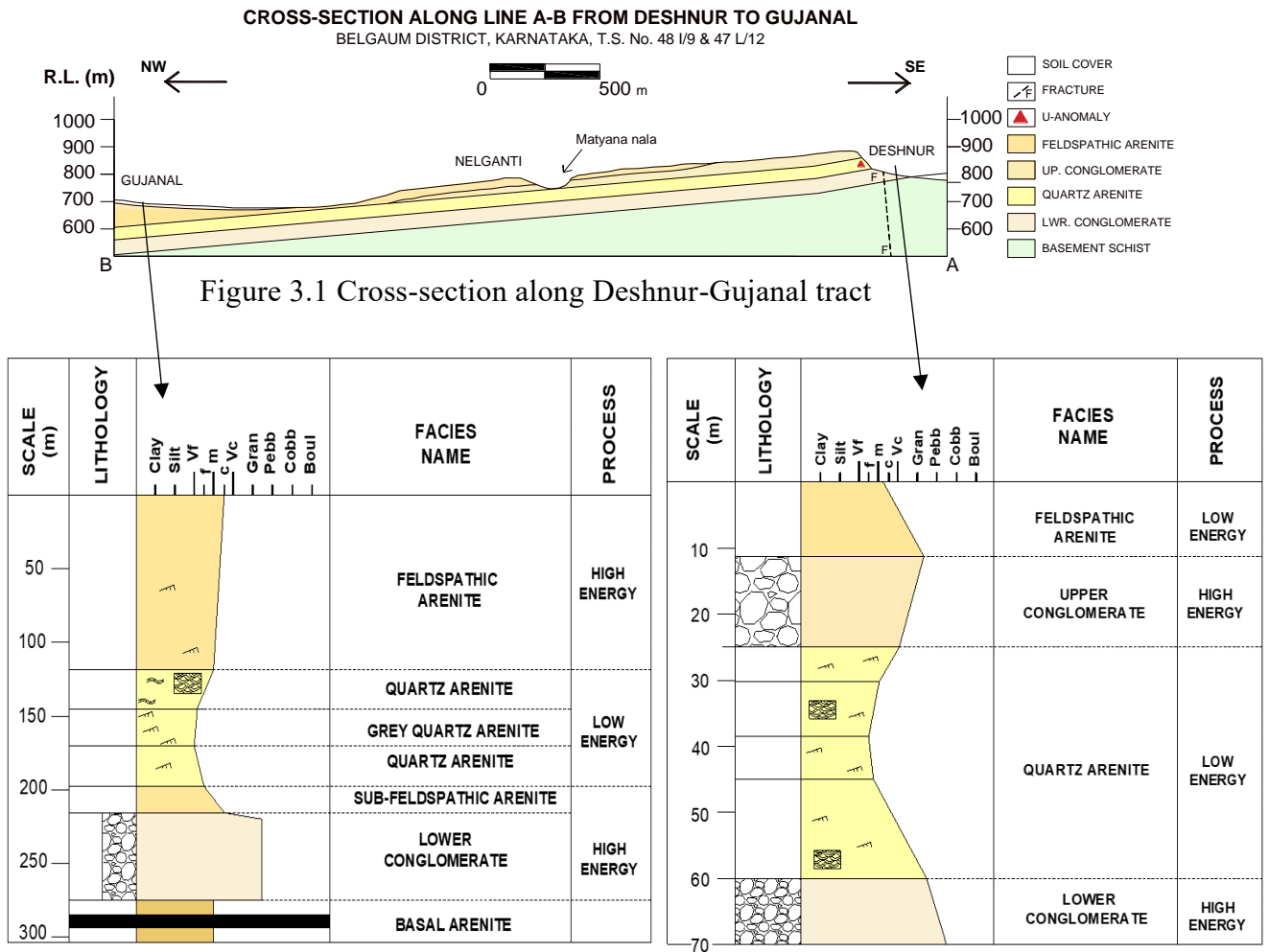
The exposed outcrops on basin margin at Deshnur show two fluvial cycles, starting from lower conglomerate followed by quartz arenite and upper conglomerate on top. The upper conglomerate is indicative of fan type deposit, grading into upper feldspathic arenite near Nelganti. Borehole data was used in Gujanal to understand the depositional system and thereby deciphering the geological environment of deposition.

Sedimentological studies were conducted on available outcrops at basin margin in Deshnur and borehole cores drilled at Gujanal. Based on field observations 3 main sedimentary cycles have been identified, starting from conglomerate and culminating with arenite however, the second cycle fluvial cycle gives way to marine cycle separated by transitional fluvio-marine cycle. A total of three boreholes (18 km NNW of basin margin at Deshnur) had been taken up for study, of which 2 (SLD-100 and SLD-102) have been reported with mineralization in pebbly feldspathic arenite/lower conglomerate. The third borehole, SLD-99 is a vertical borehole and was used to carry out the lithofacies analyses. The mineralized boreholes, with primary focus on host rock of mineralization viz. lower conglomerate were exhaustively studied to understand the nature of occurrence and control of uranium mineralization in the study area.

### **3.1 Sedimentary logs**

Stratigraphic succession at basin margin, exposes repeated sedimentary cycles of conglomerate and arenite of Cave Temple Arenite Member. Sedimentary beds are generally trending NE-SW with 8-10° degree dip in NW direction along the basin margin which gradually grades into sub horizontally dipping beds at interior of the basin.

Detailed sedimentary logs were prepared across sections from surface outcrops exposed at basin margin in Deshnur and vertical borehole (SLD-99) drilled near Gujanal. An attempt was made to mark the spatial continuity of lithounits thereby displaying the stratigraphic disposition of beds (Fig.3.1).



Litholog prepared from borehole SLD-99

Litholog prepared from vertical section Deshnur

The succession in Deshnur exposes well sorted medium to fine grained, hard and compact quartz arenite sandwiched between underlying matrix supported, polymictic lower conglomerate and overlying ill-sorted polymictic, clast supported upper conglomerate. The topmost unit feldspathic arenite is not exposed at basin margin and can only be mapped, where the upper conglomerate unit grades into feldspathic arenite near Nelganti at Matyana nala.

### **3.2 Lithofacies analysis**

Sedimentary facies refer to the sum of the characteristics of a sedimentary unit. These characteristics include its color, dimensions, sedimentary structures, grain size and types and biogenic character. For example, a 'cross bedded medium sandstone' would be a rock consisting mainly of sand grains of medium grade and exhibiting cross-bedding as the primary sedimentary structure. If the description is confined to the physical and chemical characteristics of a rock this is referred to as the lithofacies. However, if the description is confined to flora and fauna or trace fossils of a given rock, it is referred to as biofacies and ichnofacies respectively (Nichols, 2009). The different facies form a facies association that reflects the depositional environment.

Lithofacies analyses were undertaken in a vertical borehole section of SLD-99. Each sedimentary cycle is associated with a set of lithofacies. Due to limited surface exposures in study area, careful observation was made from borehole drill cores and different lithofacies were identified in each cycle. Along the basin margin these sedimentary cycles are having clasts sizes of 1cm to 4 cm with coarse grained, immature, angular to sub angular nature of clasts, while in the distal facies towards the center of the basin, the clasts sizes are reduced to 2 mm to 10 mm sizes, showing mature, sub-rounded. to rounded nature, mainly matrix supported pebbly conglomerate and feldspathic arenite.

#### **Cycle I**

Cycle I consist of 10-20 m thick Basal conglomerate and Basal arenite, directly overlying the quartz sericite schist of underlying Chitradurga group of rocks. Basal conglomerate is clast supported and consist of sub-angular to angular clasts of quartz, chert, jasper and BHQ. The borehole data indicates only 5-10 m of thickness of the unit. The



overlying Basal arenite only intercepted in boreholes consist of framework grains of quartz and feldspar, with variable thickness between 5-10 m. Facies encountered in Cycle I:

1. **Clast supported conglomerate (Facies A)** – Clast supported, polymictic, poorly sorted sub rounded to angular clasts of quartz, feldspar, chert, jasper with average grain size of 2 mm. Generally overlain by matrix supported conglomerate.

**Interpretation:** Driven by high velocity flow with in channels, designated as channel lags by Allen (1982).

## **Cycle II**

Cycle II consists of pebbly feldspathic arenite/lower conglomerate (100-130 m) and quartz arenite (80-100 m) units. Pebbly feldspathic arenite/Lower conglomerate unit representing the second major depositional cycle is the major host of uranium mineralization intercepted in both Deshnur as well as Gujanal exploration blocks. This particular litho-unit comprising of feldspar clast rich conglomerate is far from being a thick and homogenous conglomerate horizon as conceived from exploration terminology, it comprises of more than 30 channel fill cycles starting from conglomerate and culminating with thin shale bands. Small sub-cycles of conglomerate and sub-feldspathic arenite also present. The channel fills are smallest of larger sedimentary packages, which records filling of major channels during channel avulsion and abandonment (Miall 2014). Lateral as well as vertical juxtaposition of channel fills as well as flood plains give way to channel belts. The largest of these genetically related packages are valley fill cycles demarcated by largest order of bounding surfaces, equivalent to basin-wide unconformities. Facies encountered within pebbly feldspathic arenite/lower conglomerate unit:

1. **Matrix supported conglomerate (Facies B)** – Greyish to whitish colored, poorly sorted, matrix supported, composed of framework grains of Quartz and feldspar with



chert and jasper present in minor amounts. This unit is generally overlain by cross-stratified pebbly sandstone.

**Interpretation:** Debris flow deposits

2. **Cross-stratified pebbly sandstone (Facies C)** – Grey to brown colored, poorly sorted sandstone, containing bimodal distribution and floating grains of pebble size of Quartz and feldspars. This unit is intercalated by alternate silty-shale intercalations. These facies transform as medium to coarse sandstone occurring with rare oversized pebbles up the core. It is white to brownish in color, oxidized with reduced patches in places with well-developed cross stratification. Intermediate green clay intercalations also observed with reduced frequency.

**Interpretation:** Channel fill sandy transverse bars.

3. **Thinly laminated silty-shale intercalations (Facies D)** – Green to purple silty-shale intercalations, occurring abruptly as intercalation in cross-stratified pebbly sandstone. Over bank or waning flood deposits. Frequent reoccurrence of thinly laminated non-cohesive silt/clay layers/partings in the sequence may be due to quick mobilization of finer material from the channel-cut banks during flash-floods which due to lack of land plants during Proterozoic (Miall, 1980).
4. **Trough cross-stratified sub-feldspathic arenite (Facies E)** – White to brownish, oxidized with reduced patches in places with well-developed cross laminations. Coarse sand-sized with rare oversized pebbles. Intermediate green clay intercalations also observed.

**Interpretation:** Thoroughly trough cross-stratified nature manifests dune migration along the channel floor at the upper level of the lower flow regime (e.g., Miall 1985, 1988; Hadlari et al. 2006; Sambrook Smith et al. 2006; Sarkar et al. 2012)

Pebbly feldspathic arenite grades into quartz arenite unit, which is marked by rounded and well sorted grains with less matrix and high maturity, thereby indicating deposition under relatively low energy conditions and increasing sea influence. Quartz arenite unit encompasses a hard and compact, medium to fine grained and reduced in nature with oxidized patches, Grey quartz arenite. This unit is marked by influence of marine conditions, sandwiched between quartz arenite units signifying fluvial-marine transition. Presence of black shale and sulphides along So plane is indicative of reducing environmental conditions at the time of deposition. Presence of penecontemporaneous deformation along the intercalations of black shale and silt can be observed in the core. Facies encountered within Quartz arenite unit:

1. **Tabular cross stratified quartz arenite (Facies F)** – Hard and compact, tabular body geometry with sharp and planar upper and lower boundaries. Medium to fine size, well sorted grains of Quartz.

**Interpretation:** Planar cross bedding is produced by downstream migration of two dimensional bedforms under the influence of current.

2. **Trough cross stratified quartz arenite (Facies G)** – Greyish to brownish white in colour cross bedded unit, consisting of medium to coarse grains of quartz and very less amount (<5%) of feldspar.

**Interpretation:** Thoroughly trough cross-stratified nature manifests dune migration along the channel floor at the upper level of the lower flow regime (e.g., Miall 1985, 1988; Hadlari et al. 2006; Sambrook Smith et al. 2006; Sarkar et al. 2012).

3. **Wavy parallel laminated shale (Facies H)** – Thinly laminated black shale beds occurring as intercalations in Grey quartz arenite. Sulphides are present along So planes. This facies grades into thinly laminated intercalations of silt and shale, affected by penecontemporaneously deformed laminations.

**Interpretation:** Anoxic conditions indicating marine influx.

Due to density contrast, silt sized grain loaded on the surface of thinly laminated clay layers, very shortly after deposition and before consolidation of sediment.

### **Cycle III**

The quartz arenite unit grades into third and topmost fluvial cycle starting from Upper Conglomerate. The upper conglomerate unit is well exposed in basin margin at Deshnur. However, it grades into feldspathic arenite near Nelganti. As shown above (Fig. 9) in litholog created for correlation between lithounits at Deshnur and Gujanal, the quartz arenite unit of Cycle II, is directly overlain by feldspathic arenite in Gujanal. This unit marks the topmost unit of the litho-column. The grains are medium to coarse, with pitted appearances invariably and intercalated conglomerate horizons. Facies encountered at surface outcrops in Deshnur and borehole core in Gujanal are:

1. **Clast supported conglomerate (Facies I)** – This lithounit is ill-sorted, polymictic clast supported conglomerate consisting majorly of quartz, feldspar, chert and jasper. It is distinguished from Facies A in the sense, that it contains less feldspar content.

**Interpretation:** Debris flow deposits.

2. **Trough cross stratified feldspathic arenite (Facies J)** – Greyish to brownish white in color trough cross bedded unit, consisting of medium to coarse grains of quartz and high amount of feldspar. This unit is invariably pitted in nature, indicating removal of feldspars due to alteration.

**Interpretation:** Thoroughly trough cross-stratified nature manifests dune migration along the channel floor at the upper level of the lower flow regime (e.g., Miall 1985, 1988; Hadlari et al. 2006; Sambrook Smith et al. 2006; Sarkar et al. 2012).

Table 3.1 Facies encountered within Cave Temple Arenite Member of Badami

<b>Facies</b>	<b>Description</b>	<b>Interpretation</b>
Clast supported conglomerate (Facies A)	Clast supported, polymictic, poorly sorted sub rounded to angular clasts of Quartz, feldspar, chert, jasper with average grain size of 2 mm. Generally overlain by matrix supported conglomerate.	Driven by high velocity flow within channels, designated as channel lags by Allen (1982)
Matrix supported conglomerate (Facies B)	Greyish to whitish colored, poorly sorted, matrix supported, composed of framework grains of Quartz and feldspar with chert and jasper present in minor amounts. This unit is generally overlain by cross-stratified pebbly sandstone.	Debris flow deposits
Cross-stratified pebbly sandstone (Facies C)	Grey to brown colored, poorly sorted sandstone, containing bimodal distribution and floating grains of pebble size of Quartz and feldspars. This unit is intercalated by alternate silty-shale intercalations.  These facies transform as medium to coarse sandstone occurring with rare oversized pebbles up the core. It is white to brownish in color, oxidized with reduced patches in places with well-developed cross stratification.	Channel fill sandy transverse bars.

	Intermediate green clay intercalations also observed with reduced frequency.	
Thinly laminated silty-shale intercalations  (Facies D)	Green to purple silty-shale intercalations, occurring abruptly as intercalation in cross-stratified pebbly sandstone.	Over bank or waning flood deposits. Frequent reoccurrence of thinly laminated non-cohesive silt/clay layers/partings in the sequence may be due to quick mobilization of finer material from the channel-cut banks during flash-floods which due to lack of land plants during Proterozoic times (Miall, 1980).

Trough cross-stratified sub-feldspathic arenite  (Facies E)	White to brownish, oxidized with reduced patches in places with well-developed cross laminations. Coarse sand-sized with rare oversized pebbles. Intermediate green clay intercalations also observed.	Thoroughly trough cross-stratified nature manifests dune migration along the channel floor at the upper level of the lower flow regime (e.g., Miall 1985, 1988; Hadlari et al. 2006; Sambrook Smith et al. 2006; Sarkar et al. 2012).
Tabular cross stratified quartz arenite. (Facies F)	Hard and compact, tabular body geometry with sharp and planar upper and lower boundaries. Medium to fine size, well sorted grains of Quartz	Planar cross bedding is produced by downstream migration of two dimensional bedforms under the influence of current.
Trough cross stratified quartz arenite (Facies G)	Greyish to brownish white in colour cross bedded unit, consisting of medium to coarse grains of quartz and very less amount (<5%) of feldspar.	Thoroughly trough cross-stratified nature manifests dune migration along the channel floor at the upper level of the lower flow regime (e.g., Miall 1985, 1988; Hadlari et al. 2006; Sambrook Smith et al. 2006; Sarkar et al. 2012).

Wavy parallel laminated shale  (Facies H)	Thinly laminated black shale beds occurring as intercalations in Grey quartz arenite. Sulphides are present along So planes.  This facies grades into thinly laminated intercalations of silt and shale, affected by penecontemporaneously deformed laminations.	Anoxic conditions indicating marine influx.  Due to density contrast, silt sized grain loaded on the surface of thinly laminated clay layers, very shortly after deposition and before consolidation of sediment.
Clast supported conglomerate (Facies I)	This lithounit is ill-sorted, polymictic clast supported conglomerate consisting majorly of quartz, feldspar, chert and jasper. It is distinguished from Facies A in the sense, that it contains less feldspar content.	Debris flow deposits
Trough cross stratified feldspathic arenite (Facies J)	Greyish to brownish white in colour trough cross bedded unit, consisting of medium to coarse grains of quartz and high amount of feldspar. This unit is invariably pitted in nature, indicating removal of feldspars due to alteration.	Thoroughly trough cross-stratified nature manifests dune migration along the channel floor at the upper level of the lower flow regime (e.g., Miall 1985, 1988; Hadlari et al. 2006; Sambrook Smith et al. 2006; Sarkar et al. 2012).



a



b



c



d



e





f



g

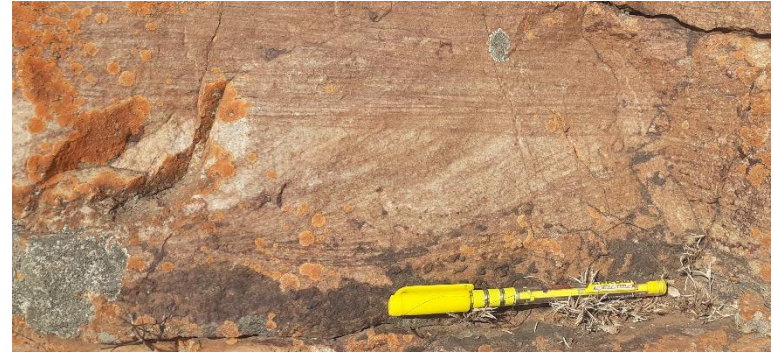


h

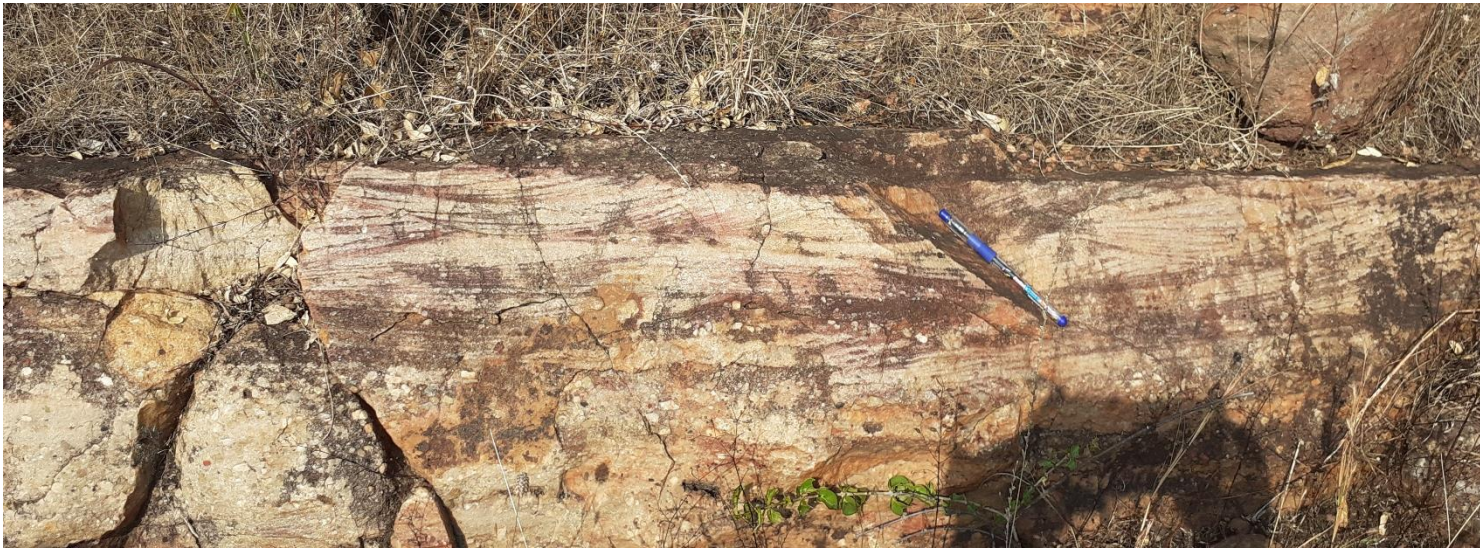




k



l



m





n



p



o



q



r





s



t



u

**Figure 3.2** a) Lithofacies A - Clast supported conglomerate; b) Lithofacies B - Matrix supported conglomerate; c, d) Lithofacies C - Cross-stratified pebbly sandstone; e) Lithofacies D - Thinly laminated silty-shale intercalations; f) Lithofacies E - Trough cross-stratified sub-feldspathic arenite; g, h) Lithofacies F - Tabular cross stratified quartz arenite; i, j, k, l, m) Lithofacies G - Trough cross stratified quartz arenite; n, o, p) Lithofacies H - Wavy parallel laminated shale; q, r, s) Lithofacies I - Clast supported conglomerate; t, u) Lithofacies J - Trough cross stratified feldspathic arenite.

### 3.3 Paleocurrent analysis

Paleocurrent analysis involves using the primary sedimentary structures, to determine direction of flow or orientation of flow of a stream or group of streams within a basin. Individual sedimentary structures indicate the flow direction at that geographic point and at that instant in time. In order to solve a true regional scale problem, a statistical analysis of a collective average of the current directions within a region over a period of time is essential (Boggs, 1995). Primary sedimentary structures like asymmetric ripples, trough cross bedding, tool marks and parting lineation provide sufficient information to decipher palaeoflow direction.

Extensive systematic paleocurrent data was collected from Cave Temple Arenite member to understand the directional variability in fluvial system. Due to lack of surface exposures in the study area, outcrops available at basin margin in Deshnur were taken up for paleocurrent analysis. Cross bedding data were collected from the quartz arenite units containing well preserved trough and planar cross beds (Fig. 3.3) for paleocurrent flow direction. The poorly-sorted clasts, in the overlying upper conglomerate exposed in basin margin are a product of debris flow unit thereby lacking imbrication.

Paleocurrent readings were recorded from cross-beds. The true dip direction of planes cannot be determined from a single vertical face (faces A or B), hence, two different apparent dip measurements were used to calculate the true dip and dip direction. Readings were also recorded from the topsets of trough cross beds wherever exposed. Data if collected from folded or tilted beds must be corrected, in order to restore bedding to its original horizontal position. However, gently dipping beds in basin margin at Deshnur, did not require any correction.

A total number of 65 cross bedding azimuths were recorded. When measurements of structures which show direction of movement are plotted, the rose diagram indicates the

direction towards which the current moved (Fig. 3.4). The distribution is clearly unimodal as all the bearings are in the NW quadrant, with 344° as vector mean. It reveals that sediment was transported from the source in SE to NW direction during the deposition of Cave temple arenite member.

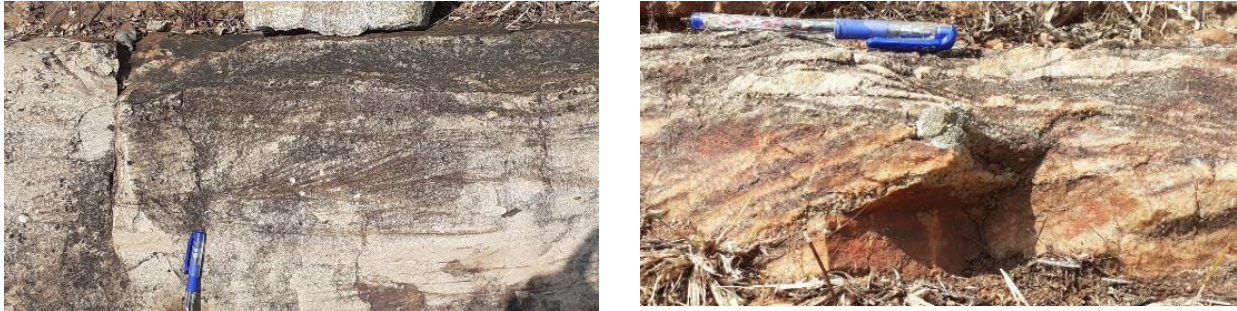


Figure 3.3 Well preserved trough and planar cross beds

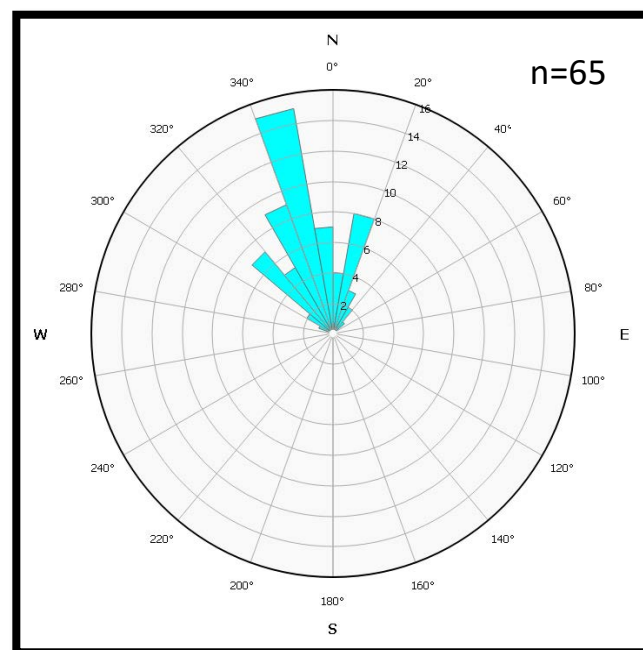


Figure 3.4 Paleocurrent direction in basin margin

### 3.4 Depositional Setting

The study area is marked by three fluvial cycles, wherein majorly two cycles are invariably present. The upper conglomerate unit as part of third cycle grades into upper feldspathic arenite, near Nelganti along Deshnur-Gujanal tract and is defined by the topmost brown colored feldspathic arenite unit (Fig. 3.5) consisting of framework grains of quartz



and feldspar. The grains are medium to coarse; sub-rounded to angular with moderate to poor sorting indicating high energy fluvial environment. However, some intercalations of gritty/conglomeratic bands and silty-shale intercalations (Fig.3.6) indicate fluctuation between high and low energy conditions. The decrease in grain size with increasing depth, complimented by increase in sorting and roundness, indicate high maturity and relatively low energy depositional conditions. Small intercalations of quartz arenite (Fig. 3.7) are also observed in feldspathic arenite indicating the transitional environment wherein marine influence is increases. This is further substantiated by the presence of grey quartz arenite with intercalations of glauconite bearing grey and black shale indicating the presence of marginal marine depositional setting. The presence of sulphides along the So planes (Fig. 3.8) in black shale, indicates anoxic environment during deposition. This lithounit is followed by pebbly feldspathic arenite/lower conglomerate, separated by sub-feldspathic arenite occurring as a transition towards higher energy fluvial conditions. This lithounit is marked by ~30 cycles of alternate gravel and sandy bars, culminating with shale beds on top.



Figure 3.5 Feldspathic arenite; a) cross-stratification, b) ferruginisation along fracture plane c) gritty feldspar and quartz grains.



Figure 3.6 Intercalations of conglomerate and silty-shale horizons



Figure 3.7 Quartz arenite



Figure 3.8 Sulphides along  $S_0$  plane within black shale



### 3.5 Uranium mineralization

Exploration activities in Deshnur and Gujanal has led to delineation of signification sub-surface correlatable mineralization in both the areas. Uranium mineralization is mainly hosted by feldspar clast rich conglomerate and pebbly feldspathic arenite confined to bedding planes. The mineralized pebbly feldspathic arenite/lower conglomerate unit has been extensively covered from boreholes SLD-99, SLD-100 and SLD-102, wherein SLD-99 was used to map the number of small sedimentary channel fill cycles and SLD-100 and SLD-102 were categorically used to correlated the grain size control with uranium mineralization.

Borehole SLD-99, represents an approximately 80m thick lower feldspar clast rich conglomerate succession comprising of 26 channel fill cycles (Fig. 3.9) starting with matrix supported conglomerate (Facies B), grading into pebbly feldspathic arenite (Facies C) and ending with thinly laminated silty-shale intercalations (Facies D). In some instances, silty-shale bands can be observed as intercalations in conglomerate units (Fig.3.10). Thickness of a channel fill cycle ranges from 30 cm to 4 meters with shale bands ranging in thickness from 2 to 15 cm. For proper representation, the end of each cycle has been marked with a dashed line. Sc here represents smaller sub-cycles of matrix supported conglomerate (Facies B) and trough cross stratified sub-feldspathic arenite (Facies E).

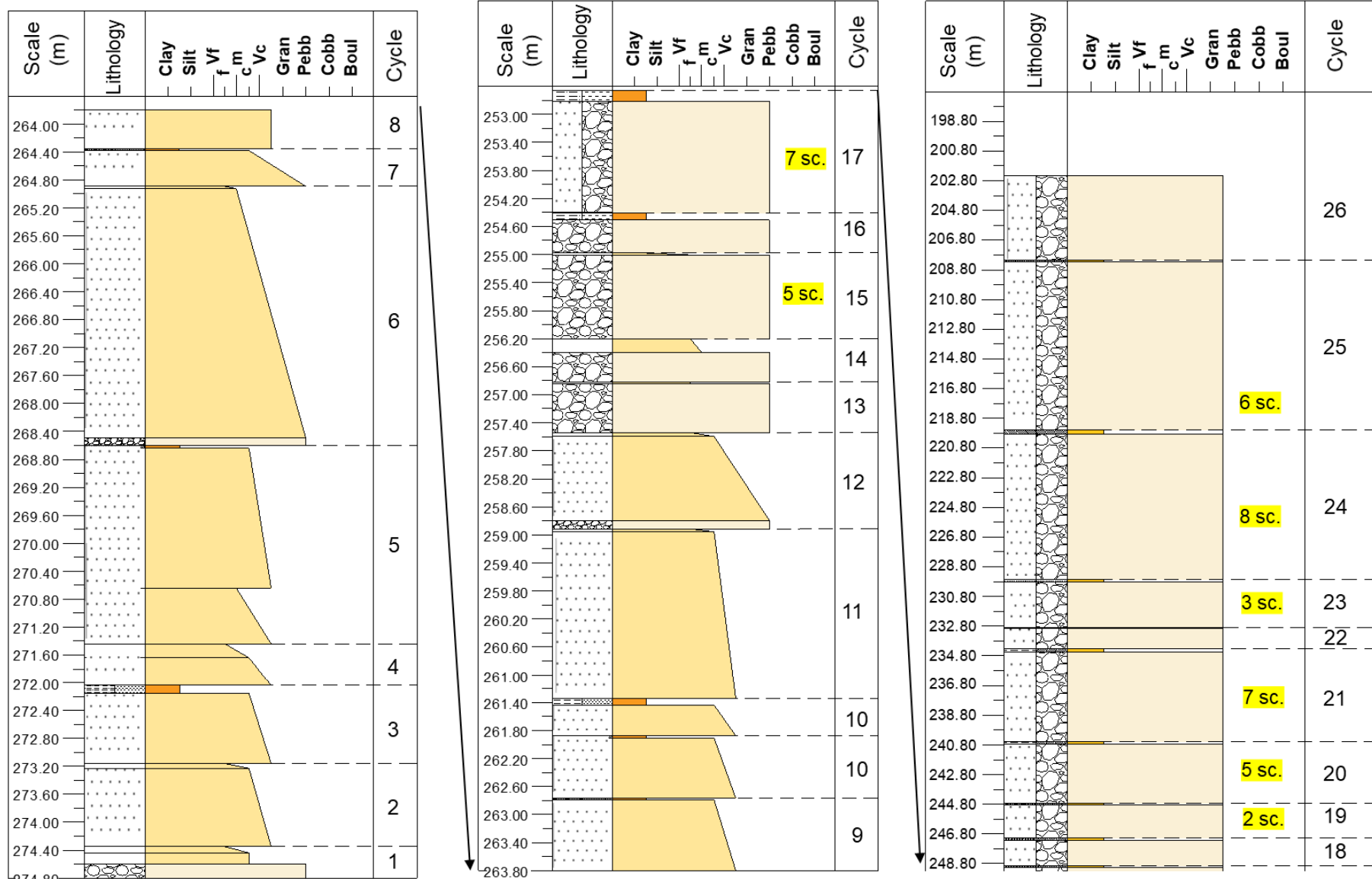


Figure 3.9 Detailed lithology of pebbly feldspathic arenite/lower conglomerate unit from borehole SLD-99



Figure 3.10 Silty shale intercalations in pebbly feldspathic arenite/lower conglomerate

Radioactive horizons of mineralized boreholes SLD-100 and 102 were also taken up for detailed lithofacies studies to understand the nature of occurrence of uranium mineralization. SLD-100 is a vertical borehole drilled in Suldhal-Gujanal block. The lower conglomerate unit in this borehole is 122 m thick. Radioactivity has been reported in 6 lenses in over 40m thick horizon, with each lens ranging in thickness from 1-3 m. Mineralization is identified in lenses between 150 m to 190 m depth with RL 461 and 507 m represented by channel fill cycle from 11 to 13. Mineralized lenses identified in 40 m thick horizon have been highlighted against the core assay data (Fig. 3.11 (i), (ii), (iii)) for representing mineralization and associated lithounit.

The pebbly feldspathic arenite/lower conglomerate unit is highly fractured and altered at places. The fracture planes are 30-40° and sub-parallel to parallel at places. Bedding plane vary between 70 to 90° with respect to core axis. Mineralization is identified in reduced and altered fractured horizons and along the intercalations of shale bands with conglomerate, associated with disseminated sulphides.

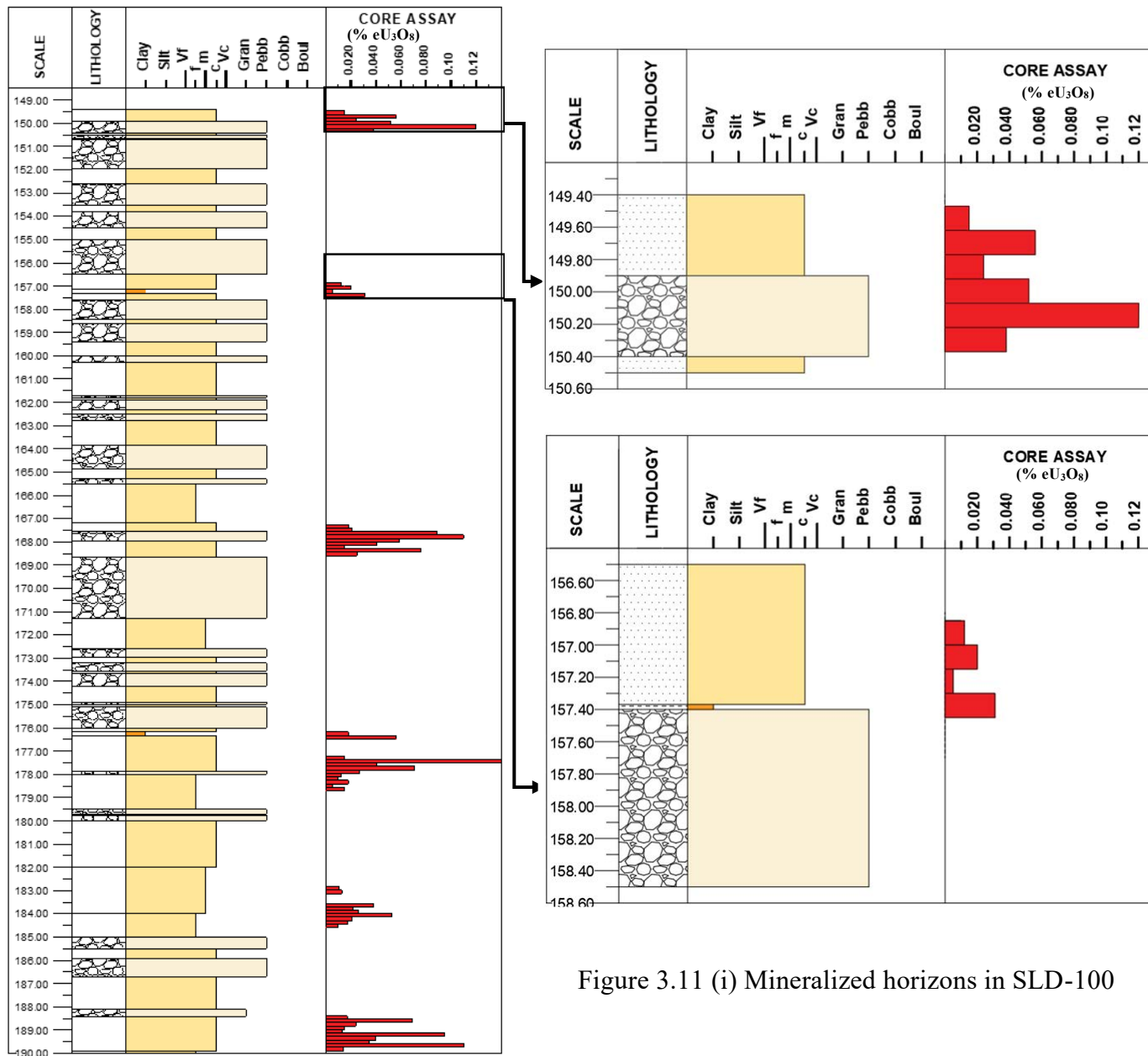
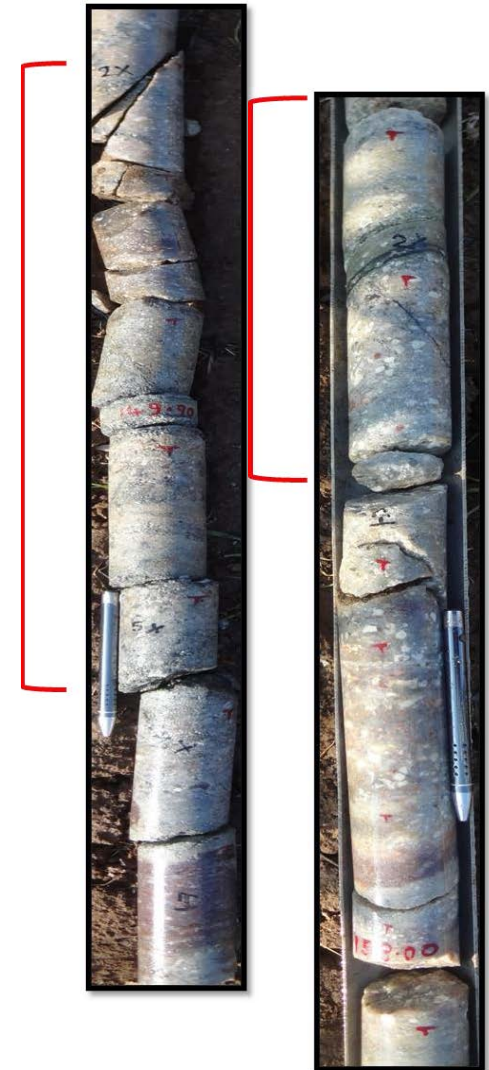


Figure 3.11 (i) Mineralized horizons in SLD-100



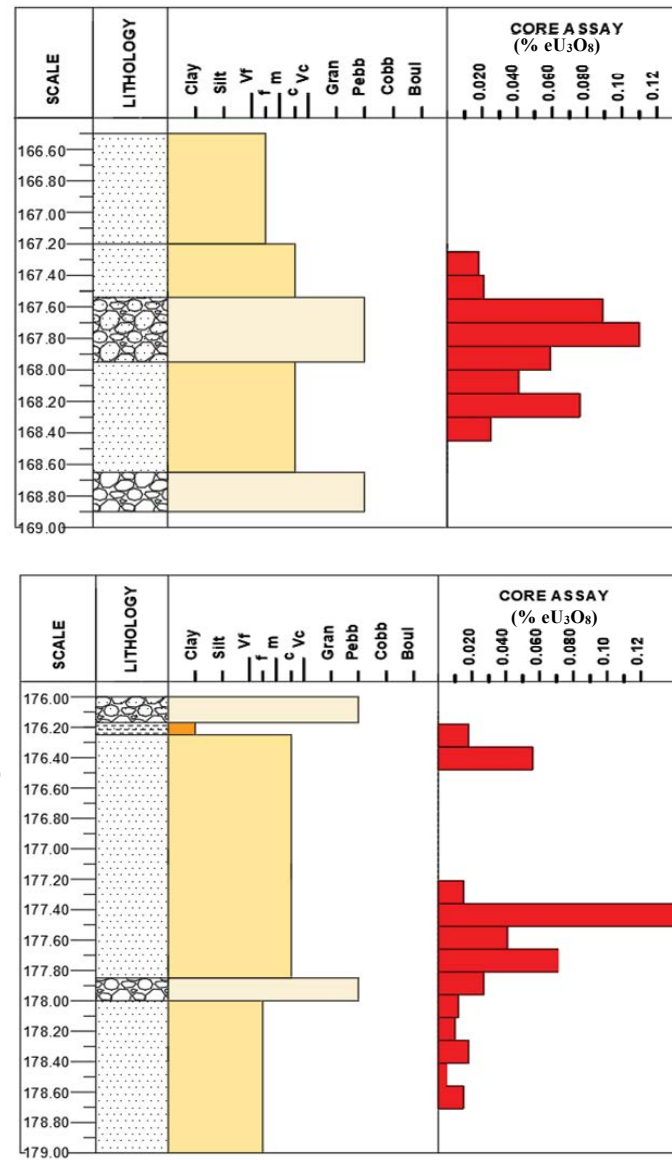
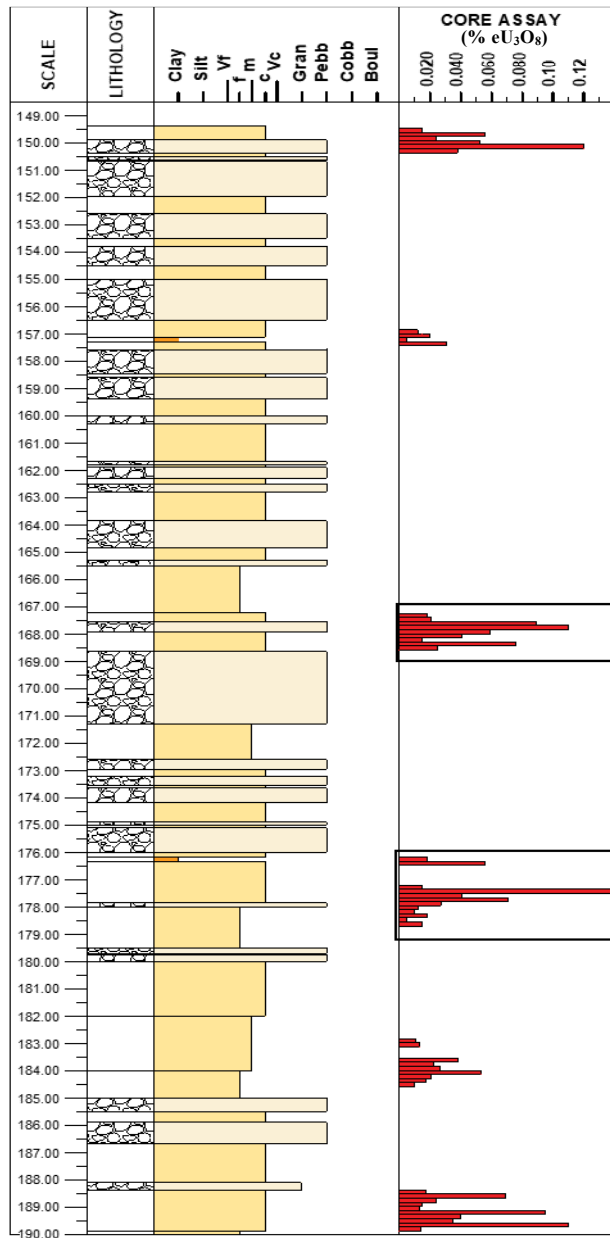
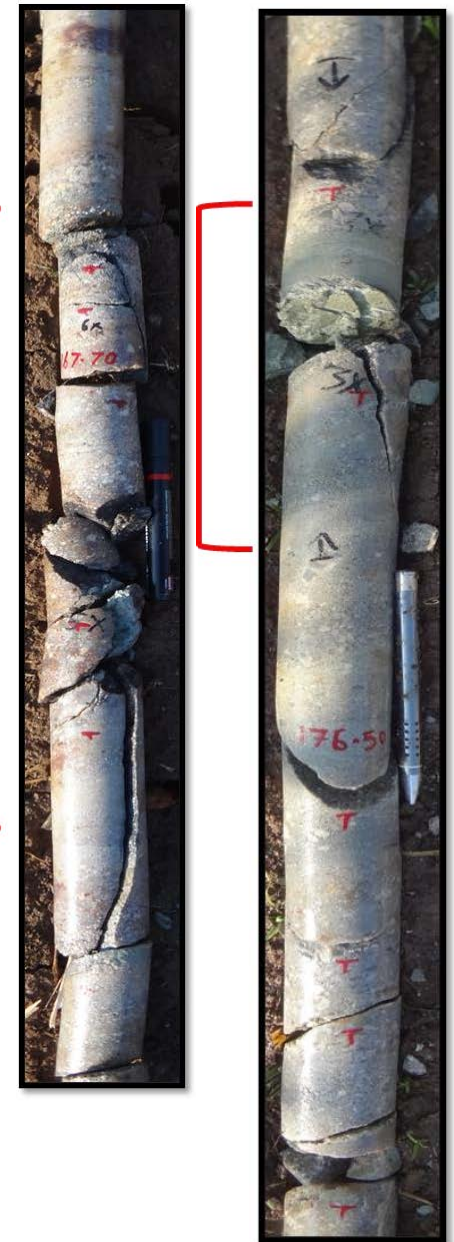


Figure 3.11 (ii) Mineralized horizons in SLD-100





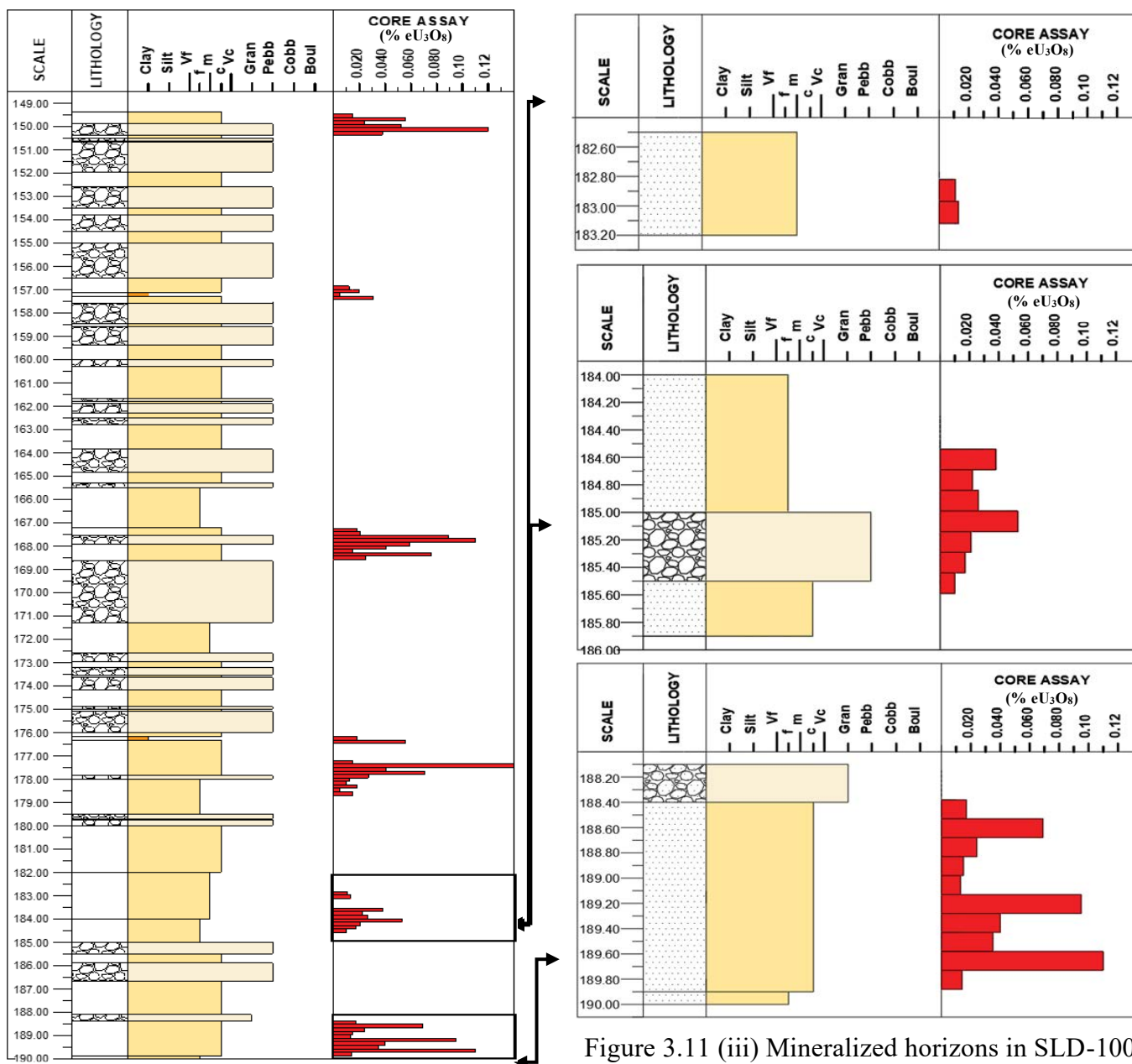


Figure 3.11 (iii) Mineralized horizons in SLD-100

SLD-102 is an inclined borehole drilled in Suldhah-Gujanal block with an inclination of 75° towards N30°W. Major mineralization has been intercepted in ~5 m thick horizon between 180 to 185.40 m. Mineralized horizons are intercepted between RL – 476 to 481 m and channel fill cycle number 26 to 30 in pebbly feldspathic arenite/Lower conglomerate unit. Mineralized lenses identified in 5 m thick horizon have been highlighted against the core assay data (Fig. 3.12) for representing mineralization and associated lithounit.

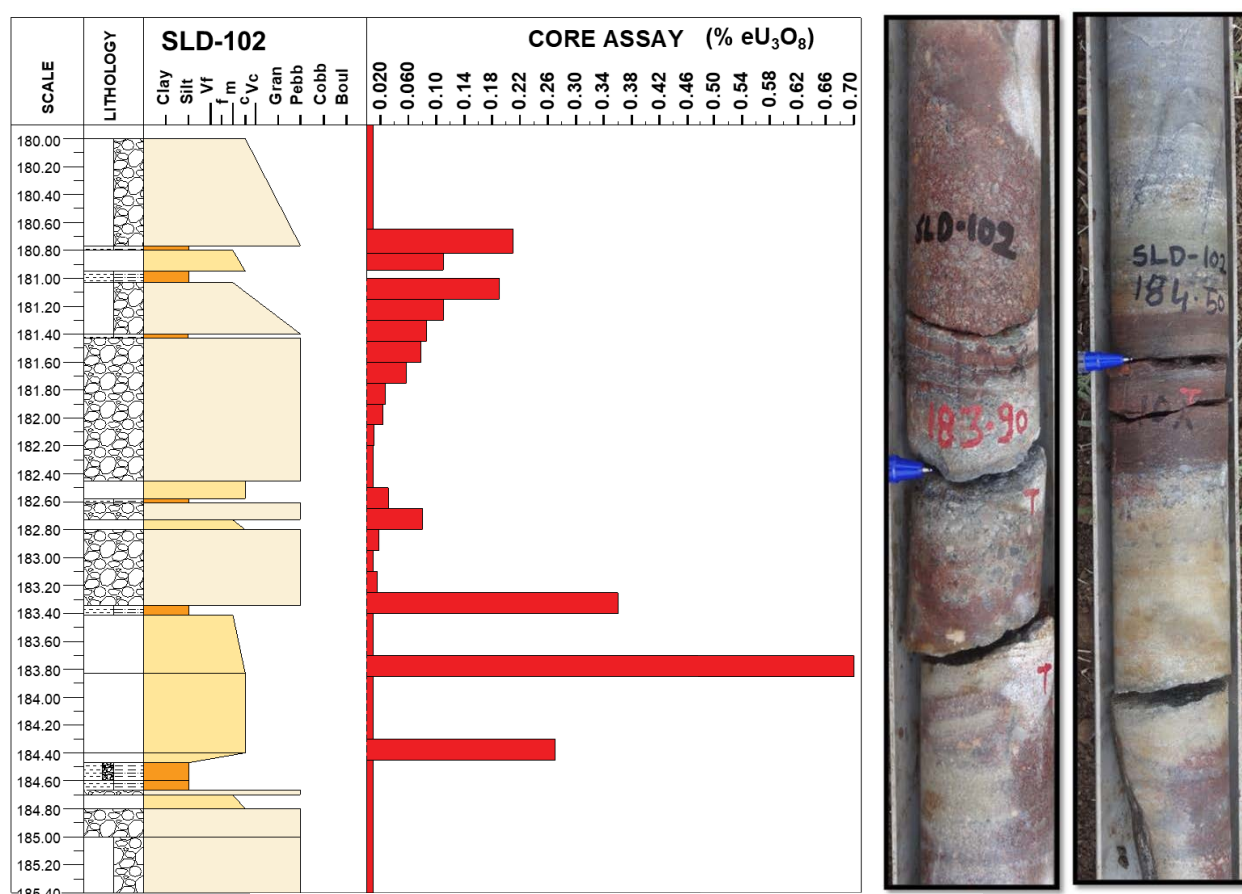


Figure 3.12 Mineralized horizons in SLD-102

Radioactivity was recorded in reduced (with frequent oxidized patches) lower conglomerate/ pebbly feldspathic arenite with finely laminated intercalated reddish-brown clay. High activity is recorded at the arenite/clay contact. Association of sulphides, mainly yellowish green chalcopryite is observed, exhibiting partial to complete alteration to azurite.

### **3.6 Mineralized host rock characteristics**

The mineralized lower conglomerate is greyish to white in color comprising of sub angular to sub rounded clasts with low to medium sorting. The unit is soft and friable, consisting both clast and matrix rich horizons, with clasts comprising majorly of feldspars (mainly microcline & orthoclase) and quartz. Relict detrital biotites of clast sizes 0.5 to 2cm are set in quartzo feldspathic matrix. The samples show moderate to intense alteration, in which feldspars are highly altered to clay minerals. The lithounit is reduced in nature with abundant in sulphides minerals occurs in the matrix portion as disseminated, along the grain boundaries and interstices of grain contacts. In contrast to the mineralized part, the non-mineralized part is hard and compact showing oxidized nature and devoid of sulphides. Sulphides can be seen occurring along grain boundaries as disseminated grain and fracture fillings.



## **CHAPTER 4**

### **PETROGRAPHY**

Petrographic studies facilitate diagnosis of constituent framework mineral phases, their relative abundance and understanding of the textural attributes of the rock. This helps in reconstructing the source rock composition, paleo depositional energy setting, subsequent diagenetic alteration and analysis of deformations which the rock has undergone over time. Present study is based on the representative cover-sediments samples belonging to Cave Temple Arenite Member collected along Deshnur – Gujanal tract.

#### **4.1 Methodology**

Petro-mineralogical studies were carried out using conventional transmitted and reflected light optical microscope. Reflected light microscopy was specifically used to study uranium bearing minerals and associated ore minerals. Leica DM2700 M polarizing microscope with an attached Leica DFC500 camera was used for micro-photography at the Petrology Laboratory, AMD-SR, Bengaluru. Systematic sampling of structurally oriented representative samples from surface outcrops available in basin margin at Deshnur and borehole core samples at Gujanal was conducted for petromineralogical studies. Owing to the friable nature of shale intercalated pebbly feldspathic arenite/lower conglomerate unit, extra care was taken during the sampling and preparation of thin sections. Megascopic observations of all the rock samples were made prior to section cutting and thin section making. This further assisted in identifying the desired sections.

Identified radioactive samples in field were first checked for any occurrence of secondary uranium phases under ultraviolet light using UVGL-15 handheld mineralight® lamp of Ultraviolet Products Inc., USA, in a dark room. The presence of secondary uranium phases is confirmed by their distinguishing property of fluorescence. However, no secondary

mineral phases have been identified during the course of study. This is further followed by checking for leachable primary uranium minerals using Chromogram tests. Following are steps to conduct a Chromogram test:

1. Ready a B/W photographic printing paper which is already treated with sodium thiosulphate [fixer] and dried.
2. Apply coating of nitric acid (1:1) on the smooth side of treated photographic printing paper.
3. Keep the even side of the rock slab in contact with the nitric acid coated photographic printing paper for 1 to 2 min.
4. Paper is removed and treated with potassium ferrocyanide solution. Precipitates of uranyl potassium ferrocyanide (brown), chromium potassium ferrocyanide (brown), iron potassium ferrocyanide (blue) and copper potassium ferrocyanide (pale pink).
5. The brown stain of uranyl potassium ferrocyanide is removable by nitric acid/sodium hydroxide but the brown stain of chromium potassium ferrocyanide remains unaffected.

Conducting a successful chromogram further assists in choosing the suitable surface for thin section preparation. The cut slices of fractured, weathered and soft samples were cooked in Canada balsam. Similarly, friable samples from pebbly feldspathic arenite/lower conglomerate unit were cooked in Canada balsam diluted with xylene for better binding before slicing. The saw-cut face is polished and attached to the glass slide using epoxy glue/thermoplastic cement or Canada balsam. The samples were further polished till thickness of 30  $\mu\text{m}$  was achieved. This fine polishing was carried out by abrading the rocks against metal and glass plates using Silicone Carbide (SiC, also known as carborundum) powder of varying granule sizes of 220#, 400#, 600#, 800# and 1000# sieve mesh. This section was further polished by alumina (AlOH) solution and Gold paste to impart superfine

polish and brilliant reflecting surface to the opaque metallic minerals. In addition to this, Cellulose Nitrate (CN) film study was also carried out for the identification of radioactive minerals. Following are the steps for conducting a CN film test:

1. Place indicators mixed with radioactive minerals/materials on four corners of the specimen on thin section/polished slab/bakelite or araldite moulds.
2. Cut the transparent CN – 85 alpha sensitive film of the thin section/mould and place the CN film on the top of the specimen. Make sure that the film has even and close contact with the specimen.
3. After 3 days of exposure through the contact, the exposed CN film is removed and ‘etched’ in 10% aqueous solution of sodium hydroxide (NaOH) for about 6 to 10 hours at room temperature.
4. The exposed and etched CN film now shows variable intensity of alpha tracks matching with concentration of radioelements in minerals and their size/shape.

#### **4.2 Badami sediments**

Badami sediments underlain by Chitradurga schist belt, and exposed along Deshnur-Gujanal tract comprises of Lower Conglomerate, followed by Quartz arenite and Upper Conglomerate/Feldspathic arenite unit of Cave Temple Arenite Member. Both grab (Deshnur) and core samples (Gujanal) from different depths were studied for petrographic observations.

Previous radiometric exploration surveys have led to delineation and correlation of significant sub surface uranium mineralization in pebbly feldspathic arenite/lower conglomerate unit in both Deshnur and Gujanal. During the course of study, radioactivity was reported in Quartz arenite, exposed along basin margin at Deshnur and in pebbly feldspathic arenite/lower conglomerate unit drilled from boreholes SLD-100 and SLD-102.

The lower conglomerate is marked by ~30 cycles starting from matrix supported conglomerate, grading into pebbly feldspathic arenite and culminating with silty-shale intercalations. Mineralization is recorded in both matrix-supported conglomerate, feldspathic arenite.

Primary focus of the present work is to study the matrix portion of the host rock and understand the difference between radioactive and non-radioactive samples from the study area.

#### **4.2.1 Pebbly feldspathic arenite/ lower conglomerate**

##### **Megascopic observations**

The Lower Conglomerate/pebbly feldspathic arenite unit of the study area as observed in the borehole cores in Gujanal is light to dark grey colored, slightly friable and matrix supported with grain size varying from 1mm to 4 mm; a few clasts show even up to 6 mm. Clasts of quartz, vein quartz, fresh and altered kaolinized feldspars and jasper, were identified in arkosic matrix. Abundant sulphides can be observed occurring in the form of veins/veinlets/disseminations marking the presence of reduced patches in overall unit deposited under oxidizing conditions.

##### **Microscopic studies**

It is a matrix-supported, polymictic type conglomeratic unit, with clast size varying from coarse sand to granule. It is composed of sub-rounded to angular clasts of quartz, polycrystalline quartz, quartzite, mylonite, chert, K-feldspars, plagioclase feldspars and jasper. The clasts are bounded by arkosic and clayey (sericite/illite) matrix (Fig. 4.1a). Quartz clasts (4mm-1cm) are subrounded to rounded and depict silica overgrowth as diagenetic modification. Quartz clast show undulatory extinction. Their proportion varies from 65 to 70% approximately in representative samples from SLD-102. Proportion of feldspars also

varies from 15 to more than 30%. K-feldspars (microcline and perthite) occur in abundance relative to plagioclase. Predominantly feldspars are fresh (Fig. 4.1c), however former feldspars are probably altered to sericite/illite & forming binding material (Fig. 4.1d). Detrital biotite is also present. Biotites are altered, sericitized/illitized, chloritized and getting merged with matrix material (Fig. 4.1e). Interstitial spaces between the larger clasts are filled with arenaceous matrix, mainly of quartzo-feldspathic composition. Crypto to microcrystalline silica, clay also constitute as significant part of the matrix. Sericitization and clay formation are chief manifestations of feldspar alterations. Sericite can be observed as flowage texture, surrounding clasts and replacing them. Cementation due to silica overgrowth and pressure solution is also observed, thereby indicating burial impact. Accessories as confirmed by heavy mineral studies, occur in the form of opaques, zoned zircons, apatite, few monazite and clusters of titanites. The presence of angular to sub-rounded clasts, show low to intermediate maturity with very poor to moderate sorting, indicate the transportation of detritus over short distance. Opaques are identified as uranium rich minerals and sulfides (Fig. 4.2a, b). Very fine metallic sulphide phases such as chalcopyrite, chalcocite and pyrite can also be spotted. Radioactivity primarily occurs as pitchblende along grain boundaries and microfractures of grains (Fig. 4.2c, d, e). Polymetallic sulphides (Fig. 4.2f) such as chalcopyrite, covellite and bornite show sulphide precipitation of different generation. Chalcopyrite can be seen replaced by bornite and bornite by chalcocite and traces of covellite.

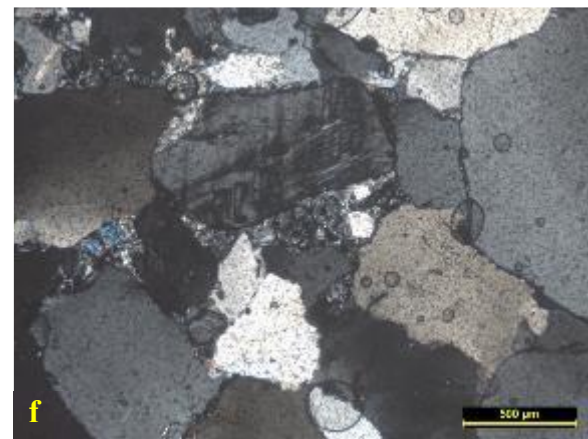
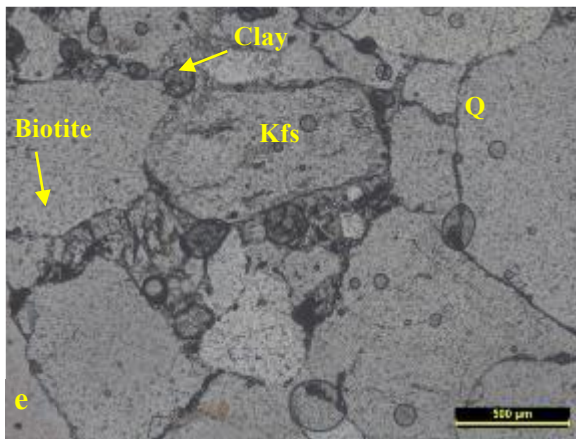
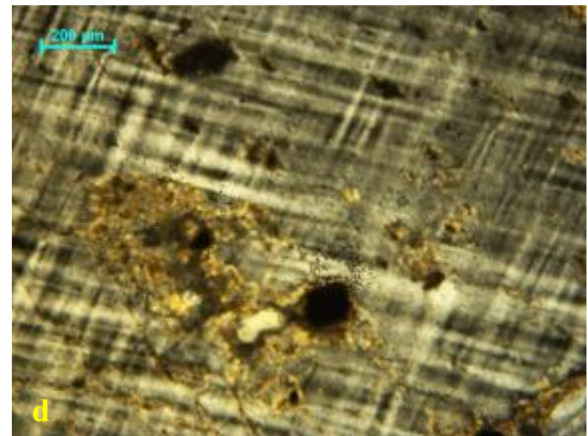
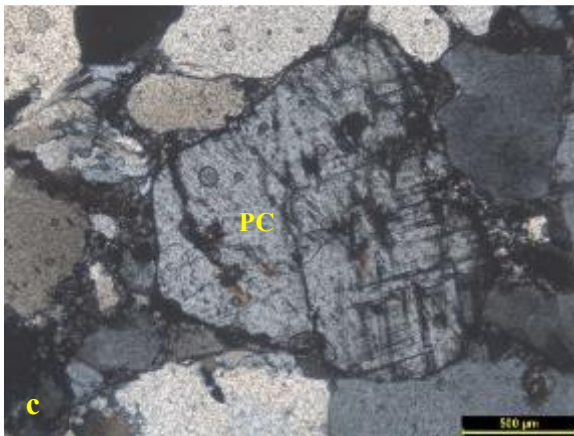
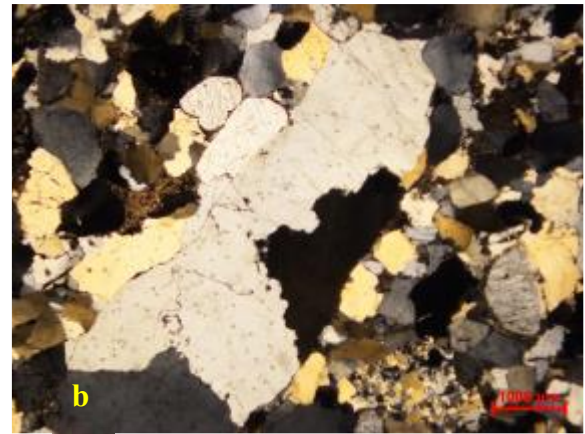
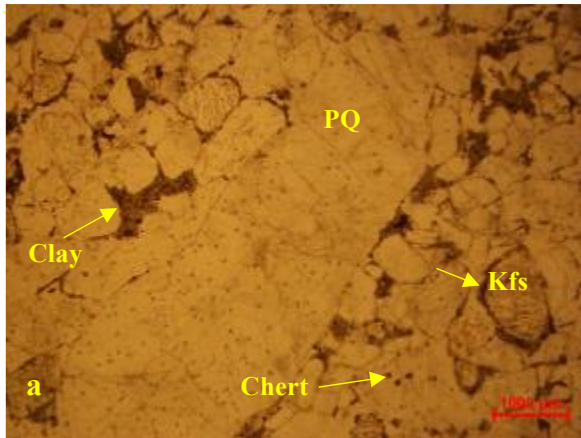


Figure 4.1 (a) Non-radioactive conglomerate, polycrystalline quartz (PQ), clay and K feldspar (kfs), TL 1N, (b) RL, XN, (c) perthite clast (PC), (d) feldspar altering to clay, Pitchblende (P) and Pyrite (Py) TL, XN, (e) detrital biotite and diagenetic clay occurring as matrix around framework grains of Quartz (Q) and feldspar (Kfs)



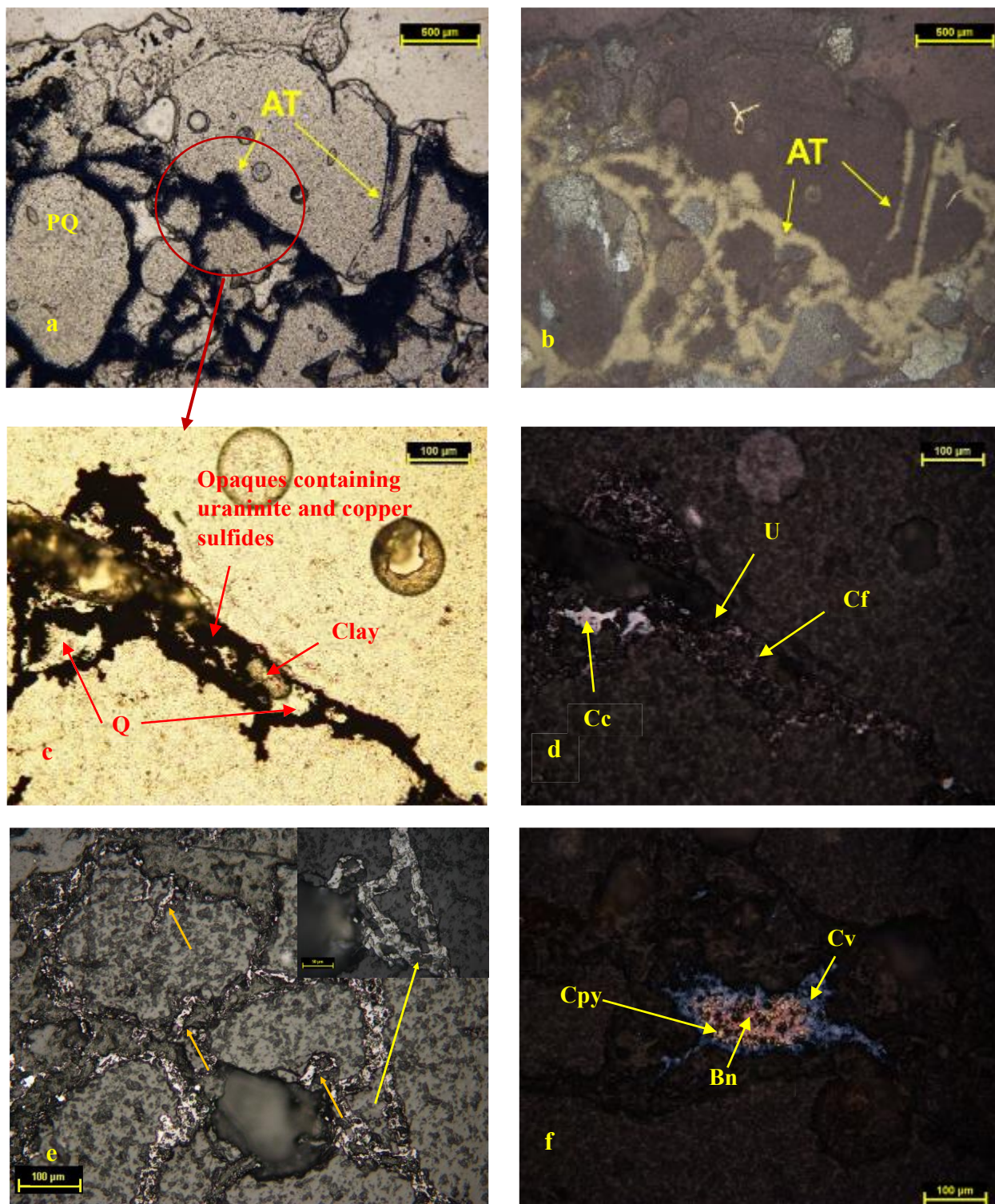


Figure 4.2 Radioactive conglomerate, (a), (b), (c) Uraninite and copper sulfide in quartz microfractures and replacing quartz & clay minerals present as matrix. (d) Uraninite (U) and suspected coffinite (Cf) associated with chalcocite TL, 1N, (e) Uraninite occupying secondary dissolution pore-spaces (indicated by small arrows) and also engulfing etched quartz fragment (inset), RL, 1N., (f) Different generation of copper sulfides, wherein chalcopyrite is replaced by bornite which is replaced by covellite.

### **4.2.2 Feldspathic arenite**

#### **Megascopic observation**

This occurs as medium to coarse grained compact to slightly friable intercalated lithounits in lower conglomerates. It is pink to greyish color, consisting of clasts of quartz and feldspars, filled with arkosic matrix. This unit occurs as small patches in pebbly feldspathic arenite/lower conglomerate unit.

#### **Microscopic observation**

This unit is mineralogically and texturally immature because of poor sorting, sub angular to angular clasts of quartz, polycrystalline quartz, microcline, perthite, orthoclase, and plagioclase feldspar and rock fragments of chert, quartzite and mylonite forming as framework clasts. Feldspars constitute for more than 15-25% (Fig. 4.3a) as observed by visual estimation comprising of clasts of perthite, orthoclase, microcline & plagioclase feldspars. Quartz grains are subangular to rounded and ovoidal in shapes. In the same section, the framework grains consisting of quartz and feldspar are arranged in a compact nature. In some places Quartz show pressure solution and overgrowth formation as diagenetic modification. Due to this silica is released and getting merged with the binding material, however the uranium bearing samples can be identified with significant amount of clayey matter occurring as matrix (Fig. 4.3g, h). Pitchblende with varying shades of grey alterations occurs with chalcopyrite along the intergranular spaces (Fig. 4.3c, d, e, f). In some cases, sulfides can also be seen occurring the grain boundaries, however no presence of uranium mineral was identified.



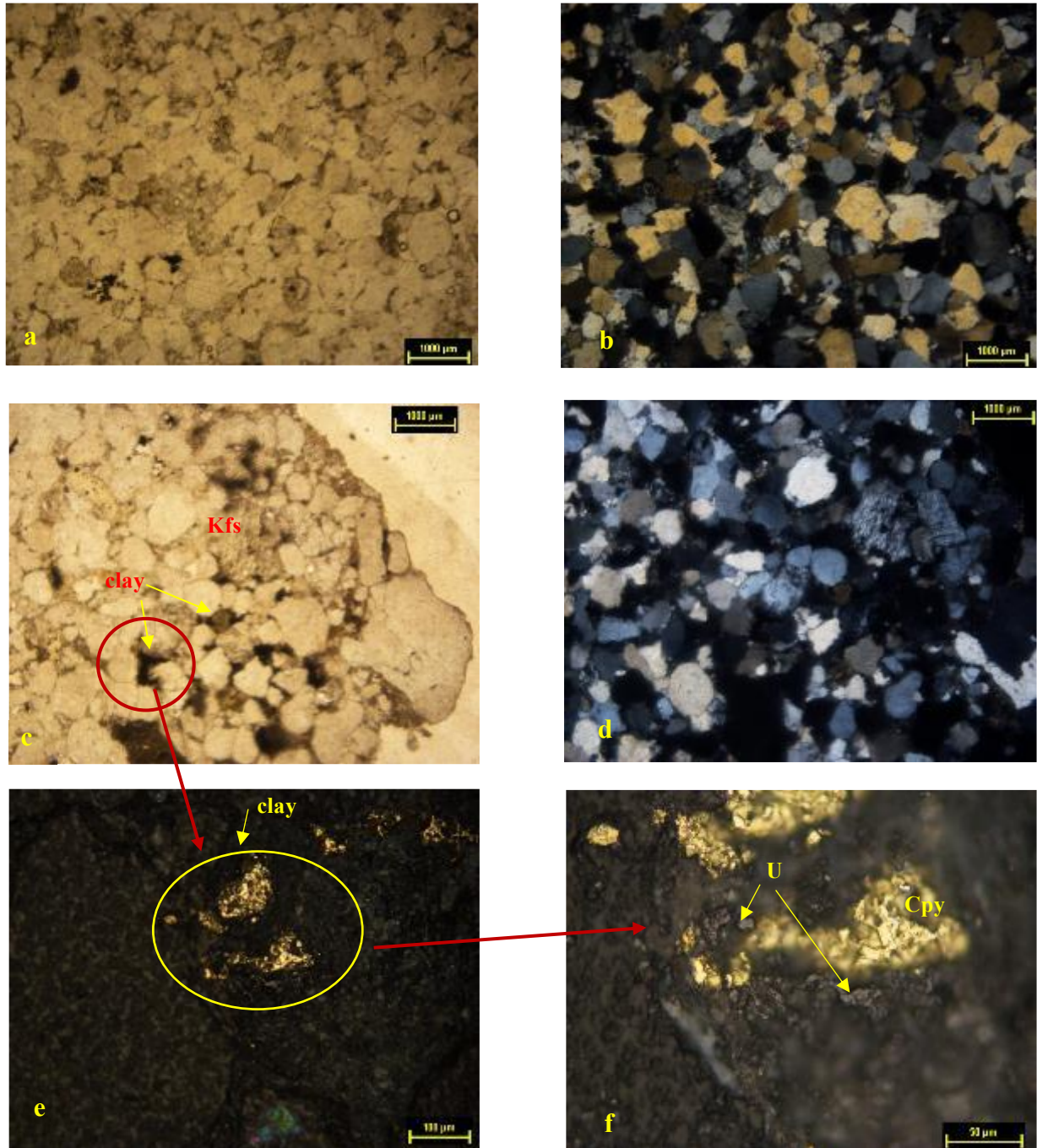
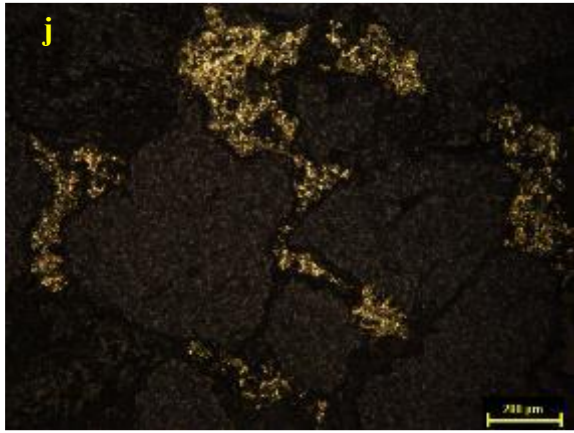
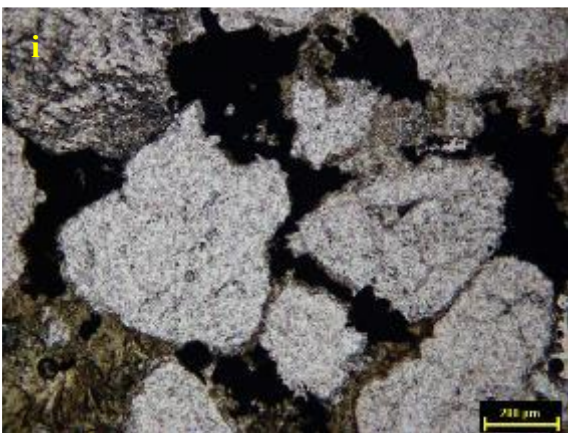
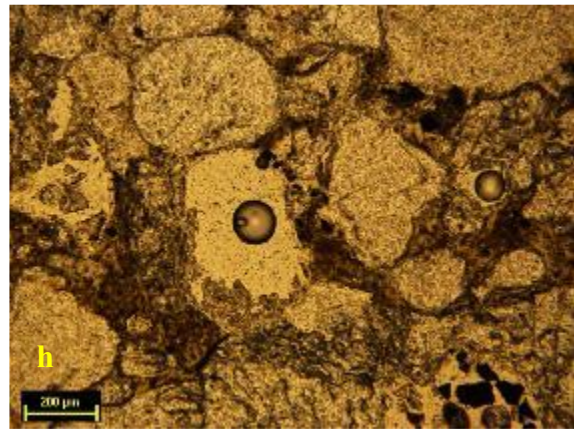
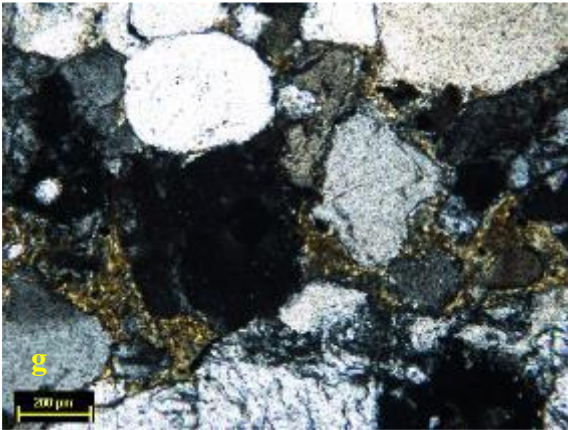


Figure 4.3 Feldspathic arenite showing compact nature with less matrix content (a) TL, 1N (b) TL, XN; Uraninite associated with chalcopyrite along grain boundaries replacing clay matrix (c) TL, 1N, (d) TL, XN. Magnified view of uraninite (U) associated with chalcopyrite TL, 1N, (e) RL, 1N; (f) RL. Biotite can be seen converting to clay minerals in matrix (g) TL XN, (h) TL, 1N. Occurrence of sulphides along grain boundaries (i) TL, XN (j) RL, XN,



### 4.2.3 Quartz Arenite

#### Megascopic observations

This lithounit is hard, compact, medium to fine grained containing profuse laminations. It is both texturally and mineralogically matured, predominantly composed of detrital quartz grains with remaining fraction constituted by minor feldspar, muscovite and chert.

#### Microscopic studies

Quartz grains showing both straight as well as undulose extinction are tightly packed thus exhibiting appreciable pressure-welded contacts yielding interlocking mosaic texture (Fig. 4.4a). Constituent arenaceous grains are subrounded to angular in nature and share long



as well as sutured contacts. Minor quartz-overgrowth is also conspicuous. Inherent high porosity of this particular lithounit owing to good mineralogical and textural maturity have been reduced during incipient mechanical compaction and subsequently reduced completely during cementation by pressure-solution and syntaxial overgrowths (Fig. 4.4b).

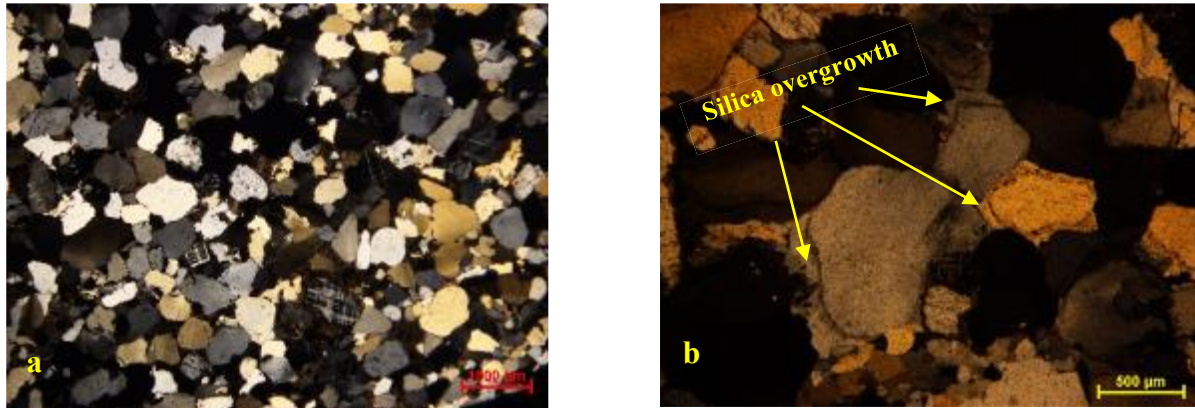


Figure 4.4 (a) Non-radioactive quartz arenite showing interlocking texture TL, XN (b) Silica overgrowth TL, XN

High order surface radioactivity was recorded in Quartz arenite unit at Deshnur. Radioactive phases represented by alpha tracks have been outlined on opaques occurring in intergranular spaces and micro-fractures within the grains (Fig. 4.5). Radioactive phases are also in matrix composed of mylonites, quartzitic and chert fragments. Uranium bearing minerals spotted by alpha tracts, can be seen occurring in association with pyrite along grain boundaries and microfractures in quartz (Fig. 4.5 a, b, c, d).

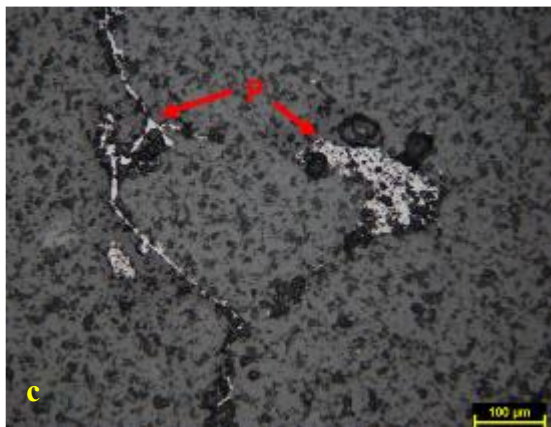
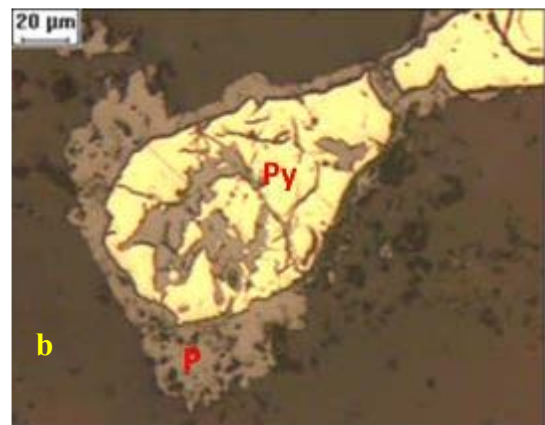


Figure 4.5 (a) Pitchblende (P) vein in hairline fractures in quartz arenite giving very dense tracks, TL, XN, (b) Fractured Pyrite (Py) surrounded and infiltrated by pitchblende, RL,1N, (c) Pitchblende present in the intergranular spaces, Offset track image RL, XN, (d) TL,1N

### 4.3 Radioactivity

These conglomerates are devoid or contain traces of sulphides. Uraninite, as discrete oxide occurs mainly as disseminated form in association with copper sulfides. However, as seen in (fig. 4.3 i&j), the presence of sulphides does not assures the occurrence of uranium bearing minerals. Pyrite and chalcopyrite occur as predominant ore mineral followed by bornite and traces of covellite. Paragenetically pyrite is being replaced by chalcopyrite and chalcopyrite in turn by pitchblende and coffinite. Uranium minerals associated with copper sulphide occur along intergranular spaces of poorly sorted matrix portion of the conglomerate/feldspathic arenite and as micro-fracture fillings in quartz and cleavage planes of feldspars. Matrix in conglomerates is quartzo-feldspathic in nature and predominantly clay which is the inter mixture of sericite/illite, chlorite, kaolinite, iron oxide and decayed/disintegrated biotites. Biotites are stretched, strained and kinked. They are disintegrated and the cleavages are obliterated with the release of hydrated iron oxide. Biotites are also altered to chlorite and sericite/illite. However, mineralization is confined to sulphide rich arenaceous and clayey matrix. Contrary to radioactive, non-radioactive ones are compact, mature and bound by ferruginous matter indicating oxidized nature of the rocks.

The petromineralogical studies of non uraniferous matrix supported conglomerate (core) is more or less similar to its radioactive counterpart. The low uraniferous conglomerate show presence of silica overgrowth and pressure solution due to which the pore spaces were reduced and which might have inhibited the movement of uranium bearing solution. The rock shows relatively lesser amount of sulphide bearing minerals than its radioactive counterpart and more of hematite and goethite in places.

Petrographic studies of samples from in and around study area suggest overall prevalence of oxidizing conditions at the time of deposition and diagenesis of the Badami

arenites. It is testified by presence of hematitic cementing material and iron coatings on the constituent detrital heavy minerals.

#### **4.4 Diagenetic History**

Mechanical compaction marks the beginning of diagenetic processes wherein constituent detritus manifested as close packing of grains, localized fracturing of quartz and feldspars, bending of detrital micas, pressure solution at point contacts and interpenetration of neighboring grains. Precipitation of iron oxide-hydroxide and clay was concurrent with mechanical readjustment as exhibited by hematitic-limonitic coating within the vacuoles over the grains. Subsequent to initial compaction of the sediments, the residual intergranular spaces were filled by silica cement, precipitated around the quartz grains giving rise to syntaxial overgrowths. Such overgrowths lead to development of euhedral crystal faces in optical continuity with detrital quartz which may be delineated on account of presence of clayey and more commonly ferruginous dustlines. With further burial and thermal maturation, chemical alteration of unstable mineral phases such as feldspars and biotite by the action of circulating corrosive fluids is noticeable. Similarly, dissolution of quartz is also evident on account of appearance of the grain boundaries and irregular overgrowths. Chemical alteration and dissolution of framework minerals might have given rise to the formation of secondary pore-spaces which were subsequently filled by authigenic minerals, mainly clays.

Possibility of occurrence of detrital clays cannot be ruled out. However, predominantly substitutive relationships of clays with early diagenetic cements suggest their authigenic nature. Due to size constraints, it is difficult to distinguish between different clay phases and their transformations in response to changing physico-chemical conditions. Interstitial clays exhibit ferruginous staining which may be attributed to simultaneous authigenesis of iron oxides-hydroxides which probably represent alteration products of



detrital ferromagnesian minerals such as biotite (Eren and Kadir, 1999; Hoeve and Quirt, 1984). Clay authigenesis is commonly associated with release of silica which may be observed to be form overgrowths or as pore-filling material.

Post-diagenetic effects of diastrophism on the rocks from in and around study area may be observed in terms of fracturing. Such fractures may have acted as vents for solution movement which might have caused subsequent localized bleaching of the beds, deposition of sulphides and remobilized silica along the fractures or replacing pre-existing cementing material.

#### **4.5 Interpretation**

The Badami cover sediments from the study area indicate an overall mineralogical and textural sub mature to immature nature. This is substantiated by the presence of appreciable amount of detrital feldspars and lithic fragments and high ICV values. Study of clast composition of representative samples suggest granitoid source with subordinate contribution from sedimentary provenance. Critical examination of the diagenetic events implies sedimentation under oxidizing conditions.

Higher concentration of uranium bearing minerals is observed at the interface of thin shale/silty with the bed suggesting lateral spreading along the bedding plane guided by the porosity and permeability of the host granule beds.

Uranium minerals mainly occur along the primary intergranular spaces in the poorly sorted matrix portion of the host rock. Uranium and sulphides bearing opaque minerals Pitchblende occupying the secondary pores formed due to dissolution of quartz grain along the etched grain boundaries is also observed. Secondary porosity is a result of dissolution of quartz (Fig. 4.6) caused by acidic brines circulating in the basin. Infilling of clays within the intergranular spaces may have prevented syntaxial silica overgrowths over etched surfaces

of the quartz grains. Subsequent post-diagenetic- partial to complete removal of pore-filling clayey material may have opened up both primary and secondary pore-spaces facilitating precipitation of sulphides and uraniferous minerals. The above observation indicates epigenetic nature of mineralization characterized by precipitation of pitchblende along both, primary as well as secondary pore-spaces

Paragenetically early sulphides phases mainly chalcopyrite replaced by pitchblende along the margins and cleavage planes is well observed suggesting uranium precipitation in later phase or in multiple pulses. Suspected coffinitization of pitchblende attests subsequent epi-thermal alteration process.

Petrological studies of samples from study area confirm quartz dissolution and development of secondary porosity. Study also insinuates probable bleaching of sediments associated with minor deposition of sulphides as a result of flushing of sediments by reducing fluids either concomitant or subsequent to post-diagenetic tectonic activity which is in principle considered to be conducive for uranium precipitation from circulating oxidized brines.

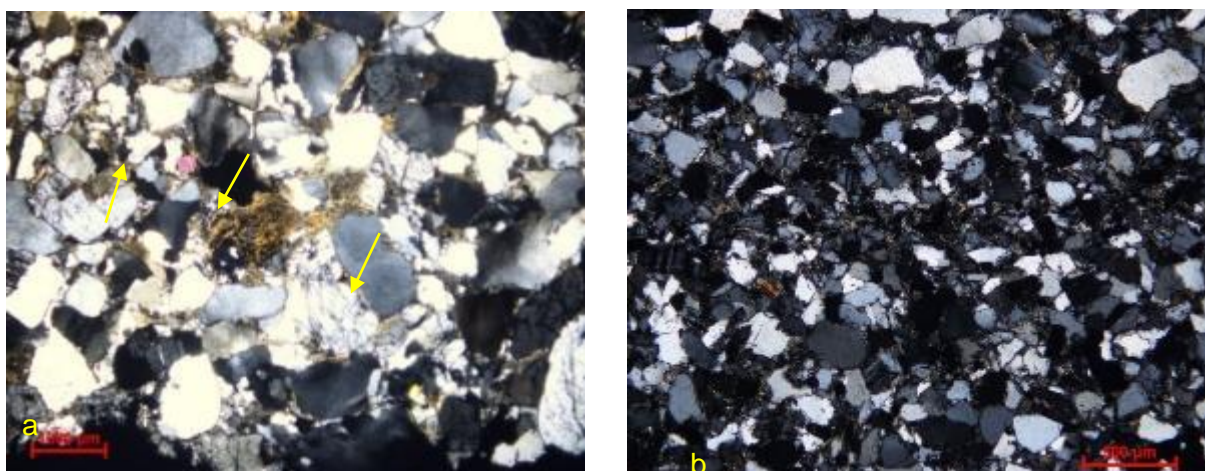


Figure 4.6 (a,b) Irregular grain boundaries (filled with clay minerals) creating pore spaces due Quartz dissolution due to acidic brines.

## **CHAPTER 5**

### **HEAVY MINERALS**

Heavy minerals are high density accessory mineral constituents occurring either as essential rock forming minerals (pyroxene, amphibole, mica) or as accessory component such as zircon, apatite, tourmaline etc. These minerals are characterized as minerals with specific gravities greater than those of the major framework grains. A series of processes take place from the moment minerals are released from the rock and deposited, to the time when they are extracted again for study. The heavy mineral suite in a sedimentary rock are sensitive indicators of source area and thereby hold paramount importance in understanding sedimentary provenance. The other factors controlling its distribution involve source area weathering, process of transportation, deposition and post depositional alteration.

The subsidiary processes rarely affect the assemblage of heavy mineral suite, however hydraulic conditions during deposition and subsequent diagenesis may cause major modification and hence need to be reviewed before undertaking provenance reconstruction studies. The most effective way to counteract these problems is to examine varieties of one mineral species using classical method of optical differentiation.

#### **5.1 Methodology**

A total of 6 representative samples weighing 150-200 gm were selected from Borehole SLD-102. The sampling was undertaken with an objective to classify the heavy mineral assemblage and evaluate its association in both radioactive and non-radioactive horizons. For immature sandstones or volcanoclastics, a sample of 100-200 gm will usually yield a sufficient quantity of heavy concentrate, but mature sediments and those which contain high proportion of cement require large bulk sediment sample size. Following steps were carried out for heavy mineral separation:

1. Disaggregation of coherent sediments using compressive force by jaw crusher to 5 mm size small chips.
2. This is followed by the use of an iron percussion mortar and pestle to liberate individual grains by complete disaggregation. The pestle was applied with a crushing action (to exert force vertically) to avoid destroying the original shape and size. Fine particles were simultaneously sieved out frequently to avoid over-grinding.
3. Sieving was carried out in different size fractions (-40 to +60#, -60 to +140#, -140 to +240# and -240#) to obtain heavy minerals in various fractions.
4. Maximum recovery of grains was obtained in -60 to +140#, however heavy minerals were also separated from -140 to +240# size. Preliminary observation stated the presence of iron coating over the heavy mineral assemblage thereby barring the identification of non-opaque grains.
5. An attempt (as suggested by Leith 1950) was made to remove the pervasive iron oxide grain coating using oxalic acid and aluminum by gently boiling the solution. However, the results were still not encouraging.
6. Concentration of heavy minerals was performed upon its immersion in high density liquids (Bromoform sp. gr. 2.89, followed by Methylene iodide, sp. gr. 3.32), wherein higher and lower density fractions are produced and separated. Bromoform lights are usually comprised of dominant framework grains of quartz and feldspar. Bromoform heavies are further separated using methylene iodide. As the specific gravity of methylene iodide is 3.31, minerals such as biotite, apatite, few pyroxenes etc., whose specific gravity is between 2.88 and 3.31 would separate out as methylene iodide lights fraction.
7. All separations were carried out in a separating funnel filled with high density fluid by gravity settling. Heavy minerals accumulate in the bottom of the funnel above the pinch

clip. When no more grains sink, the pinch clip is opened slowly, thus allowing heavy fraction to pour onto filter paper in lower funnel. The pinch clip is closed, leaving a layer of clear liquid below the light fraction. A new funnel with filter paper is placed under the separating funnel to collect lighter fractions.

8. The separated methylene iodide heavies were dried and separated based on their magnetic susceptibility. Electromagnetic separator was used to separate magnetic from non-magnetic methylene iodide heavies.
9. After the non-magnetic grains were separated, they were taken up for heavy mineral studies.

Out of 6, only three samples showed significant recovery. The pervasive iron coating (Fig. 5.1 i, j, k, l) on the surface of heavy minerals made it difficult for identification of the non-opaque mineral grains. Hence, the quantitative analysis encompassing the calculation of relative/absolute abundances of heavy or ZTR index using heavy mineral assemblage was avoided.

After careful and keen observation, only zircon (Fig. 5.1a, b, c, d), besides a few monazites (Fig. 5.1 e, f, g, h) and sphene grains (Fig 5.1 m, n, o, p) was identified out of the entire heavy mineral assemblage. Most stable of the heavy minerals found in sedimentary rocks and unconsolidated sediments; Zircon, is easily distinguished by its extreme relief, characteristic morphology and high interference colors. It is colorless, pink, purple, red, orange yellow, rarely blue or grey. Majority of detrital Zircon grains are colorless. However, very weak pleochroism is observed in stronger colored varieties. Zircon also has high birefringence and shows parallel extinction. The grains usually exhibit rounded to prismatic shape based on the transportation of the sediments.

Based on the preliminary observations, numerous grains of Zircon (iron coated mostly) were identified from the heavy residue. Therefore, an attempt was made to understand the morphometry of zircon and draw inferences about the transportation history thereby contributing towards provenance studies.



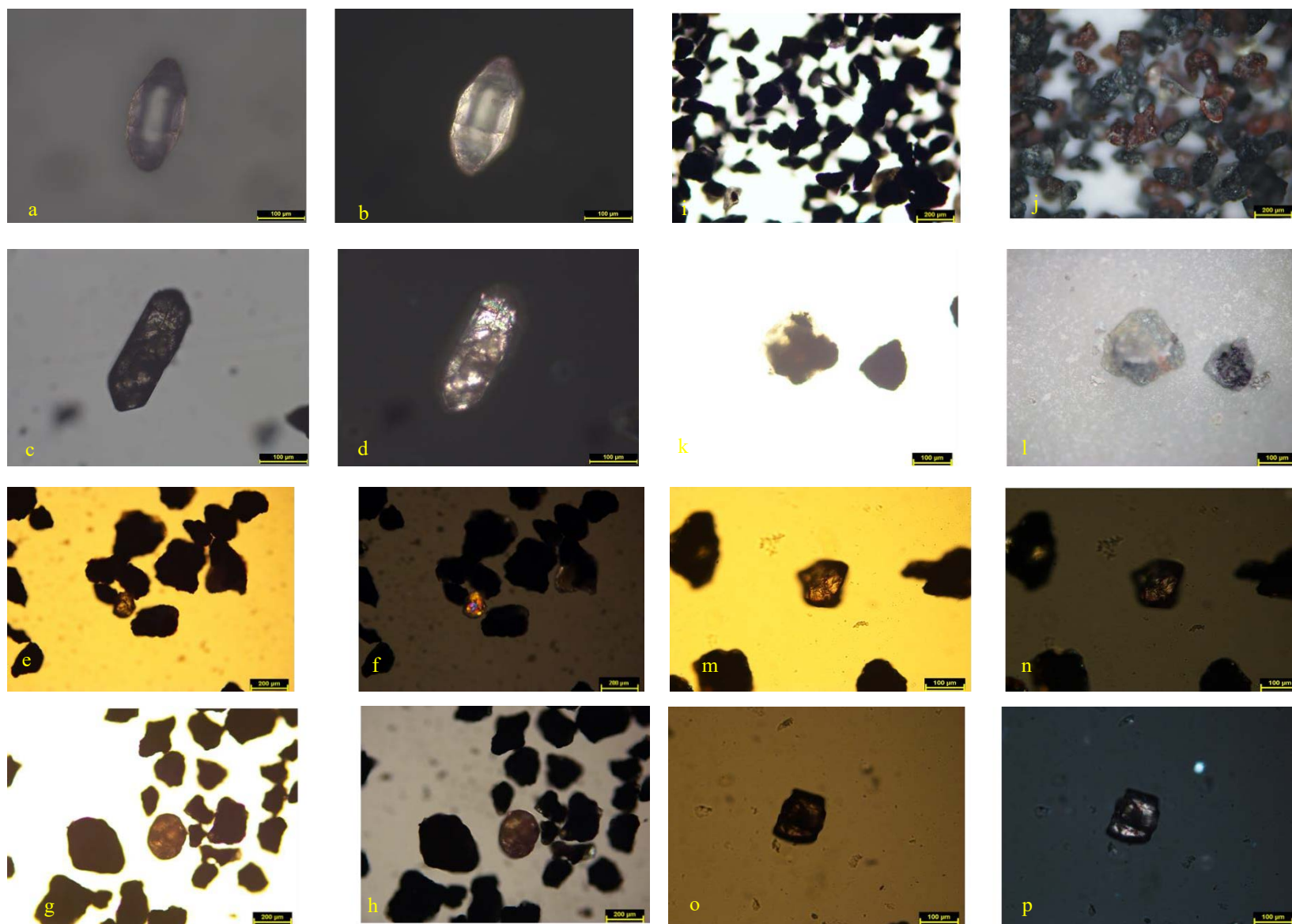


Figure 5.1 Zircon 20X, TL, 1N (a), (c); Zircon 20X, TL, XN (b), (d); Monazite 10X, TL, 1N (e), (g), Monazite 10X, TL, XN (f), (h); Iron coating 10X, TL, 1N (i), (k); Iron coating 10X, RL, XN (j), (l); Sphene 20X, TL, 1N (m), (n), (o), (p).

## 5.2 Morphometric analysis of Zircon

Morphology of Zircon crystal grains, especially in sediments, may indicate distance and medium of transport thereby acting as an additional tool for common provenance analyses. Notable investigations in the past revealed a widespread variety in attributes of zircon crystal morphology (e.g. Freise 1931, List 1966, Saxena 1966, Voggenreiter 1986, Finger & Haunschmid 1988, Tejan-Kella et al. 1991, Sinha et al. 1992, Balan et al. 2001, Moral Cardona et al 2005) wherein primary focus has been laid on roundness or crystal habit as well as surface characteristics. An attempt has been made to combine these aforementioned properties as suggested by Gartner et al. (2013)

### 5.2.1 Roundness

Roundness as suggested by Murawsky & Meyer (2010) is the smoothening of crystal edges caused by abrasion. It indicates the energy conditions affecting zircon grains during the entire transport process (Köster 1964, Dietz 1973). Compared to the aeolian environments, fluvial transport is ineffective in rounding sand grains. The ten classes of roundness after Pupin (1980), are as defined as



Figure 5.2 Completely unrounded Zircon grains with sharp edges 20X, TL, 1N (a), (b), Zircon 20X, TL, XN (c)

Table 5.1 The ten classes of roundness, after Pupin 1980

Class	Features
Completely unrounded	The grain shows very sharp edges without any exception, the single crystal faces are distinguishable without problems; classification <i>sensu</i> Pupin (1980) is possible.
Almost completely unrounded	Some edges of the grain are slightly rounded, the single crystal faces are distinguishable without problems; classification <i>sensu</i> Pupin (1980) is possible.
Very poorly rounded	Most edges and angles are slightly rounded, the single crystal faces are distinguishable without problems; classification <i>sensu</i> Pupin (1980) is possible.
Poorly rounded	Almost all edges and angles are rounded, only few angles show lesser rounding in the contour of the whole grain. Nevertheless, the single crystal faces are distinguishable without problems and a classification <i>sensu</i> Pupin (1980) is possible.
Fairly rounded	All edges and angles are rounded. Partially, some crystal faces show a smooth transition to the neighboring ones. Nevertheless, the single crystal faces are distinguishable without problems and a classification <i>sensu</i> Pupin (1980) is possible.
Rounded	In consequence of progressive rounding, all edges and angles are clearly rounded. All crystal faces show a smooth transition to the neighboring ones. Normally, the single crystal faces are

	distinguishable and a classification <i>sensu</i> Pupin (1980) is possible in most cases. Due to rounding, some smaller faces can be undistinguishable, but are often reconstructible using the remaining faces
Well rounded	Some edges and angles are rounded in a way that they are not recognizable anymore. Hence, the differentiation of some crystal faces is not possible. In some cases, a classification <i>sensu</i> Pupin (1980) is possible, depending highly on the visibility and the arrangement of the crystal faces.
Very well rounded	All edges and angles are very well rounded and not recognizable in larger parts, the classification <i>sensu</i> Pupin (1980) is not possible anymore.
Almost completely rounded	Only few edges and angles are partially recognizable. Remains of crystal faces are visible in some cases, but differentiation and classification <i>sensu</i> Pupin (1980) are impossible.
Completely rounded	There are no edges and angles anymore. Only few remains crystal faces are hardly recognizable in some cases. The classification <i>sensu</i> Pupin (1980) is impossible

The zircon grains, identified in the samples are completely unrounded as the grains show sharp edges without any rounding and the crystal faces are distinguishable without any problem. As the smoothening of crystal edges is caused by abrasion, lack of smoothening indicates lesser transport (Köster 1964, Dietz 1973).

### **5.2.2 Elongation**

The ratio of width divided by length is to be termed as elongation, which is bounded by the minimum value of 0 and the maximum value of 1. Another possible ratio with changed dividend and divisor after Poldervaart (1955, 1956) is called elongation, too (List 1966). The two equations are reciprocal to each other; thus, the results are comparable. Former studies used elongation as an indicator for possible host rocks (e.g. Poldervaart 1955, 1956, Hoppe 1963, List 1966). For example, zircons of granitic origin usually are more elongated than Zircons of sedimentary origin (Poldervaart 1955, 1956, Hoppe 1963, Finger & Haunschmid 1988). Furthermore, differences in Zircon morphology are also observed within magmatic rocks, caused by their cooling rates. The faster cooling takes place, the more elongated are the Zircons (Kostov 1973, Zimmerle 1975). For studies including sediments it is to consider that this parameter is conditioned by the distance of transport, because grains tend to be shorter within a longer way of transport (Wyatt 1954, Poldervaart 1956, Dietz 1973). Furthermore, there is a limited variability even within the host rocks (Hoppe 1962). Thus, the significance of elongation for provenance analyses is more or less restricted to the more elongated zircon grains.

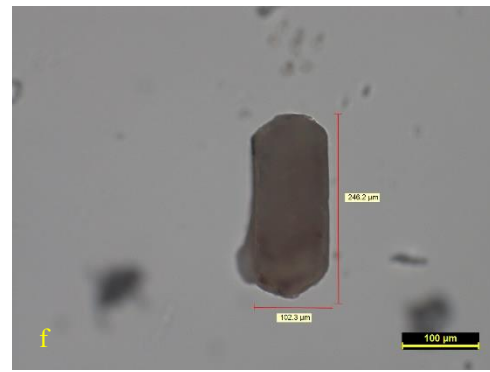
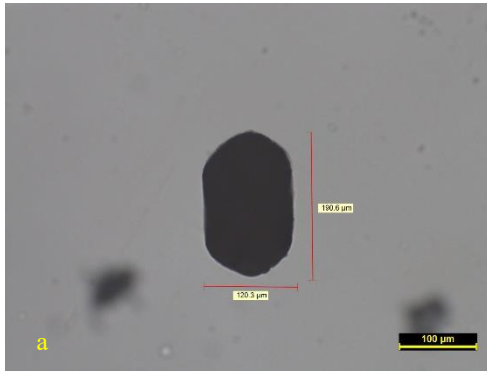


Figure 5.3 Elongate Zircon grains 20X, TL, 1N, (a), (b), (c), (d), (e), (f)



Table 5.2 Ratios and classification after Mitterer (2001) for both common possibilities of calculation of elongation

Crystal habit	stubby		stalky		Columnar or prismatic		Needle-like
	short	long	short	long	short	long	
<b>Elongation</b> (width/length)	1-0.67	<0.67-0.50	<0.50-0.40	<0.40-0.33	<0.33-0.25	<0.25-0.17	<0.17
<b>Elongation</b> (length/width)	1.0-1.5	>1.5-2.0	2.0-2.5	>2.5-3.0	>3.0-4.0	>4.0-6.0	>6.0

Length and width of Zircon crystals (n = 61) were recorded and the average value was found out to be 2.039 (width/length) and 0.505 (length/width), which signifies, that the crystal habit of Zircon is stalky and it is short in size.

### 5.2.3 Surface characteristics

Zircons show a widespread variety of surface characteristics like fracturing, cracks, scratches, striations, and impact pits all resulting from transport processes. Due to iron coating it was difficult to identify any surface characteristics except for fracturing.

- **Fracturing:** Fracturing of Zircon grains is controlled by the effective energy during the transport process and only possible in two directions: parallel or nearly perpendicular to the c-axis of the crystal. Caused by geometry and structure (Rösler et al. 2006), predominant direction of fracturing is through the c-axis. Depending on the number of fractured grains, the sample is determined as mainly influenced by high or low energy of

transport. As can be seen in the samples identified, fracturing can be observed occurring perpendicular to c axis.

- Cracks: Due to iron, coating, it was difficult to identify cracks, however some of the cracks can be identified due to collision effect during transport.

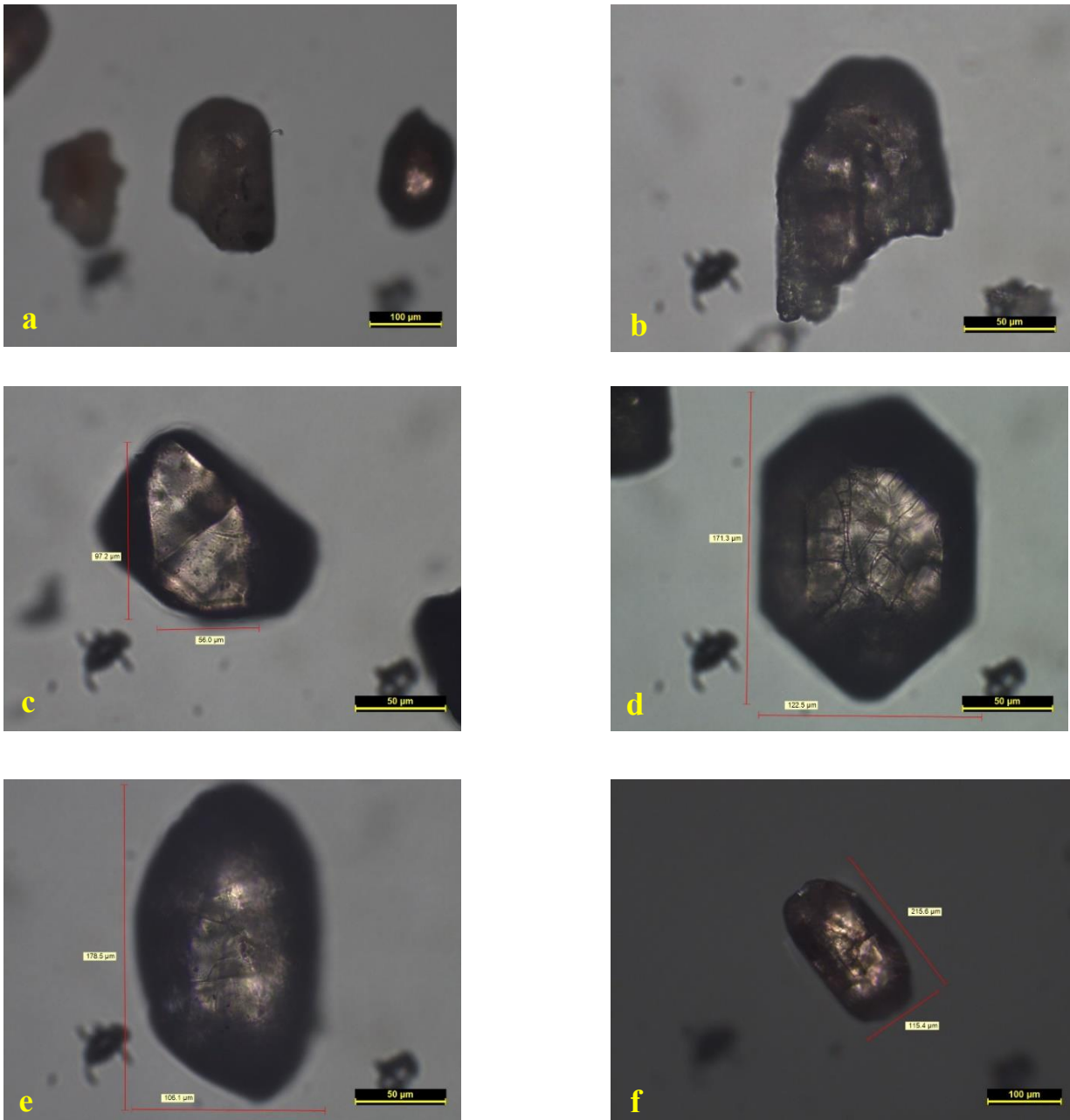


Figure 5.4 Zircon grains exhibiting fracturing perpendicular to c axis in a & b, TL, 1N;  
Zircon grains with cracks developing in c, d, e and f, TL, 1N.

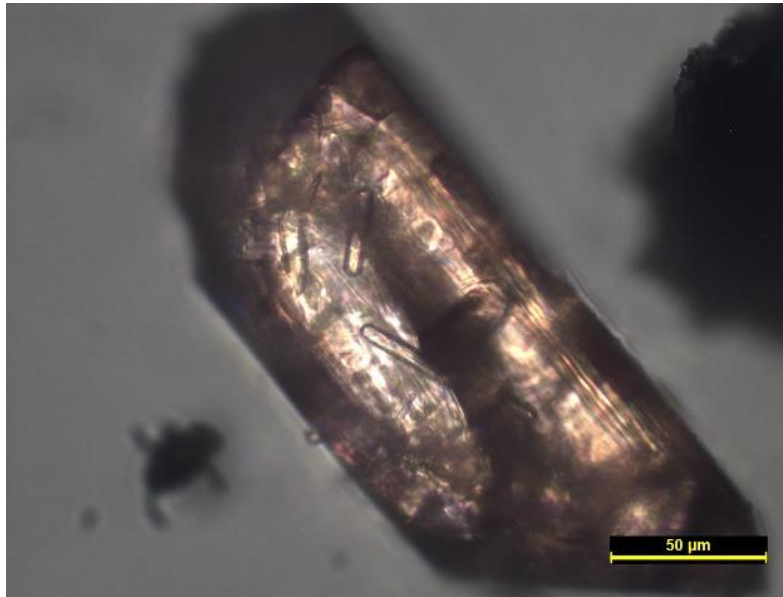


Figure 5.5 Zoned zircons with fluid inclusions 50X, TL, XN

The zircon grains identified from the heavy mineral suite, are mainly colorless and their dominant crystal habit is prismatic, although stubby and needle like shapes were also observed. The grains have preserved all their corners, edges and crystal faces, and show no to little degree of abrasion. According to the classification by Pupin 1980, they are completely unrounded. According to Poldervaart (1955), predominance of euhedral grains of Zircon is suggestive of magmatic origin. Poldervaart (1956) stated that the majority of Zircons from magmatic granite have an elongation-ratio 2.0-3.0. but Chowdhary (1971) found this ratio between 2.0 and 4.0 for magmatic granitic rocks. The average elongation ratio for the grains is 2.039.

The presence of euhedral grains, high proportion of completely unrounded Zircon and elongation ratio  $<3$  indicates that, the sediments were deposited with little or no reworking due to short distance transportation from granitic magmatic source.

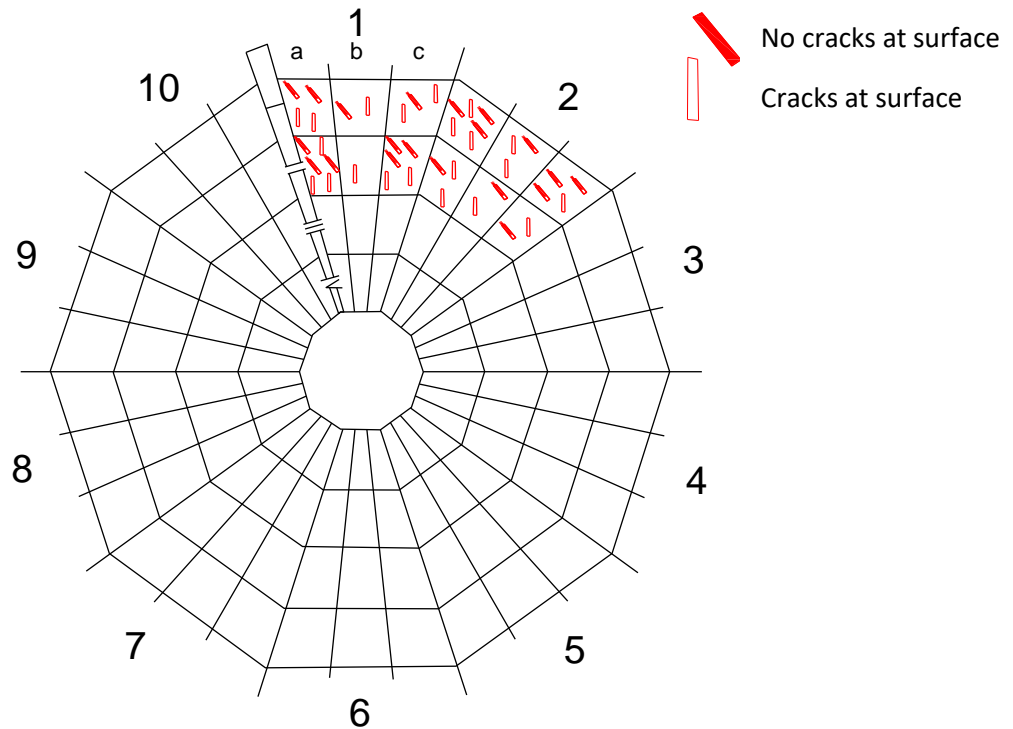


Figure 5.6 A representative spider plot showing the interrelations between roundness, collision marks, type of fraction, cracks at the crystal surface. After (Gartner et al 2013)

**Subdivisions were made into 3 groups:**

1. Roundness with ten classes (1 to 10)
2. Elongation with seven classes (1 to 7)
3. Surface characteristics with 2 sub-groups:
  - a. Fracturing with three classes (a to c)
  - b. Cracks at the surface of the crystal with two classes (i and ii)
  - c. Collision marks with four classes (I to IV)

The five-dimensional spider plot created from representative sample, as shown in Fig. 5.6 contains information about roundness, collision marks, type of fraction, cracks at the crystal surface, and location. All given characteristics are replaceable against others, e.g. elongation. Thus,

this plot provides the better illustration of interrelations between some of the single characteristics within one diagram.

An attempt to study the variation in heavy mineral assemblages was conducted in Deshnur (Ramchandran et al. 2019), wherein borehole core samples from DNR-58, were analyzed. It was identified that more unstable heavy minerals for example olivine, pyroxene and hornblende occurred besides most stable zircon, tourmaline and rutile in younger sediments (top part of the core). However, in the older sediments (Lower conglomerate), only the most stable heavy mineral assemblage i.e. zircon, tourmaline and rutile are identified. This indicates the effect of post diagenetic alteration by intrastratal solution, thus manipulating the heavy mineral assemblage (Morton, 1984). Hence, heavy mineral studies in this area does not give absolute information regarding as provenance indicators. However, the morphological studies conducted on identified zircon grains, such as its roundness, surface characteristics and elongation, providing insights into the transport history, the processes associated, possible host rocks. The studied zircon grains indicate less transport of sediments derived from nearby granitic source rock.

## CHAPTER 6

### GEOCHEMISTRY

#### 6.1 Cave Temple Arenite sandstones:

The mineralogical and chemical composition of clastic sedimentary rocks is controlled majorly by source rock characteristics, weathering, sorting process during transportation, depositional environment and post depositional processes (Hayashi et al., 1997). Based on the geochemical signatures of siliciclastic rocks, several studies have contributed towards developing the understanding of geological processes and identification of paleotectonic settings of provenances (e.g., Dickinson and Suczek, 1979; Bhatia, 1983; Bhatia and Crook, 1986; Roser and Korsch 1986; McLennan and Taylor, 1991). The present study examines the geochemical characterization of 24 representative samples (13 Sandstone and 11 Conglomerates - matrix portion) of Cave Temple Arenite Member to classify sandstone, and decipher their provenance and tectonic setting. Major, minor and trace elements were analyzed by WDXRF spectrometry.

Weathering indices such as CIA and ICV are calculated to understand the weathering at source and post deposition alteration of sandstones. During the calculation of these indices CaO correction is required in case of presence of dominant Calcite cement or calcite associated with non-silicate minerals. In case of  $\text{CaO} > \text{Na}_2\text{O}$ , %CaO is taken equal to  $\text{Na}_2\text{O}$ . A-CN-K plots are used to understand if the sandstones have undergone any potash metasomatism. The interpretations drawn from the geochemical characterizations are being corroborated with the petrographic observations to draw wholistic inferences.

Geochemical studies (n=24) indicates that the sandstones contain moderate to high  $\text{SiO}_2$  (75.91% - 97.40%, Avg – 88.78),  $\text{Al}_2\text{O}_3$  (0.44% - 12.03%, Avg – 4.87),  $\text{K}_2\text{O}$  (0.00% - 5.10%,



Avg – 1.55%), Fe<sub>2</sub>O<sub>3</sub> (0.36% - 9.10%, Avg – 1.87%) and moderate to low CaO (0.02% - 1.04%, Avg – 0.11%) and Na<sub>2</sub>O (0.00% - 0.70%, Avg – 0.23%).

High average Silica content of 88.78% and moderate to high average Al<sub>2</sub>O<sub>3</sub> content 4.87% is suggestive of high feldspar/clay content in the sandstone. Higher K<sub>2</sub>O (avg 1.55%) than Na<sub>2</sub>O (avg 0.23%) and CaO (avg 0.11%) content and K<sub>2</sub>O/Na<sub>2</sub>O > 1 suggest that K-feldspars dominate over plagioclase feldspars. The high negative correlation between SiO<sub>2</sub> and Al<sub>2</sub>O<sub>3</sub> (r = -0.94) and strong positive correlation between K<sub>2</sub>O and Al<sub>2</sub>O<sub>3</sub> (r = 0.78) further substantiates contribution of feldspar and that is supported by petrographic observations. Higher values of K<sub>2</sub>O/Na<sub>2</sub>O (avg 5.7) indicate the presence of K bearing minerals. Negative correlations of SiO<sub>2</sub> with major elements confirm that bulk of the SiO<sub>2</sub> is present as quartz grains. Strong negative correlation between SiO<sub>2</sub> and K<sub>2</sub>O (r = -0.67) indicates the decrease in clay content with increase of quartz. Correlation coefficient data of major and minor oxides is

Table 6.1 Correlation coefficient data of major and minor oxides of Cave Temple Arenite sandstones

	SiO <sub>2</sub>	TiO <sub>2</sub>	Al <sub>2</sub> O <sub>3</sub>	Fe <sub>2</sub> O <sub>3</sub>	MgO	MnO	CaO	Na <sub>2</sub> O	K <sub>2</sub> O	P <sub>2</sub> O <sub>5</sub>
SiO <sub>2</sub>	1.00									
TiO <sub>2</sub>	-0.57	1.00								
Al <sub>2</sub> O <sub>3</sub>	-0.95	0.58	1.00							
Fe <sub>2</sub> O <sub>3</sub>	-0.62	0.17	0.36	1.00						
MgO	-0.67	0.51	0.74	0.08	1.00					
MnO	-0.27	0.12	0.30	0.10	0.45	1.00				
CaO	-0.37	-0.01	0.33	0.26	-0.11	-0.18	1.00			
Na <sub>2</sub> O	-0.53	0.57	0.64	0.03	0.62	0.26	-0.14	1.00		
K <sub>2</sub> O	-0.67	0.65	0.78	0.03	0.84	0.40	-0.21	0.78	1.00	
P <sub>2</sub> O <sub>5</sub>	0.52	-0.43	-0.67	0.09	-0.53	-0.12	0.01	-0.74	-0.71	1.00

Sandstones in the present study have been classified as per the scheme proposed by Herron (1988). In the bivariate log (Fe<sub>2</sub>O<sub>3</sub>/K<sub>2</sub>O) vs log (SiO<sub>2</sub>/Al<sub>2</sub>O<sub>3</sub>) plot (after Herron, 1988), (Fig 6.1), major sandstones fall in the arkose to sub-arkose field with some falling in arkose, and Lith-arenite to Quartz arenite field. Based on Na<sub>2</sub>O and K<sub>2</sub>O contents of sandstones, Crook (1974) classified the sandstones into 3 types (quartz-rich, quartz intermediate and quartz-poor). In the K<sub>2</sub>O wt. % versus Na<sub>2</sub>O wt. % bivariate diagram (Fig. 6.2) (after Crook, 1974) the

sandstones of the present study plot essentially in quartz-rich field corroborating with comparable high SiO<sub>2</sub> values (average SiO<sub>2</sub> content 88.78%) of typical quartz rich sandstone (average SiO<sub>2</sub> content: 89 wt.%).

A Provenance diagram (Fig. 6.3) using discriminant function by Roser and Korsch (1988) has been used for plotting major element oxides. The sandstones of the present study plot in the field of Quartzose sedimentary provenance. Quartzose sedimentary provenances, according to Roser and Korsch (1988), constitute suites at either passive continental margins, intracratonic sedimentary basins or recycled orogenic provinces. The boundaries of Quartzose sedimentary provenance field in the provenance discrimination diagram of Roser and Korsch (1988) were drawn based on chemical composition of rock types of a certain terrain in New Zealand. The terrain is composed of sandstones and argillites of Ordovician Greenland Group. The source for these sedimentary rocks was either a deeply weathered granitic-gneissic terrain or from a pre-existing sedimentary terrain (Nathan, 1976). The rock types of Quartzose sedimentary provenance of the sandstones of the present study may be composed of varied sedimentary lithounit with detrital grains sourced from different crystalline rocks and/or pre-existing sedimentary rocks. Thus, the Quartzose sedimentary provenance of the present study area cannot be assessed accurately from available geochemical data, however the bulk chemical composition of “ultimate” crystalline rock source can be inferred from using Al<sub>2</sub>O<sub>3</sub>/TiO<sub>2</sub> ratio in an equation provided by Hayashi et al., (1997). Owing to the low solubility of Al and Ti oxides and hydroxides in low temperature aqueous solution (e.g., Stumm and Morgan, 1970, 2012), they remain essentially immobile. Hence, the Al<sub>2</sub>O<sub>3</sub>/TiO<sub>2</sub> ratios of sedimentary rocks derived from fluvially transported detrital siliciclastic material should be practically similar to those of their magmatic source rocks. According to Hayashi et al., (1997) the SiO<sub>2</sub> content of normal igneous rocks can be evaluated from their Al<sub>2</sub>O<sub>3</sub>/TiO<sub>2</sub> ratio using the equation below:

$$\text{SiO}_2 \text{ (wt. \%)} = 39.34 + 1.2578 (\text{Al}_2\text{O}_3/\text{TiO}_2) - 0.0109 (\text{Al}_2\text{O}_3/\text{TiO}_2)^2$$

The  $\text{Al}_2\text{O}_3/\text{TiO}_2$  ratios of the present study were substituted in the equation of Hayashi et al., (1997), and the  $\text{SiO}_2$  content of the inferred magmatic source rock is 75.42%. These values are suggestive of a felsic igneous parent rock to Quartzose sedimentary provenance. A bivariate diagram (Fig. 6.4) suggested by McLennan et al., (1980) based on the invariable properties of Al and Ti, further supports in developing and understanding towards the provenance of siliciclastic rocks. On this diagram, the sandstones of the present study plot along Granite trend line.

The provenance discriminant diagram suggested by Roser and Korsh (1988), provenance discriminant equation of Hayashi et al., (1997) and provenance discrimination diagrams of McLennan et al., (1980), together suggest that the detritus involved in the formation of sandstones were derived from Quartzose sedimentary provenance, the bulk chemical composition of which is granitic. Thus, Quartzose sedimentary provenance constitutes “Proximal” provenance and granitic terrain, “ultimate” provenance.

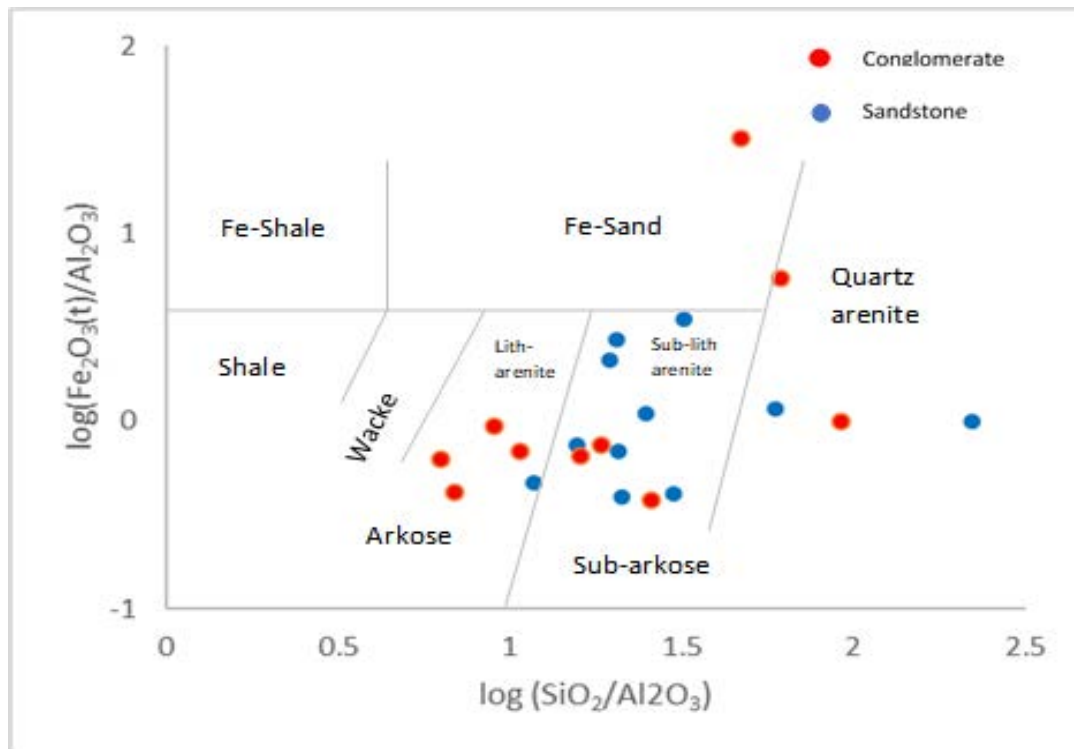


Figure 6.1 Geochemical classification of sandstones. (a)  $\log (\text{Fe}_2\text{O}_3/\text{K}_2\text{O})$  versus  $\log (\text{SiO}_2/\text{Al}_2\text{O}_3)$ .

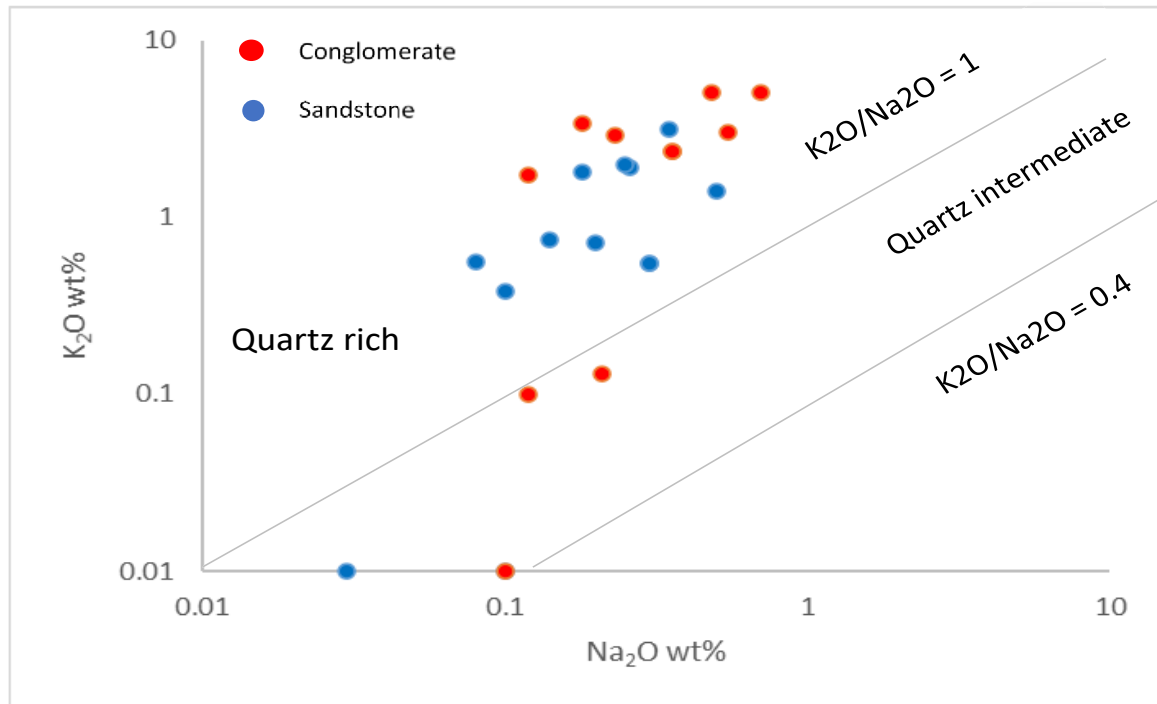


Figure 6.2 Bivariate diagram  $K_2O$  wt.% versus  $Na_2O$  wt.% bivariate diagram (after Crook 1974).

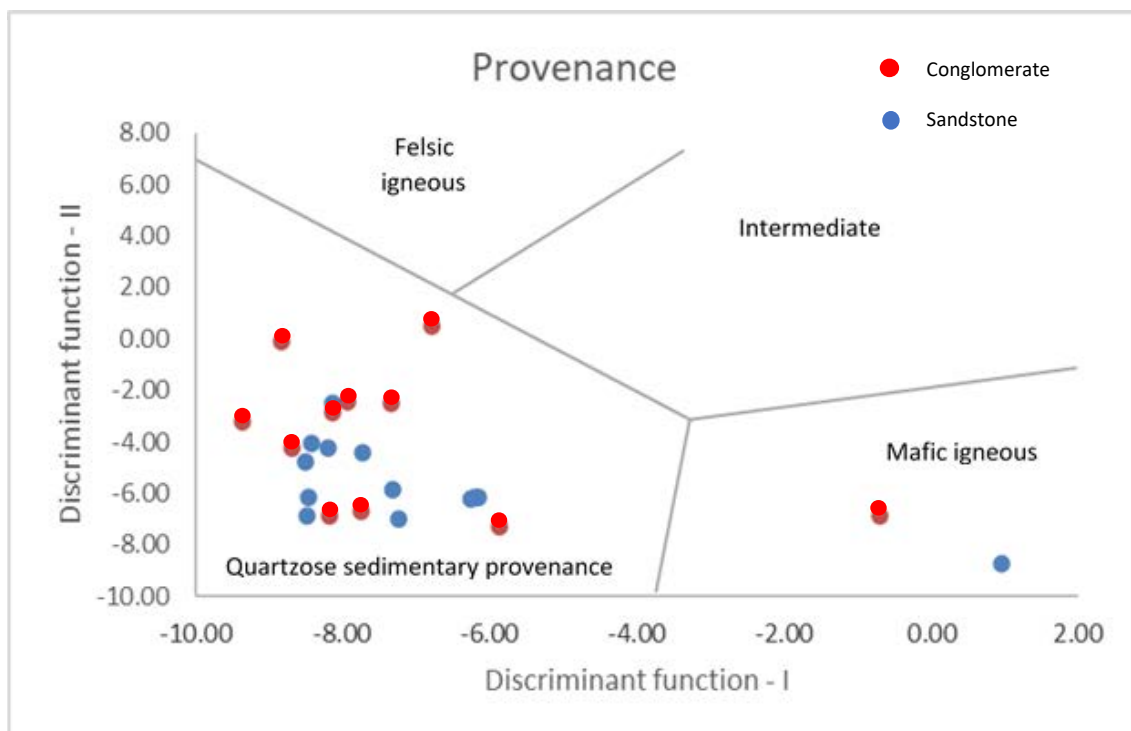


Figure 6.3 Provenance discrimination plot (after McLennan et al., 1980; Schieber, 1992)

**Discriminant Function 1** =  $(-1.773 \times TiO_2\%) + (0.607 \times Al_2O_3\%) + (0.76 \times Fe_2O_3T\%) + (-1.5 \times MgO\%) + (0.616 \times CaO\%) + (0.509 \times Na_2O\%) + (-1.22 \times K_2O\%) + (-9.09)$ .

**Discriminant Function 2** =  $(0.445 \times TiO_2\%) + (0.07 \times Al_2O_3\%) + (-0.25 \times Fe_2O_3T\%) + (-1.142 \times MgO\%) + (0.432 \times Na_2O\%) + (1.426 \times K_2O\%) + (-6.861)$

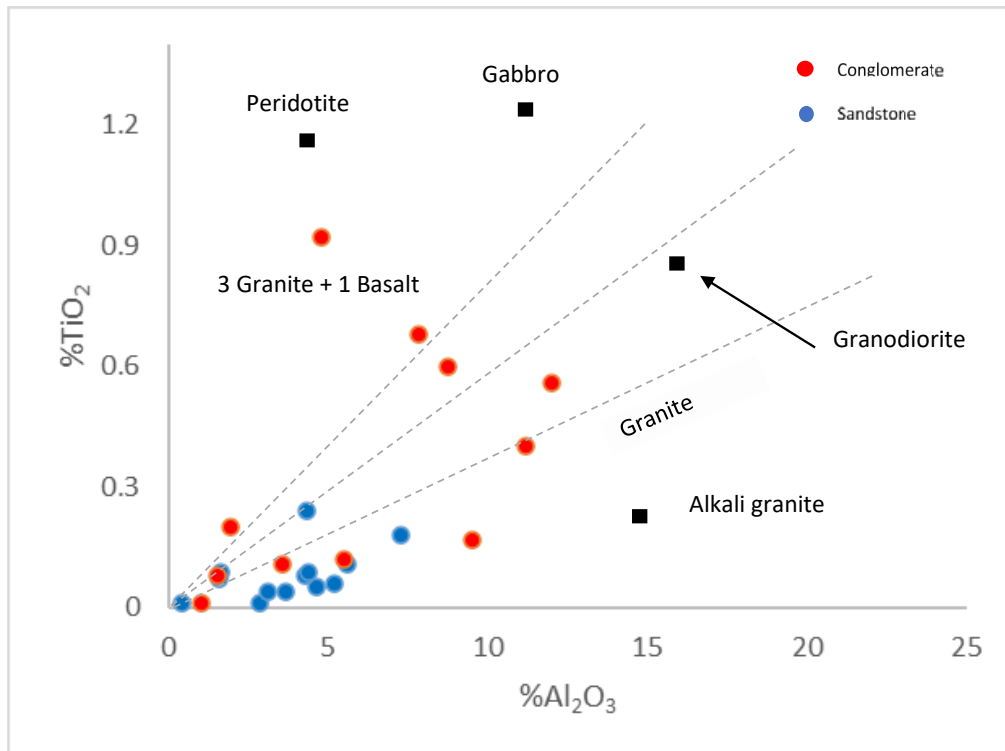


Figure 6.4 Provenance discrimination plot TiO<sub>2</sub> wt% vs Al<sub>2</sub>O<sub>3</sub> wt% (after McLennan et al., 1980). The “granite line” and “3 granite + 1 basalt line” are after Schieber, (1992).

## 6.2 Paleoweathering

The intensity of chemical weathering is a function of majorly source rock composition, duration of weathering, climatic conditions and rate of tectonic uplift of the source region (e.g., Wronkiewicz and Codie, 1987). Feldspars and volcanic glass constitute about 75% of the labile material of the upper crust. Chemical weathering of these materials results in formation of clay minerals (e.g., Nesbitt and Young, 1984, 1989; Taylor and McLennan, 1985; Fedo et al., 1995). During chemical weathering Ca, Na and K are largely removed from source rocks. If a siliciclastic sedimentary rock is free from post depositional modifications, then their alkali contents (K<sub>2</sub>O+Na<sub>2</sub>O) and K<sub>2</sub>O/Na<sub>2</sub>O ratios are considered as reliable indicators of weathering intensity of source material. Quantitative assessment of weathering has been proposed using a few indices based on molecular proportions of mobile and immobile elements oxides (Na<sub>2</sub>O,

CaO, K<sub>2</sub>O and Al<sub>2</sub>O<sub>3</sub>). Chemical Index of Alteration (CIA; Nesbitt and Young, 1982) is a well-established method for quantifying source area weathering.

$$CIA = \{Al_2O_3 / (Al_2O_3 + CaO^* + Na_2O + K_2O)\} \times 100$$

In the above equations the major oxides are expressed in molar proportions and CaO\* is the content of CaO incorporated in silicate fraction. CIA values of the sandstones was calculated, assuming the entire CaO content of the sandstones as that of silicate fraction. The CIA value of 69.32% indicates that provenance of sandstone was subjected to low to moderate weathering in source region. Source weathering and elemental distribution during diagenesis also can be assessed using Plagioclase Index of Alteration (PIA; Fedo et al., 1995)

$$PIA = \{(Al_2O_3 - K_2O) / ((Al_2O_3 - K_2O) + CaO^* + Na_2O)\} \times 100.$$

PIA values indicate the intensity of weathering varying from 61.49 to 96.36% (average = 81.82%) PIA monitors and quantifies progressive weathering of feldspars to clay minerals (e.g., Fedo et al., 1995). PIA values of the sandstones suggest moderate to intense destruction of feldspars during source weathering, transport, sedimentation, and diagenesis. During the initial stages of weathering Ca is leached rapidly than Na and K. With increasing weathering total alkali content (K<sub>2</sub>O + Na<sub>2</sub>O) decreases with increase in (K<sub>2</sub>O/Na<sub>2</sub>O) ratio. This is due to destruction of feldspars among which plagioclase is more preferentially removed than K-feldspars (Nesbitt and Young, 1984). Feldspathic material of the sandstones of the present study was subjected to variable intensities of weathering during different stages of evolution of the sandstones. Sandstones preserve the imprints of chemical weathering witnessed by feldspathic components. The mobility of elements during final stages of chemical weathering of previously and variously altered feldspars may be visualized from bivariate plots involving Na<sub>2</sub>O, K<sub>2</sub>O, CaO, SiO<sub>2</sub> and PIA. Negative correlation between Na<sub>2</sub>O wt.% and PIA may be attributed to the presence of K-bearing minerals (e.g., muscovite and illite), while the positive



correlation between PIA and  $K_2O/Na_2O$  suggest that with increase in PIA, plagioclase gets selectively altered before K-feldspars.

Weathering indices also provide useful information on tectonic activity and climatic conditions in the source region. Increase in the intensity of chemical weathering is corroborated with decrease in tectonic activity and/or change of climate towards warm and humid conditions which are more favorable for chemical weathering in source region (e.g., Jacobson and Blum, 2003). The presence of fresh and altered feldspars in the study samples indicate humid and warm climatic conditions (Folk, 1980). Suttner and Dutta (1986) proposed a binary  $SiO_2$  wt.% versus  $(Al_2O_3 + K_2O + Na_2O)$  wt.% diagram to constrain the climatic condition during sedimentation of siliciclastic sedimentary rocks. On this diagram the sandstones plot essentially in the field of humid climate (Fig. 6.5)

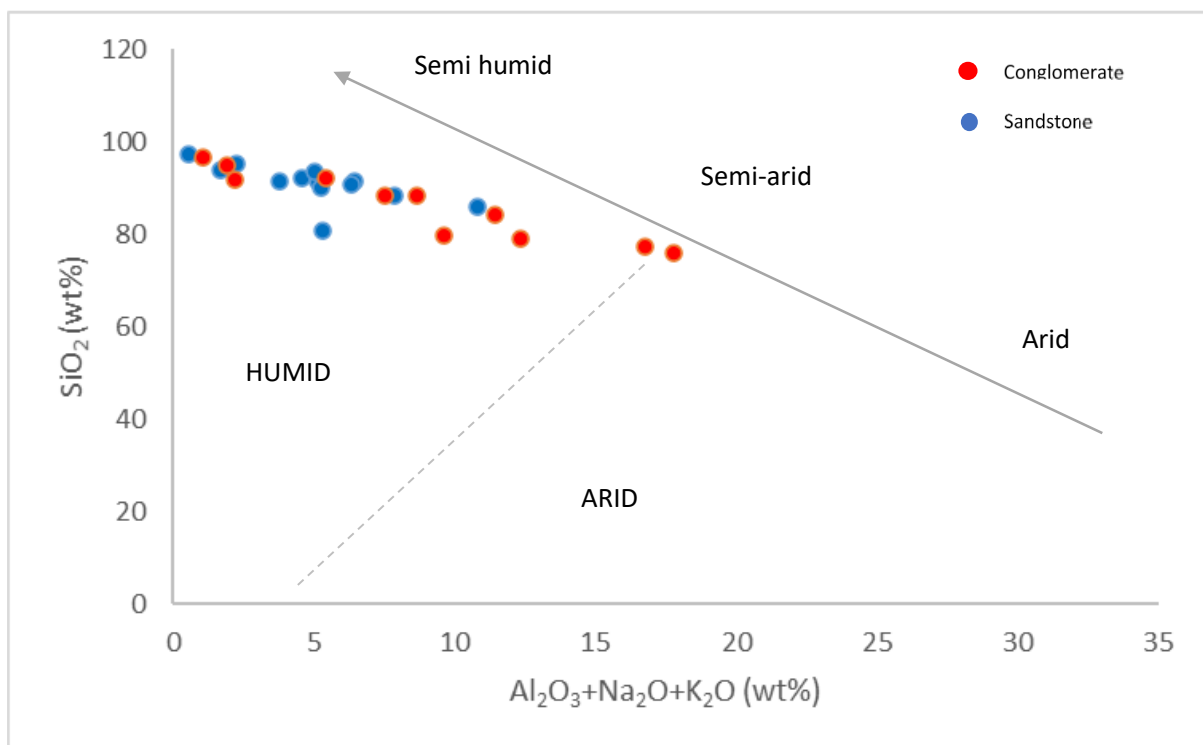


Figure 6.5  $SiO_2$  (wt%) vs  $Al_2O_3 + K_2O + Na_2O$  (wt%) binary variation plot (after Suttner and Dutta, 1986).

### 6.3 Tectonic setting

The chemical composition of siliciclastic sedimentary rocks is significantly controlled by plate tectonic settings of their provenance. Thus, the siliciclastic rocks from different tectonic settings possess terrain-specific geochemical signatures (Bhatia, 1983; Bhatia and Crook, 1986; Roser and Korsch, 1986) and provide reliable results provided the siliciclastic rocks have not been strongly affected by post depositional weathering/metasomatism/metamorphism (McLennan et al., 1993). Several tectonic setting discrimination diagrams to infer tectonic setting of provenance of ancient siliciclastic sedimentary rocks, have been proposed. However, the major element-based discrimination diagrams of Bhatia (1983) and Roser and Korsch (1986) (Fig. 6.6) are widely used wherein, the bivariate including discriminant functions, are based on immobile and variably mobile major elements, including  $\text{Na}_2\text{O}$  and  $\text{K}_2\text{O}$ . Chemical analyses data of the present study samples were plotted in the widely used  $\text{K}_2\text{O}/\text{Na}_2\text{O}$  vs  $\text{SiO}_2$  wt% diagram proposed by Roser and Korsch (1986). The sandstones from the study area plot essentially in passive margin (PM) field.

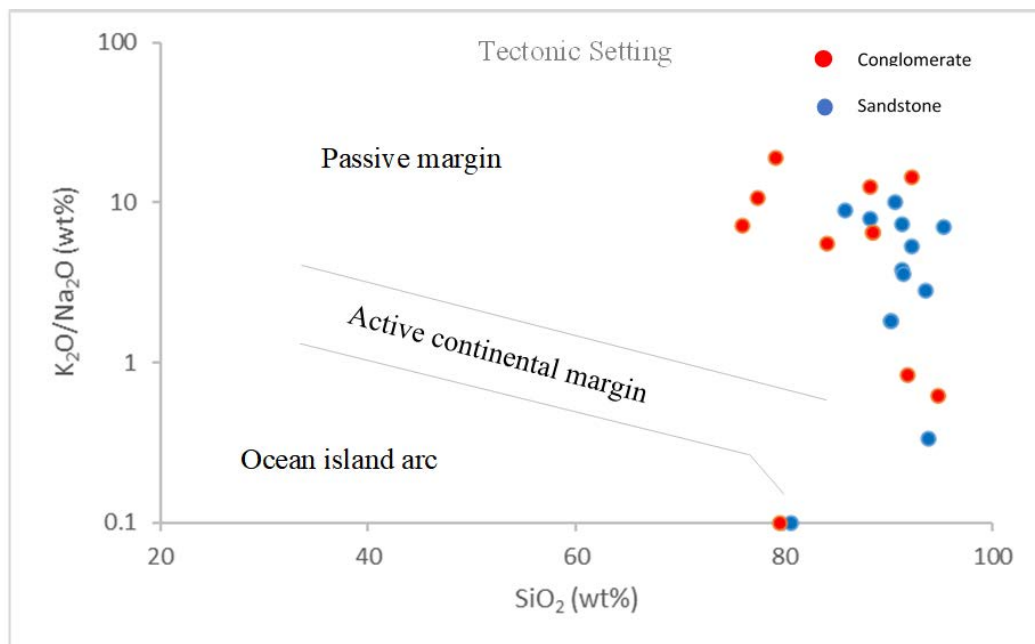


Figure 6.6  $\text{SiO}_2$  vs  $\text{K}_2\text{O}/\text{Na}_2\text{O}$  plot after Roser and Korsch, (1986) shows passive continental margin setting of the studied conglomerate

## 6.4 Geochemistry of pebbly feldspathic arenite/Lower conglomerate

Pebbly feldspathic arenite/lower conglomerate representing the second major depositional cycle is prime host of uranium mineralization in the study area. Geochemical analysis was carried out with the objective to characterize the nature of lithounit and simultaneously to draw a comparison between the radioactive and non-radioactive horizons. Radioactive (n=11) and non-radioactive (n=10) samples were selected from mineralized boreholes SLD-100 and SLD-102. All major oxides exhibit broad range in wt% as tabulated in the Table 6.2 and Table 6.3.

Table 6.2 Major, minor and trace elements of selected non-radioactive samples

Oxides in %	FG-292	FG-293	FG-294	FG-295	FG-296	FG-297	FG-298	FG-299	FG-300	FG-301
SiO <sub>2</sub>	81.70	62.61	88.74	90.76	88.40	53.51	86.78	52.94	81.81	63.88
TiO <sub>2</sub>	0.05	0.62	0.05	0.04	0.07	0.91	0.46	1.29	0.16	1.29
Al <sub>2</sub> O <sub>3</sub>	8.49	20.14	5.54	4.37	5.43	19.99	6.30	23.48	9.12	12.97
Fe <sub>2</sub> O <sub>3</sub> (t)	1.71	2.37	0.62	0.65	1.29	7.73	0.78	2.99	1.10	6.84
MgO	0.81	1.44	0.02	0.02	0.24	2.79	0.25	2.01	0.28	1.68
MnO	0.06	0.09	0.01	0.01	0.02	0.05	0.01	0.05	0.01	0.08
CaO	0.08	0.16	0.04	0.05	0.06	0.27	0.06	0.25	0.06	0.45
Na <sub>2</sub> O	0.30	0.42	0.34	0.03	0.13	0.30	0.20	0.40	0.41	0.40
K <sub>2</sub> O	4.79	8.32	3.53	2.53	3.30	8.31	3.32	9.49	5.43	4.97
P <sub>2</sub> O <sub>5</sub>	0.02	0.06	0.06	0.01	0.04	0.03	0.02	0.04	0.02	0.12
LOI	1.49	3.71	0.48	0.43	0.84	5.62	0.94	6.68	1.13	6.85
<b>Total</b>	<b>99.51</b>	<b>99.96</b>	<b>99.44</b>	<b>98.91</b>	<b>99.82</b>	<b>99.52</b>	<b>99.11</b>	<b>99.62</b>	<b>99.51</b>	<b>99.53</b>
Elements in ppm										
Ni	26	37	15	17	17	80	13	26	12	40
Cu	369	235	110	280	13	54	221	73	1223	36
Zn	50	65	11	13	16	47	16	57	12	37
Rb	158	250	126	119	122	304	135	321	168	203
Sr	71	72	64	51	58	40	48	45	84	23
Ba	556	745	466	301	438	660	379	563	648	350
Zr	101	376	86	68	85	198	308	259	152	455
Nb	<10	3	0	<10	<10	10	6	8	5	16
Pb	7	27	8	1	6	<10	4	5	10	35
U#	38	68	22	40	12	<10	27	45	58	<10

Table 6.3 Major, minor and trace elements of selected radioactive samples

Oxides in %	24/LC/9	25/LC/10	26/LC/11	27/LC/12	28/LC/13	29/LC/14	30/LC/15	37/LC/22	41/LC/26	FG-290	FG-291
SiO <sub>2</sub>	90.53	93.73	63.35	89.17	93.70	77.00	81.52	87.33	56.61	84.36	85.50
TiO <sub>2</sub>	0.01	0.02	0.52	0.01	0.01	0.19	0.01	0.01	0.01	0.10	0.06
Al <sub>2</sub> O <sub>3</sub>	4.23	2.53	16.17	5.15	2.35	12.03	10.17	6.71	20.58	7.83	6.89
Fe <sub>2</sub> O <sub>3</sub> (t)	1.94	1.60	6.89	2.44	1.56	2.67	1.62	1.01	5.93	0.94	1.26
MgO	0.32	0.32	1.35	0.39	0.61	0.80	0.66	0.34	1.88	0.21	0.23
MnO	0.03	0.02	0.17	0.06	0.01	0.06	0.03	0.02	0.25	0.01	0.02
CaO	0.07	0.06	0.20	0.08	0.12	0.11	0.06	0.05	0.31	0.06	0.05
Na <sub>2</sub> O	0.32	0.27	0.28	0.01	0.33	0.15	0.91	0.07	0.50	0.18	0.09
K <sub>2</sub> O	1.66	1.07	5.47	1.83	0.83	4.13	3.65	2.42	6.51	4.60	3.90
P <sub>2</sub> O <sub>5</sub>	0.00	0.00	0.04	0.00	0.13	0.03	0.00	0.00	0.14	0.00	0.01
LOI	0.84	0.55	5.04	1.34	0.44	2.80	1.23	1.08	7.76	1.49	1.09
<b>Total</b>	<b>99.94</b>	<b>100.18</b>	<b>99.49</b>	<b>100.47</b>	<b>100.10</b>	<b>99.96</b>	<b>99.85</b>	<b>99.03</b>	<b>100.48</b>	<b>99.78</b>	<b>99.11</b>
<b>Elements in ppm</b>											
Ni	21	23	112	23	24	46	19	14	27	42	56
Cu	1085	1144	1513	4732	309	3524	3557	7195	6271	312	2128
Zn	31	29	120	43	22	207	61	40	149	22	23
Rb	63	62	275	96	39	178	157	104	402	158	138
Sr	29	29	45	28	25	38	46	44	180	69	79
Zr	58	98	237	85	86	250	127	187	261	101	96
Nb	<10	16	15	2	<10	12	6	7	27	1	7
Ba	196	174	1101	440	77	586	472	351	2387	529	619
Pb	20	73	94	36	19	59	31	36	239	26	32
U#	122	1234	768	392	219	1339	708	500	1400	194	697

The average major oxide composition of uraniferous feldspathic arenite/lower conglomerate samples show relatively low SiO<sub>2</sub>, TiO<sub>2</sub>, Na<sub>2</sub>O and CaO, and high Al<sub>2</sub>O<sub>3</sub>, Fe<sub>2</sub>O<sub>3</sub>, K<sub>2</sub>O while other major oxides including, P<sub>2</sub>O<sub>5</sub>, MgO and MnO show similar values. Similarly, average non-uraniferous arenite show depletion in SiO<sub>2</sub>, CaO, Na<sub>2</sub>O, while marked enrichment in Al<sub>2</sub>O<sub>3</sub> and K<sub>2</sub>O. TiO<sub>2</sub>, Fe<sub>2</sub>O<sub>3</sub>, MgO and MnO show comparable values with average Proterozoic sandstone. Major, minor oxides and trace element normalized spider diagram has been generated to draw comparisons between radioactive and non-radioactive samples (Fig. 7). Geochemically, both the varieties show overlapping chemical composition, except the uraniferous conglomerates show high content of Cu, Pb and Zn indicating their association with chalcophile elements. The major, minor and trace element composition of the selected uraniferous (U > 100ppm) and non uraniferous (U < 100 ppm) samples along with Average Proterozoic Cratonic Sandstone (APCS) is given in Table 6.4.

Table 6.4 Average of major, minor and trace elements of pebbly feldspathic arenite/lower conglomerate against Proterozoic Cratonic Sandstone after Condie, 1993

Oxides in wt%	Radioactive (n=11)	Non radioactive (n=10)	APCS
SiO <sub>2</sub>	82.07	75.11	92.15
TiO <sub>2</sub>	0.09	0.50	0.17
Al <sub>2</sub> O <sub>3</sub>	8.60	11.58	3.87
Fe <sub>2</sub> O <sub>3</sub> (t)	2.53	2.61	1.32
MgO	0.65	0.95	0.55
MnO	0.06	0.04	NA
CaO	0.11	0.15	0.45
Na <sub>2</sub> O	0.28	0.29	0.51
K <sub>2</sub> O	3.28	5.40	0.88
P <sub>2</sub> O <sub>5</sub>	0.03	0.04	0.03
LOI	2.15	2.82	NA
Elements in ppm	Radioactive (n=11)	Non radioactive (n=10)	APCS
Ni	37	28	11
Cu	2888	261	NA
Zn	68	32	NA
Rb	152	191	30
Sr	56	56	27
Zr	144	209	89
Nb	8	209	4
Ba	630	511	190
Pb	60	10	20
U#	688	30	1

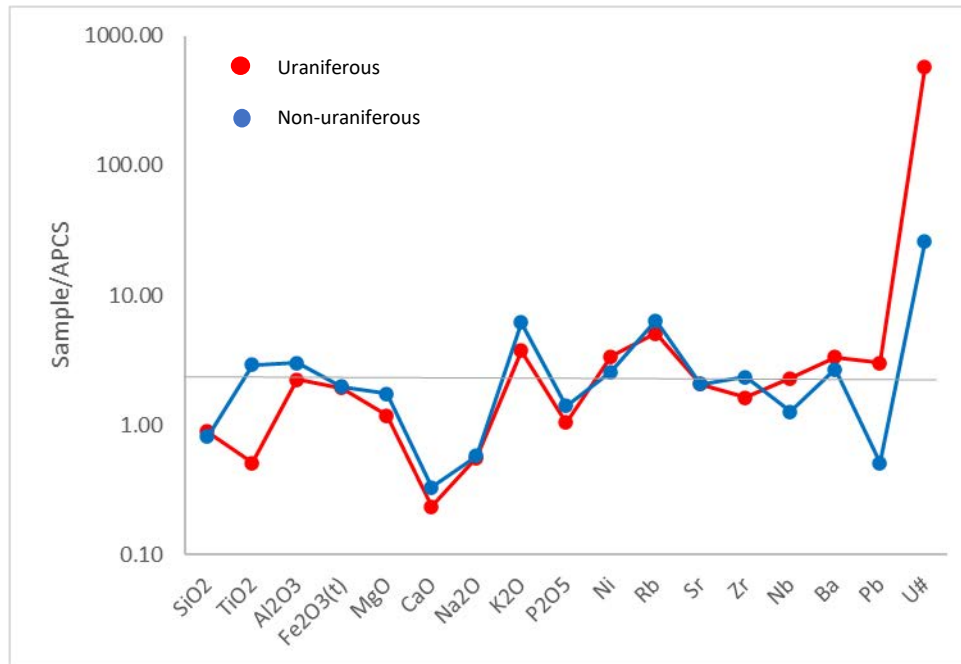


Figure 6.7 Average Proterozoic Cratonic Sandstone (APCS) normalized spider diagram for uraniferous and non uraniferous conglomerate.

In both cases, uraniferous and non uraniferous samples exhibit negative correlation of major oxides with  $\text{SiO}_2$  indicating most of it present in the form of quartz.  $\text{SiO}_2$  shows strong negative correlation with  $\text{K}_2\text{O}$  ( $r = -0.90$ ) indicating decrease of clay content with increase of quartz. Positive correlation between  $\text{Al}_2\text{O}_3$  and  $\text{K}_2\text{O}$  in uraniferous ( $r = 0.92$ ) and non uraniferous samples ( $r = 0.98$ ) suggest presence of potassic minerals. This co-variation indicates that K-bearing minerals have significant influence on Al distribution and suggests that the bulk of Al and K is primarily contributed by potassic minerals which may include K-feldspar, illite or even micas. Higher  $\text{K}_2\text{O}/\text{Na}_2\text{O}$  ratio is indicative of abundance of K-feldspar and micas while lower  $\text{K}_2\text{O}/\text{Na}_2\text{O}$  indicates predominance of clays.  $\text{K}_2\text{O}/\text{Na}_2\text{O}$  ratios of uraniferous samples show average value of 32.96 while in case of non-uraniferous samples, the average value was recorded to be 24.95 which suggests predominance of feldspars/micas over clay. The  $\text{K}_2\text{O}/\text{Al}_2\text{O}_3$  ratio may suggest how much alkali feldspar vs. plagioclase and clay minerals were present in the original rocks (Cox et al., 1995). The  $\text{K}_2\text{O}/\text{Al}_2\text{O}_3$  ratio decreases from alkali feldspar ( $\approx 0.4-1$ ), illite ( $\approx 0.3$ ) to other clay minerals ( $\approx 0$ ) (Cox et al., 1995).  $\text{K}_2\text{O}/\text{Al}_2\text{O}_3$  values for feldspar range from 0.4 to 1.0, while for clay minerals the value of  $\text{K}_2\text{O}/\text{Al}_2\text{O}_3$  is generally less than 0.3. For uraniferous samples, the average value of  $\text{K}_2\text{O}/\text{Al}_2\text{O}_3$  is 0.40 while in case of non uraniferous samples, the average value of  $\text{K}_2\text{O}/\text{Al}_2\text{O}_3$  is 0.51, thereby suggesting predominance of feldspars over clay in both the cases, however relatively lower  $\text{K}_2\text{O}/\text{Al}_2\text{O}_3$  ratios in case of uraniferous samples is indicative of correspondingly higher alteration of feldspars to clays. Also, strong negative correlation between  $\text{MgO}$  and  $\text{SiO}_2$ , uraniferous samples ( $r = -0.91$ ) and non-uraniferous samples ( $r = -0.96$ ) refutes presence of mica.



Table 6.5 Correlation matrix of major and trace elements composition of uraniferous pebbly feldspathic arenite/lower conglomerate

	<i>SiO<sub>2</sub></i>	<i>TiO<sub>2</sub></i>	<i>Al<sub>2</sub>O<sub>3</sub></i>	<i>Fe<sub>2</sub>O<sub>3</sub>(t)</i>	<i>MgO</i>	<i>MnO</i>	<i>CaO</i>	<i>Na<sub>2</sub>O</i>	<i>K<sub>2</sub>O</i>	<i>P<sub>2</sub>O<sub>5</sub></i>	<i>LOI</i>	<i>Ni</i>	<i>Cu</i>	<i>Zn</i>	<i>Rb</i>	<i>Sr</i>	<i>Zr</i>	<i>Nb</i>	<i>Ba</i>	<i>Pb</i>	<i>U#</i>
<b>SiO<sub>2</sub></b>	1.00																				
<b>TiO<sub>2</sub></b>	-0.53	1.00																			
<b>Al<sub>2</sub>O<sub>3</sub></b>	-0.99	0.48	1.00																		
<b>Fe<sub>2</sub>O<sub>3</sub>(t)</b>	-0.88	0.66	0.82	1.00																	
<b>MgO</b>	-0.91	0.39	0.89	0.90	1.00																
<b>MnO</b>	-0.93	0.42	0.89	0.94	0.95	1.00															
<b>CaO</b>	-0.87	0.35	0.83	0.89	0.97	0.96	1.00														
<b>Na<sub>2</sub>O</b>	-0.28	-0.11	0.31	0.17	0.38	0.20	0.25	1.00													
<b>K<sub>2</sub>O</b>	-0.91	0.49	0.93	0.65	0.69	0.73	0.66	0.21	1.00												
<b>P<sub>2</sub>O<sub>5</sub></b>	-0.46	-0.02	0.41	0.49	0.71	0.58	0.78	0.24	0.26	1.00											
<b>LOI</b>	-0.97	0.42	0.94	0.89	0.94	0.98	0.95	0.20	0.83	0.57	1.00										
<b>Ni</b>	-0.52	0.95	0.46	0.62	0.35	0.41	0.35	-0.16	0.54	0.02	0.41	1.00									
<b>Cu</b>	-0.36	-0.24	0.42	0.18	0.34	0.37	0.26	-0.02	0.26	0.08	0.38	-0.31	1.00								
<b>Zn</b>	-0.74	0.46	0.77	0.64	0.72	0.64	0.63	0.11	0.62	0.32	0.72	0.35	0.35	1.00							
<b>Rb</b>	-0.98	0.40	0.98	0.81	0.88	0.91	0.86	0.28	0.93	0.46	0.97	0.43	0.39	0.68	1.00						
<b>Sr</b>	-0.72	-0.09	0.73	0.47	0.67	0.72	0.72	0.23	0.75	0.55	0.78	0.03	0.41	0.35	0.83	1.00					
<b>Zr</b>	-0.84	0.51	0.86	0.70	0.79	0.73	0.70	0.08	0.73	0.37	0.81	0.41	0.52	0.88	0.80	0.49	1.00				
<b>Nb</b>	-0.74	0.27	0.73	0.64	0.73	0.74	0.67	0.17	0.63	0.37	0.76	0.28	0.42	0.62	0.77	0.66	0.77	1.00			
<b>Ba</b>	-0.92	0.22	0.91	0.77	0.88	0.93	0.89	0.23	0.84	0.57	0.96	0.27	0.45	0.59	0.96	0.91	0.71	0.77	1.00		
<b>Pb</b>	-0.82	0.13	0.80	0.76	0.88	0.91	0.90	0.24	0.65	0.62	0.92	0.14	0.43	0.58	0.86	0.84	0.69	0.86	0.93	1.00	
<b>U#</b>	-0.55	0.17	0.57	0.45	0.58	0.53	0.49	0.17	0.45	0.25	0.58	0.14	0.36	0.72	0.57	0.46	0.69	0.90	0.56	0.70	1.00

Table 6.6 Correlation matrix of major and trace elements composition of non-uraniferous pebbly feldspathic arenite/lower conglomerate

	$SiO_2$	$TiO_2$	$Al_2O_3$	$Fe_2O_3(t)$	$MgO$	$MnO$	$CaO$	$Na_2O$	$K_2O$	$P_2O_5$	$LOI$	$Ni$	$Cu$	$Zn$	$Rb$	$Sr$	$Zr$	$Nb$	$Ba$	$Pb$	$U\#$
$SiO_2$	1.00																				
$TiO_2$	-0.88	1.00																			
$Al_2O_3$	-0.97	0.80	1.00																		
$Fe_2O_3(t)$	-0.78	0.76	0.61	1.00																	
$MgO$	-0.96	0.83	0.90	0.88	1.00																
$MnO$	-0.72	0.62	0.69	0.61	0.70	1.00															
$CaO$	-0.79	0.91	0.64	0.89	0.80	0.71	1.00														
$Na_2O$	-0.62	0.52	0.63	0.36	0.49	0.56	0.48	1.00													
$K_2O$	-0.93	0.69	0.98	0.53	0.85	0.63	0.52	0.67	1.00												
$P_2O_5$	-0.37	0.56	0.25	0.51	0.32	0.58	0.73	0.50	0.14	1.00											
$LOI$	-0.94	0.96	0.85	0.84	0.91	0.72	0.94	0.56	0.76	0.57	1.00										
$Ni$	-0.75	0.56	0.65	0.89	0.88	0.57	0.64	0.25	0.60	0.22	0.67	1.00									
$Cu$	0.27	-0.38	-0.20	-0.36	-0.35	-0.31	-0.38	0.22	-0.07	-0.39	-0.37	-0.36	1.00								
$Zn$	-0.81	0.60	0.85	0.49	0.78	0.88	0.54	0.53	0.83	0.23	0.71	0.58	-0.29	1.00							
$Rb$	-0.98	0.81	0.98	0.67	0.93	0.61	0.65	0.58	0.97	0.19	0.86	0.70	-0.20	0.80	1.00						
$Sr$	0.41	-0.70	-0.24	-0.67	-0.49	-0.24	-0.74	0.13	-0.07	-0.49	-0.63	-0.45	0.68	-0.12	-0.30	1.00					
$Zr$	-0.53	0.13	0.65	0.19	0.47	0.42	0.04	0.64	0.76	-0.12	0.25	0.41	0.32	0.60	0.61	0.51	1.00				
$Nb$	-0.60	0.78	0.54	0.52	0.52	0.67	0.74	0.54	0.43	0.67	0.69	0.31	-0.21	0.49	0.47	-0.47	0.11	1.00			
$Ba$	-0.69	0.86	0.55	0.77	0.67	0.43	0.85	0.54	0.46	0.55	0.80	0.52	-0.08	0.31	0.59	-0.65	0.04	0.76	1.00		
$Pb$	-0.25	0.38	0.20	0.26	0.14	0.66	0.54	0.53	0.12	0.84	0.38	0.01	-0.04	0.30	0.08	-0.14	0.04	0.73	0.40	1.00	
$U\#$	0.07	-0.27	0.14	-0.59	-0.26	0.02	-0.45	0.22	0.24	-0.40	-0.27	-0.43	0.58	0.20	0.04	0.74	0.47	-0.06	-0.33	0.05	1.00

Mineralogical composition of sandstone other than quartz can be assessed by determination of ICV (Index of compositional variation) by Cox et.al, (1995).

$$ICV = (Fe_2O_3 + K_2O + Na_2O + CaO + MgO + MnO + TiO_2) / Al_2O_3$$

High ICV values are indicative of mineralogical immaturity of sandstone such that  $ICV > 1$  suggests predominance of plagioclase, K feldspar, amphiboles, pyroxenes and lithics. ICV values for uraniferous samples range between (0.58 to 1.48, Avg. 0.91) and for non-uraniferous samples, range between (0.67 to 1.21, Avg. 0.87) which suggests that both radioactive and non-uraniferous samples exhibit low mineralogical maturity. Based on the relative molecular proportions of the major oxides ( $Na_2O$ ,  $CaO$ ,  $K_2O$ ,  $Al_2O_3$ ), certain weathering indices have been proposed. Chemical Index of Alteration - CIA (Nesbitt and Young, 1982) are taken as measure of source rock alteration and redistribution of elements during diagenesis process.

$$CIA = (100) * [Al_2O_3 / (Al_2O_3 + CaO^* + Na_2O + K_2O)]$$

$CaO^*$  (only from silicate phases) determined as per McLennan et al. 1993, CIA values of uraniferous samples range between 55.39 and 67.93% (Avg. 62.42%) while for non uraniferous samples it ranges from 52.02 to 63.89% (Avg. 58.24%). As can be seen in the (Fig. 6.8) A-CN-K ternary plot, both uraniferous as well as non-uraniferous samples mostly exhibit low to moderate alteration while some of the uraniferous samples fall below the feldspar line indicating presence of unaltered feldspars within the matrix. In most cases, predominance of K-feldspars and its alteration product illite is indicated.

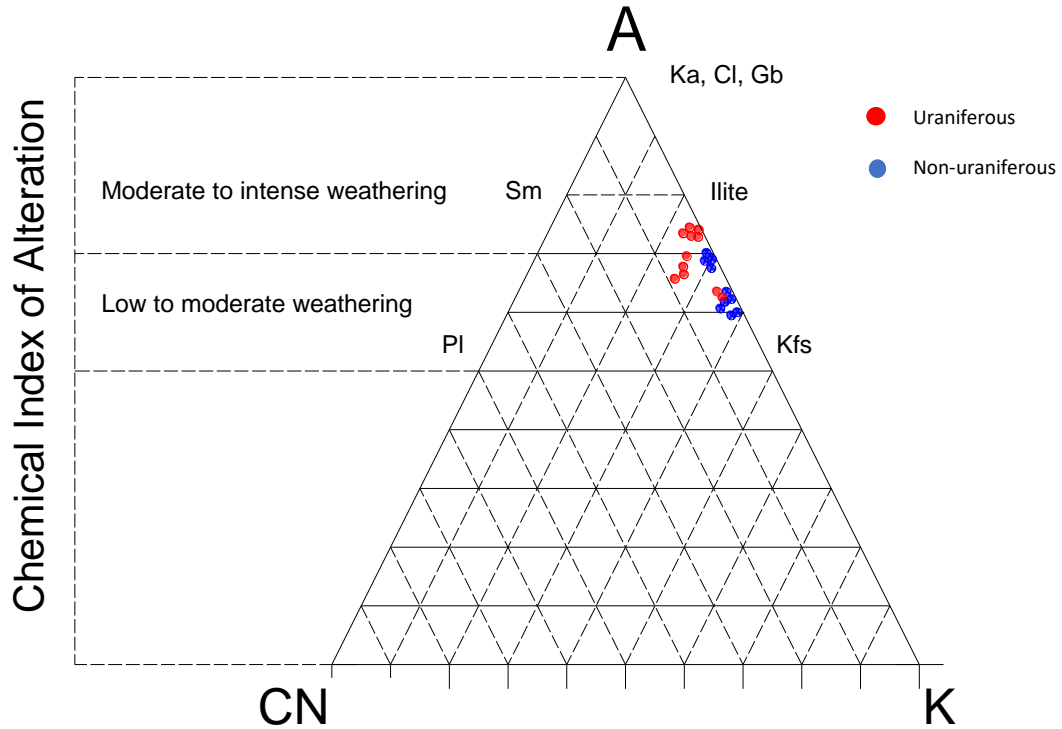


Figure 6.8 A-CN-K diagram showing the weathering trend of the high and low uraniferous matrix-supported conglomerate of the Badami Formation (After Nesbitt and Young, 1982).

A=Al<sub>2</sub>O<sub>3</sub>, CN=CaO+Na<sub>2</sub>O, K=K<sub>2</sub>O (molecular proportions).

On the binary plot between MgO/Al<sub>2</sub>O<sub>3</sub> versus K<sub>2</sub>O/Al<sub>2</sub>O<sub>3</sub> (Fig. 6.9), all uraniferous as well as non-uraniferous samples are clustered within the illite. Both TiO<sub>2</sub> and Al<sub>2</sub>O<sub>3</sub> are immobile within sedimentary environments and thereby, it is enriched with progressive weathering of the source material. Positive correlation between TiO<sub>2</sub> and Al<sub>2</sub>O<sub>3</sub> ( $r = 0.48$ ) in uraniferous samples and ( $r = 0.79$ ) in non-uraniferous samples indicates that TiO<sub>2</sub> is associated with phyllosilicates especially with illite (Dabard, 1990).

TiO<sub>2</sub> and Fe<sub>2</sub>O<sub>3</sub> ( $r = 0.60$ ) as well as between TiO<sub>2</sub> and CaO ( $r = 0.76$ ) in both radioactive and non-radioactive samples combined, indicate presence of ilmenite and sphene, respectively. TiO<sub>2</sub> also seems to exhibit strong negative correlation with SiO<sub>2</sub> in both uraniferous ( $r = -0.53$ ) and non-uraniferous ( $r = -0.88$ ) samples, suggests its concentration in detrital phases and not in adsorbed form, thereby presence of rutile, brookite also cannot be ruled out.

Non-uraniferous samples show good correlation between CaO & P<sub>2</sub>O<sub>5</sub> ( $r = 0.73$ ) and ( $r = 0.77$ ) in case of uraniferous suggesting presence of apatite.

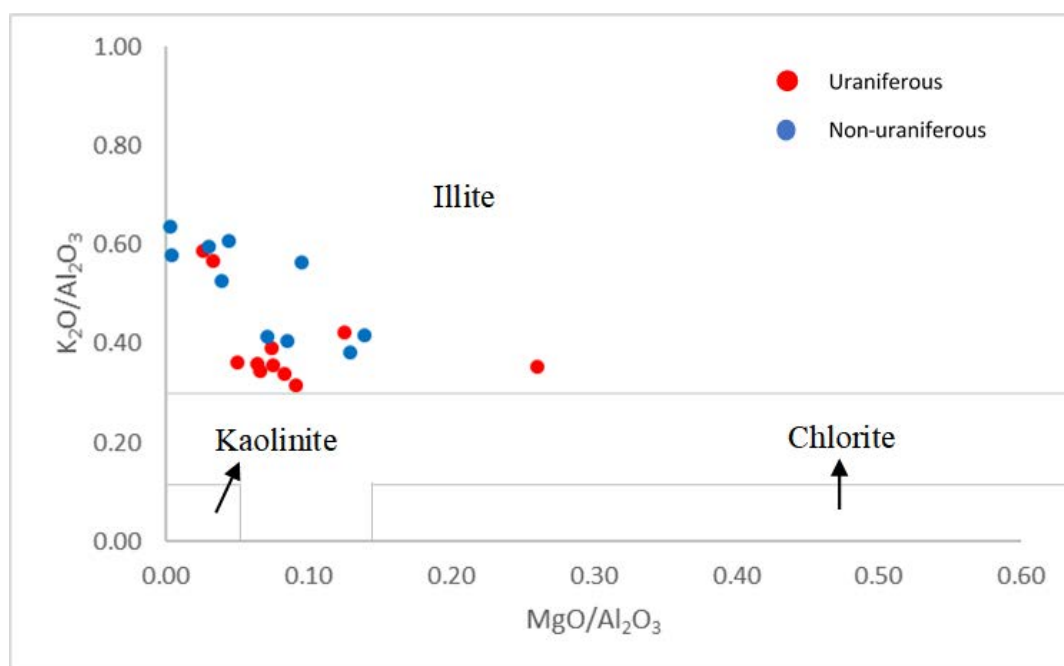


Figure 6.9 Binary plot between MgO/Al<sub>2</sub>O<sub>3</sub> versus K<sub>2</sub>O/Al<sub>2</sub>O<sub>3</sub> (after Sopuck, 1988)

Uranium shows moderately positive correlation with both CaO ( $r = 0.48$ ) and P<sub>2</sub>O<sub>5</sub> ( $r = 0.24$ ) indicating association uranium phases with apatite in case of uraniferous samples. Presence of calcium-uranium phosphatic complexes viz autunite varieties also cannot be ruled out. In case of uraniferous samples, U exhibits positive correlation Cu ( $r = 0.35$ ), Pb ( $r = 0.69$ ) and Zn ( $r = 0.71$ ) which is suggestive of close association of uranium with copper, lead and zinc sulphide phases. Presence of uranium mineralization and its association with copper sulphides has been established using petromineralogical studies. However, it has also been noticed that though, copper sulfides are usually linked to mineralization, it is does not hold true invariably as most copper sulfide assemblage can be seen occurring without any association of uranium bearing minerals. Hence a very strong correlation between U and Cu cannot be seen, despite higher concentrations up to 7195 ppm. Uranium exhibits weak positive correlation ( $r = 0.16$ ) thereby, presence of brannerite or U-Ti complexes is a possibility. In case of uraniferous samples, positive correlation of U with between Th ( $r = 0.45$ ), P<sub>2</sub>O<sub>5</sub> ( $r = 0.40$ ) and Y ( $r = 0.78$ )

is suggestive of presence of detrital monazite within the matrix. Positive correlation between U and Th ( $r = 0.45$ ) in uraniferous samples indicates presence of uranium bearing monazite. High and variable Zr both uraniferous (58 to 261, Avg. 144.18) as well as non-uraniferous (68 to 455, Avg. 208) samples point toward presence of detrital zircon. This is also complimented by heavy mineral studies.

## **CHAPTER 7**

### **DISCUSSION**

Badami Group of sediments in the study area unconformably overlie the basement Chitradurga Group of metasediments (Jayaprakash et al., 1987). Owing to the presence of a profound unconformity between basement Chitradurga group of metasediments and overlying Neoproterozoic Badami sediments and its proximity to Bababudan-Nallur shear zone (Sridhar et al. 2018), with previous exploration surveys contributing a significant correlatable sub-surface uranium mineralization, the study area becomes a potential target for uranium mineralization.

Stratigraphic evolution and architecture of Kerur formation has been extensively studied by Mukhopadhyay et al. (2019). The Cave Temple Arenite Member with its porosity, permeability, textural and mineralogical immaturity has been the most promising horizon for hosting uranium mineralisation in the Kaladgi Basin. The recent finding of uranium mineralisation in North Western part of Deshnur towards the interior of the basin gives an insight into the probable mode of mineralization in the basin (AMD 2013-2014). The present work was aimed to have a better geological understanding of the sector with reference to uranium mineralisation. A detailed sedimentological study of subsurface samples in Gujanal area is carried out with an objective to identify its control on uranium mineralization thereby suggesting an area specific model.

The Cave Temple Arenite Member in and around the study area has been investigated using sedimentology to understand the depositional setting and nature of occurrence of uranium mineralization in sediments. The detailed sedimentological study encompassed systematic collection of paleocurrent data to decipher the dominant paleo flow direction, preparation and



correlation of lithologs to delineate various fluvial elements. Systematic data of the variation in lithofacies, sedimentary structures and grain size was also collected.

The deposition took place within continental area varying from an alluvial fan to braided fluvial system. The cross-bedding data from nearby localities exhibiting lower variability (Ghosh 2014) suggests the possibility of deposition of lithounits under braided river system. Evidence in support of this interpretation are provided by the presence correlatable facies (basin margin to interior), characteristics of alluvial fan system giving way to braided river deposits in three sedimentary cycles. The trough cross stratified channel fill facies, tabular cross-stratified transverse bar facies justify the presence of braided river as depositional environment. The conglomerates are mainly clast supported in the basin margin with clast/matrix ratio 60:40 while matrix supported at the distal part along NNW with clast/matrix ratio 40:40 (Ghosh et al. 2016).

Based on the field data (n=65) collected from primary sedimentary structures, paleocurrent direction was determined. The unimodal distribution identified in the study area is 344° as the vector mean suggested the paleo flow direction from source rocks in SE to NW direction was persistent during deposition of Cave Temple Arenite Member. The north western paleocurrent direction signified the south eastern paleo-location of provenance for Badami sediments occurring in western part of Kaladgi basin. Transverse sections through boreholes along NNW-SSE direction is generated from sub-surface drilling by AMD in the study area reveal NNW paleo slope of unconformity as well as lithocontact prevailed during the geological past.

The sandstones belonging to second sedimentary cycle were taken up for detailed petromineralogical studies, revealed as texturally and mineralogically immature. Conglomerate is feldspar clast dominated and polymictic in nature, further justifying the mineralogically immature nature of the sediments. The intergranular spaces filled by arenaceous or clayey

matrix and bounded by iron oxide or silica cement. Feldspathic arenites are characterized by about 70-80% quartz, 15-20% feldspars, about 3-5% lithic fragments such as those of quartzites, etc. and 5-20% matrix composed of chlorite (Fe-rich). The presence of angular to sub-angular grains, detrital biotite, plagioclase feldspars and fresh unaltered k-feldspar clast, suggests weathering of a proximal K rich granitic source followed by rapid burial of sediments. Presence of K-feldspar clasts in the Badami sediments, petromineralogical as well as major and trace element geochemical data support such inferences. The heavy mineral identified is majorly zircon, with minor amounts of sphene and monazite, however it does not quantify the true relative abundance as identification of non-opaque heavy minerals was barred by persistent iron oxide coating over the grains. Morphological analysis of zircon grains based on its roundness, elongation and surface characteristics, indicate shorter distance of transportation derived from granitic source rock. Heavy mineral suite as suggested by (Ramachandra et al., 2019) mostly comprises of magnetite, ilmenite, monazite and zircon. Occasional presence of quartzite, jasper, BHJ, BHQ and hematite suggest that the metasediments of Chitradurga schist belts formed the subordinate source rock component.

Uranium mineralisation primarily occurs in matrix-supported conglomerate and intercalated feldspathic arenite. Pitchblende and coffinite have been identified as primary uranium minerals occurring along the grain boundaries of quartz, k-feldspar clasts. The associated sulphides identified are pyrite, chalcopyrite, chalcocite and bornite. Sulphides are seen as inclusions in pitchblende in places, indicating replacement by the later. The high uraniferous samples show sericitic/illitic, kaolinitic and chloritic alterations. In comparison, low uraniferous matrix-supported conglomerate samples (core) are hard and compact, buff to light grey in colour. The mineralogy of low uraniferous matrix supported conglomerate (core) is more or less similar to its high uraniferous counterpart. The low uraniferous conglomerate shows presence of diagenetic clay, silica overgrowth and pressure solution due to which, the

pore spaces were reduced and which might have inhibited the movement of hydrothermal solution carrying uranium. The rock shows relatively lesser amount of sulphide bearing minerals than its radioactive counterpart and more of hematite, goethite and magnetite at places.

Geochemical analysis and interpretations are in accordance with the petrographic observations. The sandstones plot majorly in the sub-arkose to arkose field on the classification plot after Herron 1988. The weathering indices suggest moderate chemical weathering at the source with an average CIA value of 69.32%. This is supported by the climatic discrimination geochemical plot which suggests a semi-arid to humid climate (after Suttner and Dutta 1986). Average PIA value of 82.81% suggests plagioclase alteration occurred post deposition. This has been observed in the petrographic study where the plagioclase feldspars are observed to alter to clay and in some places even form pseudomatrix. A negative correlation of PIA vs  $\text{Na}_2\text{O}$  and a positive correlation between PIA and  $\text{K}_2\text{O}/\text{Na}_2\text{O}$  suggest that with increase in PIA, plagioclase feldspar gets selectively altered before K-feldspars. Provenance discriminant diagram suggested by Roser and Korsh (1988), provenance discriminant equation of Hayashi et al., (1997) and provenance discrimination diagrams of McLennan et al., (1980), together suggest that the detritus involved in the formation of sandstones were derived from quartzose sedimentary provenance, the bulk chemical composition of which is granitic. Thus, quartzose sedimentary provenance constitutes “proximal” provenance and granitic terrain, “ultimate” provenance.

Geochemical analyses were carried out to draw comparisons between radioactive and non-radioactive pebbly feldspathic arenite/lower conglomerate. Uranium exhibits weak to moderate correlation with copper and strong positive correlation with lead and zinc. This is further supported by petromineralogical evidences, indicating the presence of copper sulphide minerals in association with Uraninite. Primary uranium bearing minerals identified within

pebbly feldspathic arenite/lower conglomerates are pitchblende and coffinite, which are mostly occurring along the grain boundaries of quartz and feldspar and micro-fractures in places. The mode of occurrence, textural evidence and their mineralogical and geochemical association indicate their hydrothermal nature and epigenetic origin. Sulfur isotope data (AMD, 2018-19) was obtained from pure fractions of pyrite (n=9), separated from mixed sulphides (pyrite, marcasite, chalcopyrite, pyrrhotite and galena). The samples collected from different depths in a radioactive core drilled at Gujanal show  $\delta^{34}\text{S}$  value range from -4.04 to 0.02‰ (CDT). The  $\delta^{34}\text{S}$  values in pyrites from most of the hydrothermal vary from -8 to +10 ‰ (Rye and Ohmoto Hiroshi, 1974). These values suggest hydrothermal source of Sulfur in above pyrite. Paragenetically, chalcopyrite is being replaced by bornite and covellite and later uranium phase. This indicates the presence of copper-rich solutions as pulses in different events. These sulphides are epigenetic in nature and formed during earlier phase of hydrothermal activity.

Uranium mineralisation in both Deshnur and Gujanal area is hosted by un-oxidised part of lower conglomerate and the basal arenite units occurring just above the unconformity contact of Cave temple arenite member with the Chitradurga basement, in the vicinity of NE-SW trending faults. The mineralization in Gujanal, occurs both in sulphide bearing sediments and in basement chlorite schist along the NE-SW trending post-sedimentary reactivated fracture zone (Status Report, Gujanal block, AMD, 2014-2020). The fracture zone has deformed the sedimentary succession thereby increasing secondary porosity and permeability thus allowing the movement of hydrothermal fluids and precipitation of uranium in sedimentary rocks.

## CHAPTER 8

### CONCLUSION

- Geological mapping in and around Deshnur area, Belgaum district, Karnataka has helped to identify two major fractures trending viz. NE-SW, NW-SE and also to understand general stratigraphic disposition of beds along Deshnur-Gujanal tract. The beds are trending in NE-SW direction, dipping gently (5-10°) in NW direction.
- Paleocurrent directions recorded from primary sedimentary structures exposed in the study area show unimodal distribution thereby indicating the movement of current flow from the source in South East direction towards North West direction, during the deposition of Cave Temple Arenite Member.
- Facies analysis followed by facies association have contributed towards identifying, three major cycles starting with the deposition of conglomerate in an alluvial fan depositional environment and ending with deposition of sandstone in a fluvial environment are identified. The second fluvial cycle is separated from third fluvial cycle by a depositional environment dominated by marine facies.
- The uranium mineralization is identified in lower part of Badami succession. The trend of mineralization in both Deshnur and Gujanal is recorded majorly in pebbly feldspathic arenite/lower conglomerate along the NE-SW trending fracture zones.
- Significant uranium mineralization was intercepted in borehole SLD-100 and SLD-102, hosted in pebbly feldspathic arenite/ lower conglomerate, with higher concentrations observed at the interface of thinly laminated silty shale intercalations and pebbly feldspathic arenite along the bedding plane guided by the porosity and permeability of the host granule beds.

- The mineralized host rock is polymictic matrix supported pebbly feldspathic arenite/lower conglomerate which is greyish white to greenish white in colour, immature, low to medium sorting, sub angular to sub rounded clasts, soft and friable in nature. It consists mainly of feldspars (mainly microcline & orthoclase), vein quartz, relict detrital biotites clast sizes are 0.5 to 2cm set in quartzo feldspathic matrix. Biotites are altered, sericitized/illitized, chloritized and getting merged with matrix material. Sericitization and clay formation are chief manifestations of feldspar alterations. The cement is iron oxide and silica.
- The mineralized rock is reduced in nature with abundant sulphide minerals such as chalcopyrite, chalcocite etc. occurring in disseminated form. Major part of non-mineralized rock shows oxidised nature, brown, whitish brown colour, hard and compact, less or devoid of sulphides.
- Based on the petrographic observations, uranium mineralization is mostly identified occurring in intergranular spaces and microfractures of quartz and feldspar in association with base-metal sulphides, primarily copper sulphides. This is further established by good positive correlation of U with Cu, Pb and Zn. The sulphides are epigenetic in nature and formed during the phase of hydrothermal activity. Primary uranium phases such as Pitchblende, Uraninite and Coffinite can be observed replacing the earlier formed sulphide phases suggesting uranium precipitation in later phase.
- The heavy mineral studies focussing on morphological parameters (roundness, elongation and surface characteristics) of zircon, corroborates with the fact that the sediments have endured short transport history, derived from nearby granitic source rock.
- Based on field observations complemented by petromineralogical studies, indicating the presence of fresh and altered feldspars, BIF, chert, jasper and quartzite fragments,

more than one type of source has been ascertained for the deposition of Badami sediments. Owing to presence of abundant fresh feldspars in pebbly feldspathic arenite/lower conglomerate unit, it is proposed that potash rich Proterozoic granites, might be one of the significant sources. Further studies are required pertaining to characterization of such high K<sub>2</sub>O bearing Proterozoic granite exposed in nearby areas.

- NW extension of the study area is marked by NE-SW trending post sedimentary fault (AMD, 2014-2015). The reactivated fault might have acted as the conduits for hydrothermal solutions rich in base metal which later invaded the host sediments along favourable zones.
- The present work incorporated majorly the structural and sedimentological studies to understand the depositional setup and the control of lithology on uranium mineralization. Further scope of work demands detailed study of hydrothermal alteration in mineralised (both in clasts and matrix) and non-mineralized lithounits. This will lead to develop a better understanding of the role of diagenesis, nature of ore fluid and causes of ore deposition.



## REFERENCES

- Allen, J. R. L. (1982). Sedimentary structures: Their character and physical basis. *Developments in Sedimentology*, 30(A), pp.593.
- Balan, E., Trocellier, P., Jupille, J., Fritsch, E., Muller, J. P. and Calas, G. (2001). Surface chemistry of weathered zircons. *Chemical Geology*, 181(1-4), pp.13-22.
- Bhatia, M.R. (1983). Plate tectonics and geochemical composition of sandstones. *The Journal of Geology*, 91(6), pp.611-627.
- Bhatia, M.R. and Crook, K.A. (1986). Trace element characteristics of graywackes and tectonic setting discrimination of sedimentary basins. *Contributions to mineralogy and petrology*, 92(2), pp.181-193.
- Boggs, S. (1995). *Principles of sedimentology and stratigraphy*. Prentice Hall, 2, 774p.
- Cardona, J.M., Mas, J.G., Bellón, A.S., Domínguez-Bella, S. and López, J.M. (2005). Surface textures of heavy-mineral grains: a new contribution to provenance studies. *Sedimentary Geology*, 174(3-4), pp.223-235.
- Chakraborty, P.P., Dey, S. and Mohanty, S.P. (2010). Proterozoic platform sequences of Peninsular India: implications towards basin evolution and supercontinent assembly. *Journal of Asian Earth Sciences*, 39(6), pp.589-607.
- Chowdhary, P.K. (1971). Zircon populations in Lewisian quartzite, gneiss and granite north of Loch Laxford, Sutherland. *Geological Magazine*, 108(3), pp.255-262.
- Clark Jr., S.P., Peterman, Z.E. and Heier K.S. (1966). Abundances in uranium, thorium and potassium. *Geological Society of America Memoirs Handbook of Physical Constants*, 97, pp.521-541.

- Condie, K.C. (1993). Chemical composition and evolution of the upper continental crust: contrasting results from surface samples and shales. *Chemical geology*, 104(1-4), pp.1-37.
- Cox, R., Lowe, D.R. and Cullers, R.L. (1995). The influence of sediment recycling and basement composition on evolution of mudrock chemistry in the southwestern United States. *Geochimica et Cosmochimica Acta*, 59(14), pp.2919-2940.
- Crook, K.A. (1974). Lithogenesis and geotectonics: the significance of compositional variation in flysch arenites (graywackes). *Soc. Econ. Paleo. Min., Spec. Publ.* 19, pp.304-310
- Cuney, M.L. (2005). World-class unconformity-related uranium deposits: key factors for their genesis. *Mineral Deposit Research: Meeting the Global Challenge*, Springer, pp. 245-248.
- Cuney, M. and Kyser, K. (2009). Recent and not-so-recent developments in uranium deposits and implications for exploration. *Economic Geology*, 104(4), pp.600-601.
- Cuney, M. and Kyser, K. (2009b). Unconformity-related uranium deposits. Recent and not-so-recent developments in uranium deposits and implications for exploration. *Mineralogical Association of Canada, Short Course*, 39, pp.161-219.
- Cuney, M. (2010). Evolution of uranium fractionation processes through time: driving the secular variation of uranium deposit types. *Economic Geology*, 105(3), pp.553-569.
- Dabard, M.P. (1990). Lower Brioverian formations (Upper Proterozoic) of the Armorican Massif (France): geodynamic evolution of source areas revealed by sandstone petrography and geochemistry. *Sedimentary Geology*, 69(1-2), pp.45-58.
- Deb, M. and Pal, T. (2015). Mineral potential of Proterozoic intracratonic basins in India. *Geological Society, London, Memoirs*, 43(1), pp.309-325.

- Dey, S., Rai, A.K. and Chaki, A. (2009). Palaeoweathering, composition and tectonics of provenance of the Proterozoic intracratonic Kaladgi–Badami basin, Karnataka, southern India: evidence from sandstone petrography and geochemistry. *Journal of Asian Earth Sciences*, 34(6), pp.703-715.
- Dey, S. (2015). Geological history of the Kaladgi–Badami and Bhima basins, south India: sedimentation in a Proterozoic intracratonic setup. Geological Society, London, *Memoirs*, 43(1), pp.283-296.
- Dickinson, W.R. and Suczek, C.A. (1979). Plate tectonics and sandstone compositions. *AAPG Bulletin*, 63(12), pp.2164-2182.
- Dietz, V. (1973). Experiments on the influence of transport on shape and roundness of heavy minerals. *Contributions to Sedimentology*, 1, pp.69 – 102.
- Eren, M. and Kadir, S. (1999). Color origin of upper Cretaceous pelagic red sediments within the Eastern Pontides, northeast Turkey. *International Journal of Earth Sciences*, 88(3), pp.593-595.
- Fayek, M., Horita, J. and Ripley, E.M. (2011). The oxygen isotopic composition of uranium minerals: A review. *Ore Geology Reviews*, 41(1), pp.1-21.
- Fayek, M. (2013). Uranium ore deposits: A review. *Uranium: cradle to grave*, 43, pp.121-147.
- Fedo, C.M., Nesbitt, W.H. and Young, G.M. (1995). Unraveling the effects of potassium metasomatism in sedimentary rocks and paleosols, with implications for paleoweathering conditions and provenance. *Geology*, 23(10), pp.921-924.
- Finger, F. and Haunschmid, B. (1988). Die mikroskopische Untersuchung der akzessorischen Zirkone als Methode zur Klärung der Intrusionsfolge in Granitgebieten – eine Studie

- im nordöstlichen oberösterreichischen Moldanubikum. – Jahrbuch der Geologischen Bundesanstalt, 131, pp.255-266.
- Folk, R.L. (1980). Petrology of sedimentary rocks. Hemphill publishing company, Austin, 184p.
- Foote, R.B. (1876). The geological features of the south Mahratta country and adjacent districts. Geological Survey of India, 12(1), pp.139-164.
- Freise, F.W. (1931). Untersuchungen von Mineralen auf Abnutzbarkeit bei Verfrachtung im Wasser. – Tschermaks Mineralische und Petrographische Mitteilungen, 41, pp.1-7.
- Gärtner, A., Linnemann, U., Sagawe, A., Hofmann, M., Ullrich, B. and Kleber, A. (2013). Morphology of zircon crystal grains in sediments-characteristics, classifications, definitions. *Geologica Saxonica*, 59, pp.65-73.
- Ghosh, N., Chavan, S.J., Nagaraju, M. Prakash, B.G., Sarkar, S. and Sesha Rao, R.V.S. (2016). Paleocurrent analysis of Badami Group of rocks in South Western part of Kaladgi Basin, Karnataka. *EARFAM*, 26, pp.127-135.
- Hadlari, T., Rainbird, R. H., and Donaldson, J. A. (2006). Alluvial, eolian and lacustrine sedimentology of a Paleoproterozoic half-graben, Baker Lake Basin, Nunavut, Canada. *Sedimentary Geology*, 190(1-4), pp.47–70.
- Hayashi, K.I., Fujisawa, H., Holland, H.D. and Ohmoto, H. (1997). Geochemistry of ~1.9 Ga sedimentary rocks from northeastern Labrador, Canada. *Geochimica et Cosmochimica Acta*, 61(19), pp.4115-4137.
- Herron, M.M. (1988). Geochemical classification of terrigenous sands and shales from core or log data. *Journal of Sedimentary Research*, 58(5), pp.820-829.

- Hoeve, J. and Quirt, D. (1984). Mineralization and host rock alteration in relation to clay mineral diagenesis and evolution of the Mid-Proterozoic Athabasca Basin, Saskatchewan, Canada, SRC Technical report 187p.
- Hoppe, G. (1962). Zur Morphologie des akzessorischen Zirkons. – Berichte der Geologischen Gesellschaft in der Deutschen Demokratischen Republik, 6, pp.37-41.
- Hoppe, G. (1963). Die Verwendbarkeit morphologischer Erscheinungen an akzessorischen Zirkonen für petrogenetische Auswertungen. Abhandlungen der Deutschen Akademie der Wissenschaften zu Berlin, 1, pp.1-130.
- IAEA (2013). Geological classification of uranium deposits and description of selected examples, IAEA-Tecdoc-CD-1749, 353p.
- Jacobson, A.D. and Blum, J.D. (2003). Relationship between mechanical erosion and atmospheric CO<sub>2</sub> consumption in the New Zealand Southern Alps. *Geology*, 31(10), pp.865-868.
- Jayaprakash, A.V., Sundaram, V., Hans, S.K. and Mishra, R.N., (1987). Geology of the Kaladgi-Badami Basin, Karnataka. *Purana Basins of Peninsular India. Mem. Geol. Soc. India*, 6, pp.201-225.
- Jayaprakash, A.V. (2007). *Purana Basins of Karnataka. Mem. Geol. Surv. India*, 129, pp.140.
- Kale, V.S. and Phansalkar, V.G. (1991). Purana basins of peninsular India: A review. *Basin research*, 3(1), pp.1-36.
- Köster, E. (1964). Granulometrische und morphometrische Meßmethoden an Mineralkörnern, Steinen und sonstigen Stoffen, *Zeitschrift Für Pflanzenernährung, Düngung, Bodenkunde*, 106(1), pp.1-336.

- Kostov, I. (1973). Zircon morphology as a crystallogenic indicator. *Kristall und Technik*, 8, pp.11-19.
- Krishnamurthy, P. (1996). Are early-middle Proterozoic unconformity-related uranium deposits unique to Australia and Canada? an appraisal with special reference to India. *Exploration and Research for Atomic Minerals*, 9, pp.1-40.
- Kyser, K. and Hiatt, E.E. (2003). Fluids in sedimentary basins: An Introduction. *Journal of Geochemical Exploration*, 80(2-3), pp.139-149.
- Kyser, T.K. and Cuney, M. (2009b). Introduction. In: Cuney, M. & Kyser, T.K. (Eds.), *Recent and Not-So Recent Developments in Uranium Deposits and Implications for Exploration*. Mineralogical Association of Canada. Short Course series, 39, pp.1-14.
- Larsen, L.H. and Poldervaart, A. (1957). Measurement and distribution of zircons in some granitic rocks of magmatic origin. *Mineral Mag*, 31, pp.544-564.
- Leith, C.J. (1950). Removal of iron oxide coatings from mineral grains. *Journal of Sedimentary Research*, 20(3), pp.174-176.
- List, F.K. (1966). Statistische Untersuchungen an Zirkon und Apatit in Anatexiten des südlichen Bayerischen Waldes. *Geologische Rundschau*, 55, pp.509 – 530.
- Mazumder, R. and Eriksson, P. G. (2015). Eds. *Precambrian basins of India: stratigraphic and tectonic context*. *Geol Soc London Mem*, 43, pp.352.
- Mcculloch, M.T. and Wasserburg, G.J. (1978). Sm-Nd and Rb-Sr chronology of continental crust formation. *Science*, 200(4345), pp.1003-1011.
- Mclennan, S.M., Nance, W.B. and Taylor, S.R. (1980). Rare earth element-thorium correlations in sedimentary rocks, and the composition of the continental crust. *Geochimica et Cosmochimica Acta*, 44(11), pp.1833-1839.

- Mclennan, S.M. and Taylor, S.R. (1991). Sedimentary rocks and crustal evolution: tectonic setting and secular trends. *The Journal of Geology*, 99(1), pp.1-21.
- Mclennan, S.M., Hemming, S., Mcdaniel, D.K. and Hanson, G.N. (1993). Geochemical approaches to sedimentation, provenance, and tectonics. *Special Papers-Geological Society of America*, 284, pp.21-40.
- Mclennan, S.M. (2001). Relationships between the trace element composition of sedimentary rocks and upper continental crust. *Geochemistry, Geophysics, Geosystems*, 2(4).
- Miall, A.D. (1980). Cyclicity and the facies model concept in fluvial deposits. *Bulletin of Canadian Petroleum Geology*, 28(1), pp.59-79.
- Miall, A. D. (1985). Architectural element analysis: A new method of facies analysis applied to fluvial deposits. *Earth-Science Reviews*, 22, pp.261–308.
- Miall, A. D. (1988)a. Facies architecture in clastic sedimentary basins. K. Kleinspehn & C. Paola (Editors) *New perspective in basin analysis*. Springer, pp. 67–81.
- Miall, A. D. (1994). Reconstruction of fluvial macroform architecture from two-dimensional outcrops: Examples from the Castlegate Sandstone, Book Cliffs, Utah. *Journal of Sedimentary Research*, 64(2b), pp.146–158.
- Miall, A. D. (1996). *The geology of fluvial deposits: Sedimentary facies, basin analysis and petroleum geology*. Springer, 582p.
- Miall, A. D. and Jones, B. (2003). Fluvial architecture of the Hawkesbury Sandstone (Triassic), near Sydney, Australia. *Journal of Sedimentary Research*, 73, pp.531–545.
- Miall, A. D. (2006). How do we identify big rivers? And how big is big? *Sedimentary Geology*, 186, pp.39–50.
- Miall, A. D. (2014). *Fluvial depositional systems*. Springer, 14, 316p.



- Morton, A.C., (1984). Stability of detrital heavy minerals in Tertiary sandstones from the North Sea Basin. *Clay minerals*, 19(3), pp.287-308.
- Mukhopadhyay, S., Samanta, P., Bhattacharya, S. and Sarkar, S. (2019). Stratigraphic evolution and architecture of the terrestrial succession at the base of the Neoproterozoic Badami Group, Karnataka, India. *Geological evolution of the Precambrian Indian shield*, pp.121-157.
- Murawsky, H. and Meyer, W. (2010). *Geologisches Wörterbuch*, Heidelberg (Spektrum), pp.1 – 220.
- Nathan, S. (1976). Geochemistry of the Greenland Group (Early Ordovician), New Zealand. *New Zealand journal of geology and geophysics*, 19(5), pp.683-706.
- Nautiyal, S. (1966). Precambrian of Mysore Plateau: Presidential Address (Geology and Geography Section). *Proc. 53rd Indian Sci, Congpt*, 11.
- Nesbitt, H. and Young, G.M. (1982). Early Proterozoic climates and plate motions inferred from major element chemistry of lutites. *nature*, 299(5885), pp.715-717.
- Nesbitt, H.W. and Young, G.M. (1984). Prediction of some weathering trends of plutonic and volcanic rocks based on thermodynamic and kinetic considerations. *Geochimica et Cosmochimica Acta*, 48(7), pp.1523-1534.
- Nesbitt, H.W. and Young, G.M. (1989). Formation and diagenesis of weathering profiles. *The Journal of Geology*, 97(2), pp.129-147.
- Nichols, G. (2009). *Sedimentology and stratigraphy*. John Wiley & Sons, 419p.
- Pillai, S.P. and Kale, V.S. (2007). Tectonic Controls on Sedimentation in the Proterozoic Kaladgi Basin of South India. Abstract, International Conference on Precambrian

- Sedimentation and Tectonics and Second GPSS meeting, IIT Bombay, 10-12 December 2007, pp.41-42.
- Pettijohn, F.J. (1975). Sedimentary rocks. New York: Harper & Row, 85(3), 628p.
- Pillai, S.P. and Kale, V.S. (2011). Seismites in the Lokapur Subgroup of the Proterozoic Kaladgi Basin, South India: A testimony to syn-sedimentary tectonism. *Sedimentary Geology*, 240(1-2), pp.1-13.
- Pillai, S.P., Pande, K. and Kale, V.S. (2018). Implications of new  $^{40}\text{Ar}/^{39}\text{Ar}$  age of Mallapur Intrusives on the chronology and evolution of the Kaladgi Basin, Dharwar Craton, India. *Journal of Earth System Science*, 127(3), pp.32.
- Pillai, S.P. and Kale, V.S. (2019). Interplay Between Tectonics & Eustacy in a Proterozoic Epicratonic, Polyhistory Basin, North Dharwar Craton. *Tectonics and Structural Geology: Indian Context*, Springer Geology, pp. 75-114.
- Poldervaart, A. (1955). Zircons in Rocks; 1. Sedimentary Rocks. *American Journal of Science*, 253(8), pp.433 – 461.
- Poldervaart, A. (1956). Zircons in Rocks; 2. Igneous Rocks. *American Journal of Science*, 254(9), pp.521 – 554.
- Pupin, J.P. (1980). Zircon and Granite Petrology. *Contributions to Mineralogy and Petrology*, 73(3), pp.207 – 220.
- Radhakrishna, B.P. and Naqvi, S.M. (1986). Precambrian continental crust of India and its evolution. *The Journal of Geology*, 94(2), pp.145-166.
- Radhakrishna, B.P. (1987). Purana basins of peninsular India. *Mem. Geol. Soc. India*, 6, 518p.

- Ramachandran, A., Srinivasalu, S., Ramasamy, S., Bhuvaneswari, S., Gnanaval, D. and Krishna, K.V.G. (2019). Mineralogical Studies of Kerur Formation Badami Group, Kaladgi Basin, Karnataka. *Journal of the Geological Society of India*, 93(3), pp.343-350.
- Ramakrishnan, M. and Vaidyanadhan, R. (2010). *Geology of India (Vol. 1 & 2)*. GSI Publications, 2(1), 428p.
- Roser, B.P. and Korsch, R.J. (1986). Determination of tectonic setting of sandstone-mudstone suites using  $\text{SiO}_2$  content and  $\text{K}_2\text{O}/\text{Na}_2\text{O}$  ratio. *The Journal of Geology*, 94(5), pp.635-650.
- Roser, B.P. and Korsch, R.J. (1988). Provenance signatures of sandstone-mudstone suites determined using discriminant function analysis of major-element data. *Chemical geology*, 67(1-2), pp.119-139.
- Rösler, J., Harders, H. and Bäker, M. (2006). *Mechanisches Verhalten der Werkstoffe*, pp.1-521.7
- Rye, R.O. and Ohmoto, H. (1974). Sulfur and carbon isotopes and ore genesis: a review. *Economic Geology*, 69(6), pp.826-842.
- Sambrook Smith, G. H., Best, J. L., Bristow, C. S. and Petts, G. E. (2006). *Braided rivers: Process, deposits, ecology and management* Oxford: Blackwell, 396p.
- Sarkar, S., Samanta, P., Mukhopadhyay, S. and Bose, P. K. (2012). Stratigraphic architecture of the Sonia Fluvial interval, India in its Precambrian context. *Precambrian Research*, 214, pp.210–226.
- Saxena, F.K. (1966). Evolution of zircons in sedimentary and metamorphic rocks. *Sedimentology*, 6(1), pp.1-33.

- Schieber, J. (1992). A combined petrographical–geochemical provenance study of the Newland Formation, Mid-Proterozoic of Montana. *Geological Magazine*, 129(2), pp.223-237.
- Sinha, A.K., Wayne, D.M. and Hewitt, D.A. (1992). The hydrothermal stability of zircon: Preliminary experimental and isotopic studies. *Geochimica et Cosmochimica Acta*, 56(9), pp.3551 – 3560.
- Sridhar, M., Markandeyulu, A., Chawla, A.S. and Chaturvedi, A.K. (2018). Analyses of Aeromagnetic Data to Delineate Basement Structures and Reveal Buried Igneous Bodies in Kaladgi Basin, Karnataka. *Journal of the Geological Society of India*, 91(2), pp.165-173.
- Stumm, W. and Morgan, J.J. (1970). *Aquatic chemistry; an Introduction emphasizing chemical equilibria in natural waters*, 48(12), 779p.
- Stumm, W. and Morgan, J.J. (2012). *Aquatic chemistry: chemical equilibria and rates in natural waters*, John Wiley & Sons, 126, 1040p.
- Suttner, L.J. and Dutta, P.K. (1986). Alluvial sandstone composition and paleoclimate; I, Framework mineralogy. *Journal of Sedimentary Research*, 56(3), pp.329-345.
- Taylor, S.R. and McLennan, S.M. (1981). The composition and evolution of the continental crust: rare earth element evidence from sedimentary rocks. *Philosophical Transactions of the Royal Society of London. Series A, Mathematical and Physical Sciences*, 301(1461), pp.381-399.
- Taylor, S.R. and McLennan, S.M. (1985). *The continental crust: its composition and evolution. An examination of the geochemical record preserved in sedimentary rocks*. Oxford: Blackwell Scientific, 15, 312p.

- Tejan-Kella, M.S., Fitzpatrick, R.W. and Chittleborough, D.J. (1991). Scanning electron microscope study of zircons and rutiles from a Podzol Chronosequence at Cooloola, Queensland, Australia. *Catena*, 18(1), pp.11-30.
- Unpublished annual report, AMD-SR, KBI (2004-05). Sub-surface exploration by drilling in Deshnur block, Belagavi district, Karnataka.
- Unpublished annual report, AMD-SR, KBI (2013-14). Sub-surface exploration by drilling in Deshnur block, Belagavi district, Karnataka.
- Unpublished annual report, AMD-SR, KBI (2014-15). Sub-surface exploration by drilling in Deshnur block, Belagavi district, Karnataka.
- Unpublished annual report, AMD-SR, KBI (2017-18). Sub-surface exploration by drilling in Gujanal block, Belagavi district, Karnataka.
- Unpublished annual report, AMD-SR, KBI (2018-19). Sub-surface exploration by drilling in Gujanal block, Belagavi district, Karnataka.
- Unpublished status report, Gujanal block, AMD-SR, KBI (2014-20). Sub-surface exploration by drilling in Gujanal block, Belagavi district, Karnataka.
- Vishwanathaiah, M.N. (1977). Lithostratigraphy of the Kaladgi and Badami Groups, Karnataka. *Indian Mineralogist*, 18, pp.122-132
- Kale, V. S. (1991). Constraints on the evolution of the Purana basins of peninsular India. *Journal of the Geological Society of India*, 38(3), pp.231-252.
- Kale, V. S., Ghunkikar, V., Thomas, P.P. and Peshwa, V. V. (1996). Macrofacies architecture of the first transgressive suite along the southern margin of the Kaladgi basin. *Journal of the Geological Society of India*, 48, pp.75–92.

- Voggenreiter, W. (1986). Vorläufige Ergebnisse morphologischer Untersuchungen an Zirkonen aus Quarziten und Quarzschiefen des Penninikums und Unterostalpins des Weißeneck-Schreck-Gebietes der südlichen Radstädter Tauern (Ostalpen, Österreich). *Jahrbuch der geologischen Bundesanstalt*, 129(1), pp.149 – 159.
- Walker, R.N., Logan, R.G. and Binnekamp, J.G. (1977). Recent geological advances concerning the HYC and associated deposits, McArthur river, NY. *Journal of the Geological Society of Australia*, 24(7-8), pp.365-380.
- Wronkiewicz, D.J. and Condie, K.C. (1987). Geochemistry of Archean shales from the Witwatersrand Supergroup, South Africa: source-area weathering and provenance. *Geochimica et Cosmochimica Acta*, 51(9), pp.2401-2416.
- Wyatt, M. (1954). Zircons as provenance indicators. *American Geologist: Journal of Earth and Planetary Materials*, 39(11-12), pp.983-990.
- Zimmerle, W. (1975). Accessory zircon from a Rhyolite, Yellowstone National Park (Wyoming U.S.A.). *Zeitschrift der Deutschen Geologischen Gesellschaft*, 130(1), pp.361 – 369.